Rational Pathogen Design: Extending the Host Range of *Listeria monocytogenes* by Thermodynamically Re-engineering the Internalin / E-Cadherin Interface

Von der Fakultät für Lebenswissenschaften

der Technischen Universität Carolo-Wilhelmina

zu Braunschweig

zur Erlangung des Grades eines

Doktors der Naturwissenschaften

(Dr. rer. nat.)

genehmigte

D i s s e r t a t i o n

von Thomas Wollert
aus Magdeburg

1. Referent: Honorarprofessor Dr. Dirk Heinz
2. Referentin: Professor Dr. Petra Dersch
eingereicht am: 21.05.2007
mündliche Prüfung (Disputation) am: 17.07.2007

Druckjahr 2007

Vorveröffentlichungen der Dissertation

Teilergebnisse aus dieser Arbeit wurden mit Genehmigung der Fakultät für Lebenswissenschaften, vertreten durch den Mentor der Arbeit, in folgenden Beiträgen vorab veröffentlicht:

Publikationen

Wollert, T., Pasche, B., Rochon, M., Deppenmeier, S., van den Heuvel, J., Gruber, A.D., Heinz, D.W., Lengeling, A. & Schubert, W.-D. (2007) Extending the host range of *Listeria monocytogenes* by rational protein design. *Cell* **129** (5), 891-902.

Wollert, T., Heinz, D.W. & Schubert, W.-D. (2007) Thermodynamically re-engineering the listerial invasion complex InlA / E-cadherin. PNAS, doi:10.1073/pnas.0702199104.

Tagungsbeiträge

Wollert, T., Heinz, D.W. & Schubert, W.-D.: Strengthening the binding of Internalin to human E-cadherin. (Poster) Structural Biology at Crossroads, EMBL Hamburg, Germany (2004). Poster-Prize.

Wollert, T., Heinz, D.W. & Schubert, W.-D.: Structure based re-engineering of Internalin – the intestinal invasin of *Listeria monocytogenes*. (Vortrag) Murnau Conference on Structural Biology of Molecular Recognition, Murnau , Germany (2005).

Wollert, T., Heinz, D.W. & Schubert, W.-D.: Structure based re-engineering of Internalin – the intestinal invasin of *Listeria monocytogenes*. (Vortrag) Eighth Heart of European Bio-Crystallography Meeting, Karlovy Vary, Czech Republic (2005). Best Talk Prize.

Wollert, T., Heinz, D.W. & Schubert, W.-D.: Structure based re-engineering of Internalin – the intestinal invasin of *Listeria monocytogenes*. (Poster) Meeting of the Network of Excellence (NoE) EuroPathoGenomics, Universität Würzburg, Germany (2005).

Wollert, T., Heinz, D.W. & Schubert, W.-D.: Structure based re-engineering of Internalin – the intestinal invasin of *Listeria monocytogenes*. (Vortrag) Jahrestagung der Deutschen Gesellschaft für Kristallographie, Universität Freiburg, Germany (2006).

Wollert, T., Pasche, B., Rochon, M., Deppenmeier, S., van den Heuvel, J., Gruber, A.D., Heinz, D.W., Lengeling, A. & Schubert, W.-D.: Structure based re-engineering of Internalin – an invasin *of Listeria monocytogenes*. (Poster) 23rd European Crystallographic Meeting, University of Leuven, Belgium (2006).

Wollert, T., Pasche, B., Rochon, M., Deppenmeier, S., van den Heuvel, J., Gruber, A.D., Heinz, D.W., Lengeling, A. & Schubert, W.-D.: Structure-based pathogen design – a new murine listeriosis model. (Vortrag) Cold Spring Harbor Laboratory Meeting, Genomic Perspectives to Host-Pathogen Interactions, Welcome-Trust Conference Centre, Hinxton, UK, (2006).

Wollert, T., Pasche, B., Rochon, M., Deppenmeier, S., van den Heuvel, J., Gruber, A.D., Heinz, D.W., Lengeling, A. & Schubert, W.-D.: Structure based pathogen design – extending the host specificity of *Listeria monocytogenes*. (Vortrag) Structural Biology of Pathogens, University of Birmingham, UK (2006).

Wollert, T., Pasche, B., Rochon, M., Deppenmeier, S., van den Heuvel, J., Gruber, A.D., Heinz, D.W., Lengeling, A. & Schubert, W.-D.: Structure based re-engineering of Internalin – an invasin of *Listeria monocytogenes*. (Poster) 58th Mosbacher Colloquium, Mosbach, Germany (2007).

Wollert, T., Pasche, B., Rochon, M., Deppenmeier, S., van den Heuvel, J., Gruber, A.D., Heinz, D.W., Lengeling, A. & Schubert, W.-D.: Structure based pathogen design – extending the host range of *Listeria monocytogenes*. (Poster) Annual Meeting of the American Crystallographic Association, Salt Lake City, Utah, USA (2007).

Contents

Abbreviations

Å	Ångstrøm
Amp	Ampicillin
Arf6	ADP-ribosylation factor 6
ARHGAP10	Rho GTPase-activating protein 10
Arp	Actin related protein
BHI	Brain heart infusion
Cm	Chloramphenicol
CNS	Central nervous system
DNA	Deoxyribonucleic acid
Ery	Erythromycin
FAK	Focal adhesion kinase
GFP	Green fluorescent protein
GST	Glutathion-S-transferase
hEC1	human E-cadherin ectodomain 1
Ig	Immunoglobulin
InlA	Internalin
IPTG	Isopropyl βD-thiogalactopyranoside
IR	Interrepeat
ITC	Isothermal titration calorimetry
Kan	Kanamycin
K_D	Dissociation constant
LIPI-1	*Listeria* pathogenicity island 1
LLO	Listeriolysin O
Lmo-EGD	*Listeria monocytogenes* EGD-e
Lmo-InlA^m	*Listeria monocytogenes* EGD-e isogenic mutant strain, carrying the *inlA*$^{S192N\text{-}Y369S}$-gene
LRR	Leucine rich repeat
mEC1	murine E-cadherin ectodomain 1
PAGE	Polyacrylamide gel electrophoresis
PC-PLC	Phosphatidylcholine specific phospholipase C
PCR	Polymerase chain reaction
p.i.	post infection
PI-3K	Phosphatidylinositol-3 kinase
PI-PLC	Phosphatidylinositol specific phospholipase C
PrfA	Positive regulatory factor A
SARS	Severe acute respiratory syndrome
SDS	Sodium dodecyl sulfate
TCA	Trichloroacidic acid
VASP	Vasodilator-stimulated phosphoprotein
WASP	Wiskott-Aldrich syndrome protein

Summary

Pathogens have evolved a dedicated set of virulence factors that specifically interact with individual host molecules. This specialization limits an individual pathogen to a defined range of hosts. Newly emerging diseases overwhelmingly involve existing pathogens whose virulence factors have been mutated to allow them to infect previously inaccessible hosts. The human food borne pathogen *Listeria monocytogenes* expresses two invasion proteins, internalin (InlA) and InlB, that enable bacterial uptake into distinct sets of host cells. These two molecules restrict *L. monocytogenes* to a defined range of hosts including cattle, sheep and humans but prevent infections of mice, guinea pigs or rabbits. In emulating spontaneous changes of host specificity, InlA has been rationally re-engineered to increase the affinity for its natural receptor human E-cadherin, thereby extending the specificity to allow recognition of formerly incompatible murine E-cadherin. At the atomic level, regions of low complementarity in the interaction interface of InlA and human E-cadherin were identified by analyzing the crystal structure of the recognition complex. Single amino acid substitutions in InlA that would potentially increase its weak binding affinity for human E-cadherin by improving surface complementarity were introduced into InlA. Structural changes of individual substitutions and of their combinations were verified crystallographically. Binding affinities as well as binding enthalpy and entropy were determined by isothermal titration calorimetry. All four rationally chosen, single substitutions in InlA increase binding affinity strongly. The correlation of high resolution structural data with thermodynamic characteristics provides unique insights into atomic contributions to binding enthalpy and entropy. Combining a mere two single substitutions transforms the weak interaction of wild-type InlA with human E-cadherin into a tight recognition. Biophysically, re-engineered InlA recognizes murine E-cadherin with an affinity similar to that of the wild-type InlA human E-cadherin interaction. Incorporating these two mutations into the listerial genome extends the host range of *L. monocytogenes* to include the mouse. By rationally adapting a single protein, a versatile murine model of human listeriosis has thus been created.

1 Introduction

Sudden changes in host specificity of existing pathogens are a serious threat for the global human population. Zoonotic pathogens eliciting recent pandemics (Lewis, 2006) include HIV (Heeney *et al.*, 2006) and SARS (Li *et al.*, 2005), while influenza A subtype H5N1 may be poised to do so (Stevens *et al.*, 2006). For these pathogens single amino acid substitutions in virulence factors have been identified to be responsible for changed host tropism (Feng, 2005; Yamada *et al.*, 2006). Understanding the underlying mechanisms, however, requires detailed knowledge of atomic changes in virulence factors, their influence on recognition of formerly incompatible host molecules and how this newly created interaction modifies normal cell and tissue functions to convert the previous coexistence of these species to a host-pathogen relationship.

1.1 Pathophysiology of *L. monocytogenes*

The genus *Listeria* includes six species: *L. monocytogenes*, *L. ivanvovii*, *L. inocua*, *L. welshimeri*, *L. seegligeri*, and *L. grayi* (Vazquez-Boland *et al.*, 2001). The first two are pathogenic for animals while only *L. monocytogenes* is associated with human disease (Glaser *et al.*, 2001).

L. monocytogenes is a rod shaped, ubiquitously distributed Gram-positive bacterium. It is able to grow at low temperatures and can withstand low pH and high salt conditions. This robustness makes *L. monocytogenes* problematic to the food industry, especially as regards ready-to-eat products (McLauchlin *et al.*, 2004). Healthy individuals respond to listerial infections mostly with mild symptoms like gastroenteritis (Hof, 2001), indicating that the immune system is able to control and combat the infection efficiently (Pamer, 2004). This correlates with a comparatively low incidence of severe listeriosis reported in Germany (519 cases in 2005, Koch and Stark, 2006) or the USA (1330 cases in 2002, Lynch *et al.*, 2006). In elderly or immunocompromized individuals and pregnant women, however, systemic manifestation of listeriosis occurs with symptoms including meningitis, sepsis, fetal infections and miscarriage. Among bacterial pathogens, *Salmonella enteritidis* causes the largest number of outbreaks but *L. monocytogenes* is responsible for the majority of fatal cases (Lynch *et al.*,

2006) amounting to a mortality rate of 30 %, far exceeding those of other food borne pathogens (Altekruse *et al.*, 1997).

1.1.1 Virulence factors and intracellular infection cycle of *L. monocytogenes*

The opportunistic, facultative intracellular pathogen *L. monocytogenes* uses the nutrient-rich and shielded environment of the cytosol to persist in host cells protected from humoral and cellular immune responses (Galan, 2000). *L. monocytogenes* has evolved several virulence factors (Figure 1.1-1) that specifically contribute to the intracellular infection cycle. Two of these, InlA and InlB promote cell-type specific uptake into normally non-phagocytic host cells (Cossart and Sansonetti, 2004). Following uptake, bacteria need to escape from the phagosome to avoid fusion with the lysosome and subsequent degradation by lysosomal enzymes. Release of bacteria from the phagosome is predominantly mediated by the pore-forming cytolysin listeriolysin O (LLO, Dubail *et al.*, 2001) with the help of the phosphatidylinositol specific phospholipase C (PI-PLC, Kayal and Charbit, 2006). Cytosolic bacteria grow and replicate rapidly with cell-type specific intracellular replication rates of one hour or less (Chico-Calero *et al.*, 2002). An important capacity of *L. monocytogenes* is its actin-based intracellular movement. Actin-rich filamentous structures called ‘actin comet tails’ are produced at one bacterial pole propelling the bacterium through the cytosol by continuous G-actin polymerization at the bacterial surface (Pizarro-Cerda and Cossart, 2006b). Actin polymerization is orchestrated by the polarized surface protein ActA (Kocks *et al.*, 1992). It recruits the cellular actin-polymerizing machinery including Arp2/3 and VASP, mimicking cellular actin nucleating factors like WASP (Boujemaa-Paterski *et al.*, 2001). When a bacterium encounters the cell membrane, actin-based movement leads to the formation of filopodia-like protrusions into the neighboring cell (Pust *et al.*, 2005) within which the bacterium is enclosed in a double-membrane vacuole. Release form this vacuole again requires LLO-activity supported by the second listerial phospholipase C (PC-PLC) specific for phosphatidylcholine (Alberti-Segui *et al.*, 2007). This direct cell-to-cell spread is of eminent importance in listerial pathophysiology because it allows large-scale infection of tissues without exposure to cellular or humoral components of the immune system and possibly more importantly because it allows *L. monocytogenes* to overcome tissue-barriers (Le Monnier *et al.*, 2007).

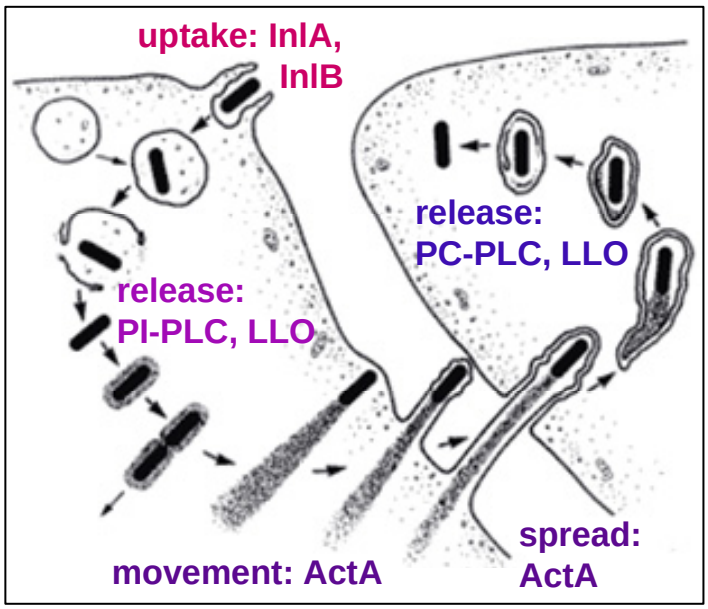

Figure 1.1-1: Infection cycle of *L. monocytogenes*. Following uptake into non-phagocytic cells induced by the invasion proteins InlA (internalin) and InlB bacteria escape from the phagosome by expressing PI-PLC (phosphoinositol specific phospholipase C) and LLO (listeriolysin O). Actin-based movement within cells is mediated by ActA and similarly enables direct cell-to-cell spreading of bacteria. Release form the double-membrane vacuole involves PC-PLC (phosphocholin specific phospholipase C) and LLO expression. Figure adapted from Tilney and Portnoy (1989).

As a consequence of the intricate interplay of these virulence factors tightly regulated by the transcription factor PrfA (Chakraborty *et al.*, 1992), *L. monocytogenes* is able to penetrate the intestinal barrier, followed by systemic dissemination, infection of hepatic and splenic tissues, and bacteremia-induced crossing of the blood-brain and the blood-placenta barriers (Lorber, 1997).

1.2 Invasion proteins – key to enter host cells

In *L. monocytogenes* at least two cell surface proteins promote the host-cell-specific uptake, InlA (Gaillard *et al.*, 1991) and InlB (Gaillard *et al.*, 1991; Dramsi *et al.*, 1995). InlA induces listerial uptake into epithelial cells (Gaillard *et al.*, 1991) by targeting the N-terminal domain (hEC1) of human E-cadherin (Mengaud *et al.*, 1996), the dominant adhesion molecule of adherens junctions (D'Souza-Schorey, 2005). The second listerial invasion protein InlB recognizes the receptor tyrosine kinase Met (Shen *et al.*, 2000) inducing uptake into a wide range of mammalian cells including hepatocytes and endothelial cells. Two further receptors of InlB have been characterized, gC1qR (the receptor for the globular part of the complement

component C1q), possibly a co-receptor for InlB (Braun *et al.*, 2000) and heparan sulfate, a negatively charged polysaccharide, present on eukaryotic cell surfaces (Jonquieres *et al.*, 2001). Whereas InlB-mediated Met-receptor activation and subsequent intracellular signaling events are well characterized (Hamon *et al.*, 2006), the precise role of the other two receptors remains to be clarified.

1.2.1 The leucine-rich-repeat family of proteins

Structurally, InlA and InlB belong to the leucine-rich-repeat (LRR) family of proteins with at least 25 members in *L. monocytogenes* (Cabanes *et al.*, 2002). LRRs share a characteristic repeat-architecture stabilized by a conserved pattern of the aliphatic amino acids valine, leucine, and isoleucine within each repeating unit creating the hydrophobic core (Takahashi *et al.*, 1985). Each repeat contributes a β-strand at the concave, and a spatially larger α- or 3_{10}-helix at the convex face generating the solenoid shape of the domain. All β-strands participate in a parallel β-sheet, lining the concave face of the domain, the most common ligand binding site of LRR proteins (Kobe and Kajava, 2001). The rigid LRR-domain predominantly functions as a protein-protein interaction motif (Kobe and Deisenhofer, 1994).

LRR-proteins are widespread in eukaryotic and prokaryotic cells with diverse functions. Interestingly, major pattern recognition receptors of the innate immune system such as Toll-like receptors (Bell *et al.*, 2003) or the recently described intracellular NOD-receptors (Inohara *et al.*, 2005) also harbor LRR-domains.

Nine homologous listerial proteins do not only possess a LRR-domain, but instead share a common fused core architecture (the internalin domain) that consists of a conserved N-terminal cap, a LRR domain, and an interrepeat (IR) domain structurally related to immunoglobulin-like domains (Schubert *et al.*, 2001; Schubert and Heinz, 2003). This LRR-subfamily consists of InlA, InlB, InlC, InlE, InlF, InlG, InlH, and the two recently identified proteins InlI and InlJ (Sabet *et al.*, 2005). Apart from the invasion proteins InlA and InlB, the other seven members are functionally less well characterized but at least InlC, InlE-H, and InlJ have been shown to contribute to listerial virulence (Dramsi *et al.*, 1997; Bergmann *et al.*, 2002; Sabet *et al.*, 2005).

1.2.2 Structural insights into the InlA / hEC1 recognition complex

The crystal structure of the complex of InlA and E-cadherin functional domains reveals atomic details of recognition (Schubert *et al.*, 2002). The internalin domain (Schubert *et al.*, 2001) of InlA includes an N-terminal α-helical cap domain (residues 36-78), a 15-repeat LRR-domain (residues 79-414) and a β-sandwich IR-domain. The LRR-domain creates an elongated yet curved, right-handed solenoid (Figure 1.2-1A).

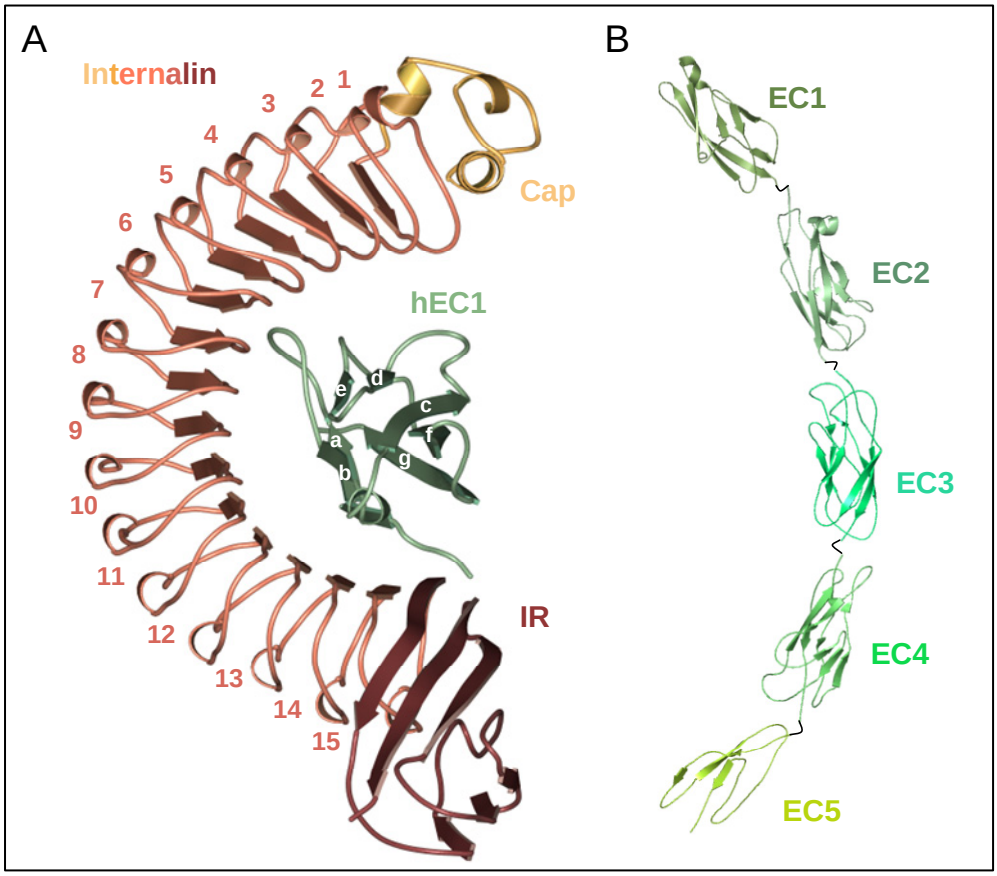

Figure 1.2-1: Structures of the InlA/hEC1 recognition complex and the E-cadherin ectodomain. (**A**) The internalin domain of InlA (Cap - orange, LRR – red, repeats are numbered, IR – dark red) is shown in complex with its receptor, the first extracellular domain of human E-cadherin (hEC1 - green, β-strands labeled). The LRR-domain is exclusively responsible for receptor binding (PDB code 1O6S; Schubert *et al.*, 2002) (**B**) Homology model of the entire ectodomain of E-cadherin based on the crystal structure of C-Cadherin (PDB entry 1L3W, Boggon *et al.*, 2002).

Compared to all other LRRs of InlA, repeat 6 is shorter by one residue and consists of 21 residues instead of the canonical 22. Conserved hydrophobic residues and an asparagine residue within the hydrophobic core of InlA at characteristic positions (xxLxLxxNxLxxLxxLxxLxxL; L = leucine, isoleucine, or valine; N = asparagine; x = undefined residue) stabilize the structure. All fifteen LRR β-strands and one β-strand of the

IR-domain combine to form a parallel β-sheet creating the concave receptor recognition face of the LRR-domain. The spatially larger 3_{10}-helices, stacked at the convex face, introduce the curvature of the LRR-domain. Additionally, each repeat is rotated by ~5° along the solenoid axis introducing an overall twist of the domain (Schubert *et al.*, 2002). The IR-domain, comprising residues 414-495, is the most flexible element of the internalin domain. Its fold is closely related to that of immunoglobulin (Ig) domains.

The IR-domain is followed by three spacer domains presumably to allow suitable presentation of InlA on the cell surface (Schubert *et al.*, 2002). The adjoining LPxTG motif is cleaved by sortase A, transferring membrane-bound InlA to the pentaglycine crossbridge of the cell-wall peptidoglycan (Ton-That *et al.*, 1999).

E-cadherin, the most abundant protein in epithelial-cell adherens junctions, is crucial in embryogenesis (Gumbiner, 2005) and in maintaining epithelial integrity (D'Souza-Schorey, 2005). It consists of five extracellular, Ig-like domains (EC1-5, Figure 1.2-1B), a transmembrane α-helix and an intracellular domain linked to the actin cytoskeleton through adaptor molecules such as α- and β-catenin (Gates and Peifer, 2005). The hEC1-domain is responsible for cell-cell contacts (Boggon *et al.*, 2002) and is also the receptor of InlA (Lecuit *et al.*, 1997; Lecuit *et al.*, 1999). It consist of seven β-strands that form two antiparallel β-sheets and a short α-helix within the **bc**-loop, connecting β-strands **b** and **c** (Figure 1.2-1A).

The crystal structure of the functional domain of InlA in complex with hEC1 revealed that InlA binds hEC1 through the concave face of its LRR-domain (Schubert *et al.*, 2002). Complex formation is Ca^{2+}-dependent but even in the presence of Ca^{2+} and despite a large interaction surface (Jones and Thornton, 1996) of 2400 $Å^2$, the binding affinity (K_D = 8 ± 4 μM) is rather weak. A comparatively low surface complementarity of both proteins allows numerous water molecules to be retained within the interaction interface restricting the number of direct contacts. Only two hydrophobic patches centered on Val3 and Pro16 of hEC1 interact tightly with corresponding regions of InlA. Hydrophilic interactions between both proteins involve only seven hydrogen bonds, three salt bridges, and eight water bridged interactions (Schubert *et al.*, 2002). Even the bridging Ca^{2+} is only directly coordinated by Glu326 of InlA. The other coordination sites are occupied by five water molecules, two of which interact with Asp29 of hEC1, creating the link between both proteins.

1.3 Bacterial invasion strategies

Pathogenic bacteria have essentially evolved two strategies to induce uptake into normally non-phagocytic eukaryotic host cells (Cossart and Sansonetti, 2004). The zipper-mechanism requires the close association of bacterial and eukaryotic cell. Specialized invasion proteins expressed on the surface of bacterial cells bind eukaryotic receptors predominantly involved in cell-cell adhesion. Examples include invasin-mediated entry of *Yersiniae* into epithelial cells by binding β_1-integrins (Isberg and Leong, 1990) and InlA-induced listerial invasion into target cells through its interaction with E-cadherin (Mengaud *et al.*, 1996). Binding of receptors leads to receptor-clustering and activation (Seveau *et al.*, 2004). The resulting signaling cascade activates mediator proteins that promote actin cytoskeleton rearrangement to form a phagocytic cup. Such mediators are FAK (focal adhesion kinase) in case of invasin-mediated entry of *Yersiniae* (Alrutz and Isberg, 1998), and α- and β-catenins in InlA induced invasion of *L. monocytogenes* (Lecuit *et al.*, 2000). Actin cytoskeletal rearrangements are essential for retraction and closure of the phagocytic cup creating the phagosome. A current model for InlA-induced uptake implicates two independent actin-remodeling processes: The first of these involves the α/β-catenin complex, associated with the intracellular domain of E-cadherin. It recruits formin-1 (Kobielak *et al.*, 2004), a major actin-nucleating factor involved in production of linear actin cables (Bershadsky, 2004). The second system involves the activation of the Arp2/3 complex, responsible for the generation of a branched actin network (Blanchoin *et al.*, 2000). Activation of Arp2/3 during listerial entry is mediated by clustered E-cadherin molecules that recruit cortactin (Helwani *et al.*, 2004) which in turn directly recruits and activates Arp2/3 (Weaver *et al.*, 2003). The synergistic action of both mechanisms is necessary to generate and maintain adherens junctions (Bershadsky, 2004) and is potentially involved in InlA-mediated entry of *L. monocytogenes* (Ireton, 2007). It has, furthermore, been shown that the motor protein myosin VIIa is a key-player in phagosomal cup closure (Kussel-Andermann *et al.*, 2000). Myosin VIIa has been proposed to move along actin-filaments creating the contractive force, required for bacterial internalization. Transition of this force to the phagosomal cup membrane is mediated by two other proteins, ARF6 and ARHGAP10 (Sousa *et al.*, 2005) that possibly link the myosin VIIa associated transmembrane protein vezatin to α-catenin and therefore to the InlA/E-cadherin recognition complex (Hamon *et al.*, 2006).

The second strategy of bacterial entry, called trigger-mechanism, does not require tight adhesion of bacterial and host cell, though physical contact is necessary. Effector molecules are directly injected into the host cell cytoplasm by type-three secretion systems (Galan and Wolf-Watz, 2006), evolved by pathogenic bacteria such as *Salmonellae* or *Shigellae* to redirect multiple cellular functions. Some of these effectors directly interact with the cellular machinery that regulates cytoskeleton dynamics inducing massive cytoskeletal rearrangements. Uptake of bacteria is indirectly caused by creation of large, dynamic membrane protrusions, called membrane ruffles (Cossart and Sansonetti, 2004), engulfing the bacterium.

The second listerial invasion protein InlB mediates uptake by a mechanism combining properties of both described bacterial uptake strategies. InlB is loosely attached to the outer leaflet of the cell-membrane through GW-repeats at the C-terminus (Braun *et al.*, 1997) and can act as soluble ligand or cell-membrane anchored protein (Ireton *et al.*, 1999). Membrane-bound InlB and its interaction with receptors on the surface of eukaryotic cells may promote tight adhesion leading to a “zipper”-like uptake, although the amount of Met would be limited due to tightly regulated expression in untransformed cells. A second complication of direct InlB/Met interaction is the accessibility of InlB which is largely buried within the peptidoglycan of the bacterial cell-wall and thus inaccessible for Met (Jonquieres *et al.*, 1999). Creating functional InlB involves either partial degradation of the peptidoglycan or release of InlB, initiated upon contact of *L. monocytogenes* with a host cell by host cell signals. Released InlB is able to activate its receptors, corresponding to direct triggering of uptake. The hepatocyte growth factor receptor Met (Bottaro *et al.*, 1991) becomes phosphorylated at two conserved tyrosine residues located within the intracellular part upon InlB-binding (Shen *et al.*, 2000). Recruitment of several adaptor proteins such as Gab1 (Basar *et al.*, 2005) leads to the activation of PI-3K (Ireton, 1996; Seveau *et al.*, 2007) and Arp2/3 (Bierne, 2001), induces actin cytoskeleton rearrangement resulting in membrane ruffling, and eventual bacterial uptake (Bierne *et al.*, 2005). Cellular signals that promote release of buried InlB upon adhesion of *L. monocytogenes* to host cells may involve the action of the other characterized receptors heparan sulphate and gC1qR. Both receptors have the potential to induce release of InlB from the bacterium producing non-buried, soluble InlB (Jonquieres *et al.*, 1999; Marino *et al.*, 2002), which is assumed to be the only functional form (Ireton, 2007). InlB-mediated membrane ruffling induces listerial uptake more efficiently than InlA-

induced “zippering”, possibly limiting the function of InlA to Met-free cells. Alternatively, a degree of synergy between both invasion proteins may exists.

1.4 Host specificity of *Listeria monocytogenes*

Pathogens have evolved a variety of virulence factors to manipulate different host cell functions. Recognition of host molecules, however, occurs predominantly at binding sites distinct from those of cellular interaction partners. During evolution only functionally important residues tend to be conserved, whereas other exposed side chains are variable and differ in homologous proteins of other species. Binding loosely conserved regions of host molecules consequently restricts the number of hosts accessible by a pathogen because of abrogated interactions of virulence factor with less conserved binding interfaces of host targets.

Studying human disease primarily requires all aspects of the disease to be mirrored in a suitable small animal model, preferentially in the mouse. This allows complex immunologic and pathophysiologic responses to be investigated. Because of host restriction, most human pathogens are non-pathogenic for mice or cause unrelated symptoms limiting the usefulness of mouse models to study human pathogens *in vivo* (Lecuit and Cossart, 2002). The identification of molecular details of host specificity has allowed mice to be humanized genetically, providing partial animal models for *Helicobacter pylori* (Guruge et al., 1998), measles virus (Patterson *et al.*, 2001), human coronavirus (Lassnig *et al.*, 2005), Group A streptococci (Sun *et al.*, 2004) and *L. monocytogenes* (Lecuit *et al.*, 2001).

L. monocytogenes is probably the best characterized and understood pathogen in terms of host tropism at macroscopic and microscopic levels and have been extensively analyzed in the past (Hamon *et al.*, 2006). InlA recognizes E-cadherin from guinea pig and rabbit but fails to bind the corresponding domain of murine E-cadherin (Lecuit *et al.*, 1999). InlB binds both murine and human Met-receptor but not that of guinea pig and rabbit (Khelef *et al.*, 2006). A small animal model that allows InlA and InlB mediated uptake and their interplay to be analyzed *in vivo* is thus not available.

For InlA a single amino acid substitution in E-cadherin has been proposed to be responsible for host specificity. Proline 16, located at the tip of loop **ab** in hEC1 (Figure 1.2-1A) is replaced by glutamate in murine E-cadherin, preventing recognition by InlA (Lecuit *et al.*, 1999). The crystal structure of the InlA/hEC1 recognition complex similarly identified proline

to be involved in a close interaction with a matching hydrophobic pocket of InlA (Schubert *et al.*, 2002). Substituting Pro16 by a glutamate would result in a sterically and electrostatically unfavorable interaction preventing recognition of murine E-cadherin.

Because InlB is functional in the mouse, a genetic approach has been used to adopt the mouse to the bacterium. Human E-cadherin c-DNA under the control of a tissue specific promoter and therefore exclusively expressed in intestinal enterocytes, was integrated into the mouse genome creating a humanized mouse model for orally acquired listeriosis. The model established the critical role of InlA-mediated uptake to overcome the intestinal barrier of mice (Lecuit *et al.*, 2001). Further studies (Khelef *et al.*, 2006) demonstrated InlA, not InlB, to be exclusively responsible for listerial uptake into intestinal epithelial cells *in vivo*. The tissue-specific restriction of human E-cadherin expression similarly limits the usefulness of this animal model. Studying the interplay of InlA and InlB in extra-intestinal tissues, and the function of InlA in breaching the placental and blood-brain barriers have not been possible so far (Lecuit and Cossart, 2002). Additionally, the co-expression of murine and human E-cadherin in enterocytes of transgenic mice inherently reduces the sensitivity of this model system.

A wide variety of applications would immediately be addressable were a more suitable mouse model available. Two new strategies to create such models have been announced in the past. The first involves the genomic exchange of crucial glutamate codon in murine E-cadherin by proline (Lecuit, 2005) to generate a transgenic mouse carrying only a single codon exchange in the entire genome. However, this model has not been published so far. The second strategy is based on co-expression of entire human E-cadherin in all murine E-cadherin expressing cells (Hamon *et al.*, 2006). This model is similarly not yet available.

The molecular reason why InlB specificity is confined to certain species still needs to be analyzed. Recently, the crystal structure of the recognition complex between functional domains of InlB and c-Met has been elucidated (Niemann *et al.*, 2007), providing atomic details of recognition necessary to analyze host specificity. The lack of genome sequences of animals, permissive for InlB mediated entry, however, currently prevents a detailed analysis.

1.5 Aim of the work

Initially, the biological consequence of the weak affinity of InlA for its natural receptor human E-cadherin was to be analyzed using a rational protein-engineering approach. A

detailed analysis of the crystal structure of the InlA/hEC1 recognition complex to postulate single amino acid substitutions in InlA that would potentially increase its binding affinity for hEC1 was to be undertaken. Anticipated structural changes were to be verified crystallographically and altered binding affinity for hEC1 determined biophysically using isothermal titration calorimetry (ITC). Single substitutions that succeed in increasing binding affinity for hEC1 were to be combined to achieve yet higher binding affinity. To reveal changes in invasion potential of this InlA-variants, transgenic listerial strains expressing these InlA-variants were to be created and analyzed using *in vitro* gentamicin infection assays with human E-cadherin expressing cell-lines. Improved affinity could potentially change the binding specificity of InlA, particularly as regards murine E-cadherin recognition. If the species barrier to infection could rationally be breached by creating an InlA-variant that recognizes murine E-cadherin, this would provide a versatile murine model for human listeriosis. Detailed biophysical and structural analyses of changes in the specificity of re-engineered InlA were to be performed.

2 Methods

All chemicals were purchased from the following companies, if not stated otherwise: Difco, Fluka, GE-Healthcare, Hampton Research, Invitrogen, Merck, Millipore, Qiagen, Riedel de Haen, Roche, Roth, Sigma-Aldrich and Stratagene. The quality standard was "*pro analysis*" (p.a.).

Molecular-biological methods used in this work are adapted from standard collections of methods and protocols (Sambrook and Russell, 2000; Coligan *et al.*, 2002; Ausubel *et al.*, 2007). These methods will not be explained in detail. Only variations of standard protocols have therefore been described below.

2.1 Protein production

2.1.1 Generation of InlA and E-Cadherin constructs

For structural and biophysical studies, functional fragments of InlA (residues 36-496) and E-cadherin (EC1, residues 1-105), were used. The corresponding constructs were cloned previously (Schubert *et al.*, 2002). Briefly, the internalin domain of *inlA* was amplified from genomic DNA of *L. monocytogenes* EGD-e serotype 1/2a (ATCC-number BAA-679) and cloned into pGEX-6P1 (Amersham) vector using restriction enzymes *Bam*HI and *Eco*RI. The first N-terminal domain of human E-cadherin was amplified from a human c-DNA library, cut with restriction enzymes *Bgl*II and *Eco*RI and cloned into the *Bam*HI/*Eco*RI-digested pGEX-6P1 vector.

Murine EC1 (mEC1, this work) was amplified from a c-DNA-library (German Resource Centre for Genome Research, clone ID IMAGp998A095392Q1) using primers 5'-GGAGGAAGATCTTGGGTCATCCCTCCCATCAG-3' (forward) and 5'-GAATTCTCAA-TCTGTCACTGTGATCACTATCTCCAT-3' (reverse). The PCR-fragment was cut with *Bgl*II and *Eco*RI and cloned into the *Bam*HI/*Eco*RI-digested pGEX-6P1 vector. The full insert was sequenced to verify the correctness of the nucleotide sequence.

Site directed mutations in *inlA*, *hEC1* or *mEC1* were introduced by QuikChange Mutagenesis according to the manufactures protocol (Stratagene) and verified by sequencing. Mutations and corresponding mutagenesis primers are summarized in Table 2.1-1.

Table 2.1-1: Primers used for mutagenesis reactions. Mutation sites are underlined and bold. Reverse primer-sequences are complementary with shown forward-primer sequences.

Protein	Mutation	Primer
InlA	S192N	5'-CTACAGCAATTA**AAC**TTTGGTAATC-3'
	G194S+S	5'-CAATTATCTTTT**AGTAGT**AATCAAGTGACA-3'
	S192N+G194S+S	5'-CAATTA**AAC**TTT**AGTAGT**AATCAAGTGACA-3'
	Y369A	5'-GCTTCAAAGATTATTTTTC**GCT**AATAACAAGGTAAG-3'
	Y369S	5'-GCTTCAAAGATTATTTTTC**TCG**AATAACAAGGTAAG-3'
hEC1	P16E	5'-CCCAGAAAATGAAAAAGGC**CCA**TTTCCTA-3'
	E64Q	5'-GGCTGAAGGTGACA**CAG**CCTCTGGATAGAGAA-3'
mEC1	E16P	5'- CCCCGAAAATGAAAAGGGT**CCA**TTCCCAA-3'
	Q64E	5'-GGCTGAAAGTGACA**AAG**CCTCTGGATAGAGAA-3'

2.1.2 Protein expression and purification

Using the pGEX-6P1 vector (ampicillin (Amp) resistance), genes are expressed as N-terminal GST-fusion proteins. Constructs containing sequences of *inlA*, *hEC1*, *mEC1* and corresponding variants (single or double mutants) were transformed into BL21-codon-plus cells (Invitrogen, chloramphenicol (Cm) resistance). Two liter cultures of plasmid-bearing bacteria were grown at 37°C and 180 rpm (Infors Af 110 incubator, Infors AG) in LB-Amp-Cm-medium, to yield an absorption of OD_{600} = 0.8. The incubation temperature was decreased to 20°C to slow protein production and gene expression was induced by adding IPTG (isopropyl βD-thiogalactopyranoside, end concentration 0.02 mM). Bacteria were shaken overnight, harvested by centrifugation at 6000 g for 10 min and resuspended in 50 ml PBS, containing protease inhibitor cocktail "Complete" (Roche) and 2 µl benzonase (4.2 U/µl, Merck). To isolate the cytosolic GST-fusion protein, bacteria were disrupted mechanically (high-pressure cell rupture system, IUL instruments) and centrifuged at 40000 g for one hour to remove insoluble material. The supernatant was incubated with glutathion-sepharose for at least one hour at 4°C. The sepharose was washed with ice-cold PBS using a glass-column with frit. The target-protein was cleaved from the resin-bound GST-tag using

PreScission™-Protease (GE Healthcare) at room-temperature overnight. The cleaved target protein was eluted from the resin and dialyzed against 10 mM Hepes buffer pH = 7.5.
All proteins were further purified by applying an anion-exchange chromatography using MonoQ-columns (Pharmacia) and a salt gradient from 0 to 250 mM NaCl. For hEC1, mEC1 and their mutants a size-exclusion chromatography (using a Superdex 75 16/60 column) was finally applied. All purification steps were monitored using SDS-PAGE. Proteins were finally dialyzed against 10 mM Hepes pH = 7.5 and concentrated by ultracentrifugation using Viva-spin-concentrators (Vivascience). Protein purity and homogeneity was analyzed using Maldi-TOF mass spectroscopy (Bruker) and dynamic light scattering (DynaPro 801, ProteinSolutions).

2.2 X-ray analysis

2.2.1 Co-crystallization of InlA-variants and receptors

Crystals were grown by vapor diffusion with 5 to 8 mg/ml of protein and a stoichiometric ratio of 1:1. For InlA-variant/hEC1 crystallization setups, the original InlA/hEC1 condition was used. Ingredient concentrations as well as buffer system and pH were optimized using 24 well plates. Table 2.2-1 summarizes different complexes and crystallization conditions that yielded crystals used for data collection and structure solution.
To crystallize the InlA$^{S192N\text{-}Y369S}$/mEC1 complex, commercially available screen solutions (Nextal) in 96-well plates were used to identify lead conditions. These were further optimized using 24-well plates (Table 2.2-1).

Table 2.2-1 : Crystallization conditions. Complexes and composition of reservoir solutions are listed.

Complex	Crystallization condition
InlA^{S192N}/hEC1	20 % PEG4000, 150 mM $CaCl_2$, 100 mM Tris pH 7.2, 100 mM Na acetate
InlA^{Y369A}/hEC1	20 % PEG4000, 100 mM $CaCl_2$, 100 mM Tris pH 7.2, 80 mM Na acetat
InlA$^{G194S+S}$/hEC1	23 % PEG4000, 50 mM $CaCl_2$, 100 mM MES/Tris pH 6.8, 100 mM Na acetat
InlA$^{S192N\text{-}G194S+S}$/hEC1	18 % PEG4000, 20 mM $CaCl_2$, 100 mM MES/Tris, pH 5.3, 100 mM Na acetat
InlA $^{G194S+S\text{-}Y369S}$/hEC1	17 % PEG4000, 20 mM $CaCl_2$, 100 mM MES/Tris, pH 5.8, 100 mM Na acetat
InlA$^{S192N\text{-}Y369S}$/hEC1	20 % PEG4000, 80 mM $CaCl_2$, 100 mM MES/Tris, pH 6.3, 70 mM Na acetat
InlA$^{S192N\text{-}Y369S}$/mEC1	20 % PEG6000, 100 mM Na citrate, pH 5.2, 500 mM LiCl

To reduce radiation damage during data collection crystals were frozen in liquid nitrogen. Ice formation was prevented by adding 18-25 % PEG400 (v/v), depending on the precipitant concentration of the mother liquor, to the reservoir solution. Crystals were transferred to this cryosolution, retrieved quickly, and plunged into liquid nitrogen. Crystals were mounted onto the goniometer using cap tubes filled with liquid nitrogen or a pre-cooled cryo-tong and maintained at 100 K throughout the data collection using a nitrogen stream.

2.2.2 Data collection, structure determination and refinement

Data were collected using synchrotron radiation and MARCCD detectors (Marresearch, Germany) at beamlines listed in Table 2.2-2. Indexing of reflections, integration and scaling was performed using XDS (Kabsch, 1988) and HKL (Otwinowski and Minor, 1997). For further data processing the CCP4 suite was used (CCP4 (Collaborative Computational Project 4), 1994). The structure was solved by molecular replacement using EPMR (Kissinger *et al.*, 1999) and Phaser (Storoni *et al.*, 2004). The structure of InlA/hEC1 was used as a search model giving first phase-estimates. Restrained refinement was performed using REFMAC5 (Murshudov *et al.*, 1997). After initial refinement cycles, water molecules were automatically identified and added to the model using ARP/wARP (Lamzin and Wilson, 1993). TLS-protocols were included to allows domain movements to be refined. The structural model was built, analyzed and validated using COOT (Emsley and Cowtan, 2004) and WHATIF (Vriend, 1990). Figures were prepared using PYMOL (www.pymol.org).

Table 2.2-2: Data collection. Wavelengths used for data collection are given in Å. Macromolecular Crystallography Beamlines at DESY are operated by the EMBL outstation Hamburg.

Complex	Synchrotron	Beamline	Wavelength
$InlA^{S192N}$/hEC1	DESY (Hamburg)	BW 6	1.05
$InlA^{Y369A}$/hEC1	DESY (Hamburg)	BW 6	1.05
$InlA^{G194S+S}$/hEC1	DESY (Hamburg)	X13	0.8
$InlA^{S192N-G194S+S}$/hEC1	DESY (Hamburg)	X11	0.8
$InlA^{G194S+S-Y369S}$/hEC1	DESY (Hamburg)	X11	0.8
$InlA^{S192N-Y369S}$/hEC1	BESSY (Berlin)	BL-1	0.95
$InlA^{S192N-Y369S}$/mEC1	BESSY (Berlin)	BL-1	0.95

2.3 Isothermal titration calorimetry

Isothermal titration calorimetry (ITC) may be used to quantify the change in heat (binding enthalpy) during complex formation of two molecules (Leavitt and Freire, 2001). For this purpose, small aliquots of one interaction partner are added to a solution containing the second partner. The heat released or absorbed upon complex formation in the sample cell is determined by quantifying the energy required to restore the temperature in the sample cell to that of a buffer-filled reference cell (isothermal). Technically, reference and sample cell are placed within an adiabatic jacket maintained at temperature T. Both cells are constantly warmed to maintain a temperature above T (e.g. T + 5 K). A feedback mechanism controls the temperature difference between both cells which should be zero. If heat is released during a titration step (e.g. because complex formation by the proteins is exothermic), the sample cell requires less heating than the reference cell to maintain identical temperatures in both cells. The recorded signal, proportional to the heat added to the sample cell, accordingly initially decreases but recovers after the binding equilibrium has been reached. This creates a downward peak, the integration of which is directly proportional to the change of heat. Plotting the changes in heat of successive titration steps against the stoichiometric ratio of both interaction partners results in a sigmoid curve, which allows binding enthalpy, binding stoichiometry, and binding affinity to be determined (Jelesarov and Bosshard, 1999).

2.3.1 Sample preparation

To reduce measuring artifacts, all protein samples were extensively dialyzed against the same buffer. A portion of the dialysis buffer was filtrated and degassed. Both protein solutions were sterile filtered and also degassed to avoid air bubble formation during titration, which would severely disturb the measurement. Concentrations of protein solutions used in the experiment depend on the dissociation constant (K_D). Useable titration curves could be obtained if $[EC1] = N \cdot K_D \cdot c$, where [EC1] is the estimated concentration of mEC1, hEC1 or their mutants, N is the stoichiometric ratio (in this case equal to one), K_D is the estimated dissociation constant and c is a dimensionless parameter (Cooper, 1999). The value of c is critical as it describes how the titration curve shape depends on the protein concentration (Perozzo *et al.*, 2004). Values for c between 20 and 1000 resulted in suitable experimental data. To achieve saturation during titration, the molar amount of the added component (InlA)

must exceed that of the component in the measuring cell (EC1) by a factor of two. The precise K_D is, of course, initially not known. An iterative set of measurements was therefore necessary to determine the correct concentration range to reliably identify K_D and the binding enthalpy (ΔH).

2.3.2 Experimental setup

Thermodynamic data were obtained using an MCS ITC (MicroCal, USA). Cells and syringe were rinsed with buffer and buffer was filled into the reference cell. The E-cadherin solution (hEC1, mEC1 and their variants) was filled into the measuring cell and the corresponding InlA(variant) solution into the syringe. Two syringes with injection volumes of 100 and 250 µl were used. All titrations were performed at 20°C, 400 rpm (syringe rotation to mix both components quickly), and 250 s duration between injections. Aliquots of 5 -15 µl of ligand were consecutively injected into the measuring cell.

2.3.3 Data evaluation

Data were analyzed using the Micro Cal Origin 2.9 software. All peaks were integrated to determine the amount of heat evolved on addition of ligand. Provided the titration curve was sigmoidal, four distinct parameters could be determined independently. The first titration heats (initial plateau of the curve) correspond to the apparent enthalpy (H_{app}), or the sum of the binding enthalpy (H) and the enthalpy of dilution (H_{dil}). The second plateau obtained after saturation has occurred allows H_{dil} to be determined. The sigmoid transition between both plateaus is used to determine the K_D, and the inflection point to determine the relative stoichiometry of the complex.

Data were analyzed using the single set of independent sites model. Because both, H and K_D are determined independently, the binding entropy (S) may be calculated using the Gibbs-Helmholtz equation.

2.4 Generation of transgenic *L. monocytogenes* strains

2.4.1 Cloning strategy to create pPL2 and pAUL-A integration vectors

The cloning strategy is schematically summarized in Figure 2.4-1. Full-length *inlA* was amplified from genomic DNA using the primers 5'-AGGAGGGATCCATGGTCGGAC-CAACGAGCCAACCGTG-3' and 5'-AGGAGGCGGCCGCTGCTTGATTGGCGTTGGCA-CGGTG-3' and cloned into the vector pPL2 (Lauer *et al.*, 2002) using *BamH*I and *Not*I (Figure 2.4-1A). The site specific shuttle integration vector pPL2, based on the listeriophage PSA, can be replicated by Gram-positive and Gram-negative bacterial strains. This allows construction in *E. coli* (TG2, Stratagene) and later integration into the listerial genome within the PSA-attachment site (encoding the $tRNA^{Arg}$-gene).

The desired mutations were incorporated by excising a 1026-nucleotide *Bcl*I-*Bsa*I fragment from pPL2 and replacing this with an equivalent fragment from a pGEX-6P-1 expression vector containing the mutation (Figure 2.4-1B). Two different constructs were created by integrating different mutations into the pPL2-*inlA* vector. This allows the effect of improved affinity of InlA-variants for hEC1 on invasion efficiency of *L. monocytogenes* to be analyzed. Only the variant, carrying the mutations S192N and Y369S, was used to construct the pAUL-A integration vector to generate the isogenic mutant strain of *L. monocytogenes* as follows: A fragment, comprising the 3'-part of *inlA* and the 5'-part of *inlB* was amplified using primers 5'-AGGAGGGATCCAACCGTGACGCAGCCACTTAAGGC-3' and 5'-AGGAGCAAGTC-CTGCTAATGCTCTTAAATCGC-3'. Digesting this with *BamH*I and *Xba*I allows its ligation into the *BamH*I/*Nhe*I-digested pETM11-*gfp*-fusion vector (Figure 2.4-1C).

The mutated 5'-part of *inlA* from pPL2-$inlA^{S192N-Y369S}$ (= $inlA^{m}$) was cloned into vector 'pETM11-$inlA^{3'}$-$inlB^{5'}$-*gfp* fusion' using restriction enzymes *BamH*I and *Afl*II. The resulting plasmid bears full-length, mutated $inlA^{m}$ while the 5'-*inlB* fragment is fused to *gfp* (Figure 2.4-1D).

The $inlA^{m}$-$inlB^{5'}$-*gfp* fragment was excised from 'pETM11-$inlA^{m}$-$inlB^{5'}$-*gfp* fusion' by digesting with *Not*I, filling in by Klenow polymerase and dNTP (NEB), heat inactivation and cutting with *BamH*I. The fragment was cloned into the pAUL-A shuttle vector (Chakraborty *et al.*, 1992) cut with *Hind*III, filled in using Klenow polymerase an dNTP's, heat inactivated and digested with *BamH*I (Figure 2.4-1E). All cloning steps were monitored by PCR-analysis and sequencing.

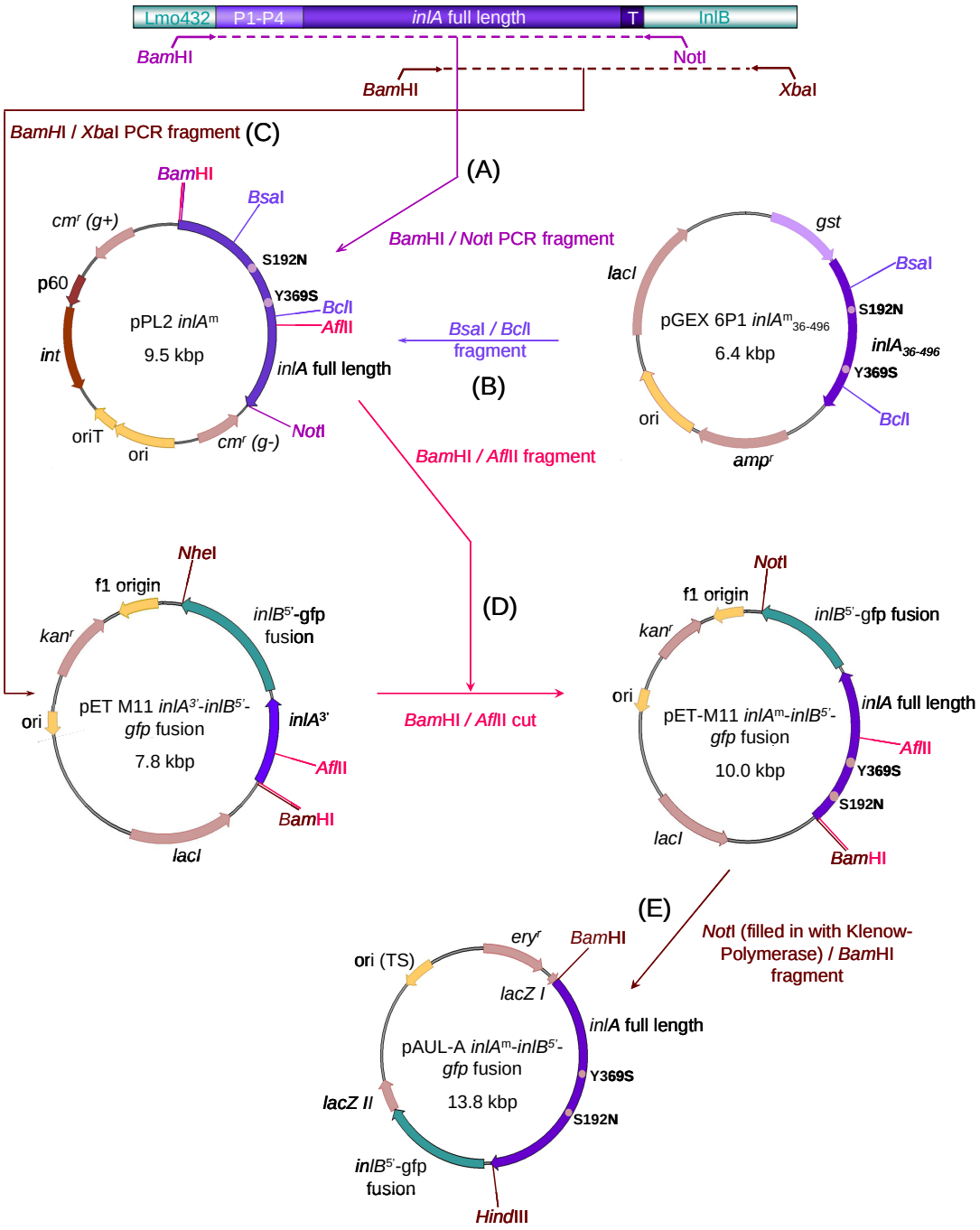

Figure 2.4-1: Cloning strategy to create the isogenic listerial mutant strain Lmo-InlA^{m}. (**A**) PCR from genomic DNA (top, P1-P4 are *inlA* promotors 1 to 4, T = termination site) using primers with *Bam*HI and *Not*I restriction sites (magenta) yields full length *inlA*, which was cloned into the pPL2 vector. (**B**) By cloning the *Bcl*I/*Bsa*I (blue) fragment of the pGEX-6P1 expression vector into the pPL2-*inlA* vector both *inlA*-mutations were introduced (yielding *inlA*^{m}). (**C**) A second PCR form genomic DNA using primers with *Bam*HI and *Xba*I restriction sites (brown) yields an *inlA*$^{3'}$-*inlB*$^{5'}$ fragment that was cloned into the pET M11 *gfp* fusion vector. (**D**) The 5'-part of *inlA*^{m} (*Bam*HI/*Afl*II fragment, red) was excised from pPL2-*inlA*^{m} and cloned into pET M11 *inlA*$^{3'}$-*inlB*$^{5'}$-*gfp* fusion vector to create pET M11 *inlA*^{m}-*inlB*$^{5'}$-*gfp* fusion, bearing full length *inlA*^{m} and the 5'-part of *inlB* fused to *gfp*. (**E**) This fragment was cloned into the final pAUL-A integration vector yielding pAUL-A *inlA*^{m}-*inlB*$^{5'}$-*gfp* fusion. cm^{r} = chloramphenicol resistance (g+, g- = Gram-positive/negative); *int* = integrase, ori(T) = origin of replication (of transfer); ori(TS) = temperature sensitive origin of replication; amp^{r} / kan^{r} / ery^{r}= ampicillin/kanamycin/erythromycin resistance, *lac*I = lac repressor gene, *lac*Z = β-galactosidase gene (interrupted by *inlA*-*inlB*-*gfp*).

2.4.2 Generation of pPL2-*inlAB* constructs

Additional pPL2 constructs were cloned that contain not only the full-length *inlA* gene but the entire *inlAB* locus. A fragment containing *inlA*$^{3'}$ and full length *inlB* was amplified from genomic DNA using primers 5'-CGGAGCCACTTAAGGCAATTTTTAATGTTAAGT-3' and 5'-AGGAGGCGGCCGCCGCATAAACAGTGCTTTTCACGCGG-3', cut with *Not*I and *Afl*II and cloned into *Afl*II/*Not*I cut vectors pPL2-*inlA*, pPL2-*inlA*^{Y369A}, and pPL2-*inlA*^{m}.

2.4.3 Generation of competent listerial cells

Transformation of integration vectors into the *L. monocytogenes* EGD-e knockout strain Δ*inlA2* or Δ*inlAB2* (Lingnau *et al.*, 1995) requires competent listerial cells to be generated. Both strains were grown in brain heart infusion (BHI, Difco) broth supplemented with 0.5 M sucrose at 37°C and 180 rpm until an OD_{600} of 0.2 was reached. Penicillin G (10 µg/ml) was added to suppress bacterial cell wall synthesis. After growing for 2 h, bacterial protoplasts were harvested by centrifuging 20 min at 3000 x g. Protoplasts were washed four times with decreasing volumes of ice-cold 1 mM Hepes pH 7.0 supplemented with 0.5 M sucrose (Park and Stewart, 1990). Glycerin (15% v/v) was added and aliquots were stored at -70°C.

2.4.4 pAUL-A *inlA*^{m}-*inlB*$^{5'}$-*gfp* integration and homologous recombination

Vectors (1 µg DNA) were transformed into *L. monocytogenes* Δ*inlA*2 protoplasts (40 µl) by electroporation. Positive transformants were selected by growth onto BHI-Ery agar plates at the permissive temperature of 30°C overnight. A positive clone was streaked out onto BHI-Ery agar plates and incubated at 42°C overnight (no extra-chromosomal replication of the plasmid in Gram-positive bacteria). Clones were purified by re-streaking onto BHI-Ery agar plates and further inoculation at 42°C. Integration and contamination with extra-chromosomal vector were monitored by PCR-analysis. Site-directed integration of the vector into the genome of *L. monocytogenes* Δ*inlA*2 requires homologous genomic sequences. The vector can therefore either integrate using the *inlA*$^{5'}$ or the *inlB*$^{5'}$ genomic sequences (Figure 2.4-2).
To facilitate vector reversion by homologous recombination, a single pure colony was inoculated into BHI medium and grown without selection pressure at 25°C overnight. 10 µl of the overnight culture were inoculated into 50 ml fresh BHI medium and grown overnight.

This procedure was repeated three times. Dilutions were plated out onto BHI-agar plates without Ery and grown overnight. A colony-lift was performed to transfer clones onto BHI-Ery agar plates. After growth overnight comparison with the original plate identified Ery-sensitive clones, which have lost their Ery-resistance through homologous recombination. Two different types of reversion in either case of integration were theoretically possible. In the first, the vector reverts as it had integrated, yielding unchanged *L. monocytogenes* Δ*inlA*2 (blue lines in Figure 2.4-2). In the second, the anticipated clone carrying *inlA*^{m} in an otherwise unmodified genome is created (red lines in Figure 2.4-2). Colony PCR of Ery-sensitive clones were performed to identify positive revertants carrying the *inlA*^{m} gene (primers are described in Table 2.4-1). The entire *inlA*^{m}-*inlB* locus of one positive clone (clone 22) was amplified using colony PCR and the PCR-fragment was purified and fully sequenced to ensure that no point-mutations except S192N and Y369S were present. Western blot of TCA-precipitated cell-wall extracts and culture-supernatants were performed to analyze expression of InlA and InlB. Antibodies were derived from hybridoma-cell supernatants (provided by Prof. Dr. Jürgen Wehland, Division of Cell and Immune Biology, Helmholtz-Centre for Infection Research, Braunschweig, Germany).

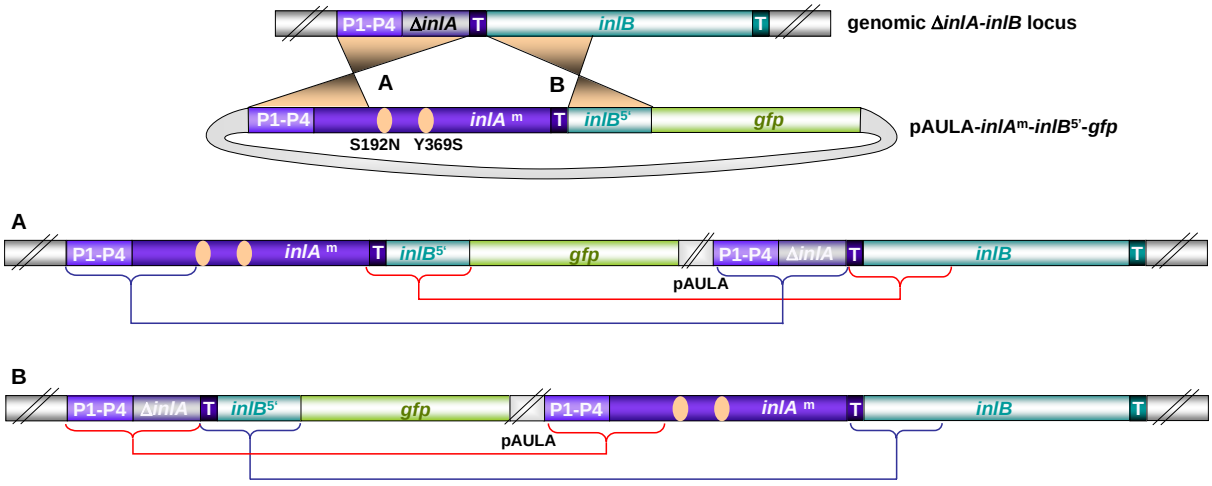

Figure 2.4-2: Integration and reversion of pAUL-A-*inlA*^{m}-*inlB*$^{5'}$-*gfp* by homologous recombination. The vector integrates into the genome (top) using homologous sequences either with Δ*inlA* (**A**) or with the 5' region of *inlB* (**B**). Reversion also requires homologous sequences. (**A**) Vector reversion through *inlB*-homology (red lines) yields the desired product (genomic *inlA*^{m}), whereas reversion via *inlA*-homology (blue lines) gives Lmo-Δ*inlA*. (**B**) Reversion via *inlA* or *inlB* homology yields the anticipated product (red) or the original strain (blue), respectively.

2.4.5 pPL2 integration

The vectors pPL2-*inlA*, pPL2-*inlA*^{Y369A}, and pPL2-*inlA*^{m} were transformed into *L. monocytogenes* Δ*inlA*2 and vectors pPL2-*inlAB*, pPL2-*inlA*^{Y369A}*inlB*, and pPL2-*inlA*^{m}*inlB* in *L. monocytogenes* Δ*inlAB*2 as described (see above) and plated onto BHI-Cm agar plates. Colonies were grown overnight at the permissive temperature of 28°C. On the next day the temperature was shifted to 37°C where no extra-chromosomal replication occurs and plates were incubated for a further 3 days. Clones were inoculated into BHI-Cm medium and grown overnight at 37°C. Integration was verified by colony-PCR (for primer details see Table 2.4-1).

Table 2.4-1: Primers for PCR-based identification of integration and reversion of pAUL-A or pPL2. Primer hybridization sites are indicated (Target), f = forward primer, r = reverse primer. int = PSA integrase gene, tRNA^{Arg} = PSA attachment site within the tRNA^{Arg}-gene.

Identification	Target	Name	f/r	Sequence
Integration of pAUL-A	*inlA*	*inlA*$^{3'}$	f	5'-GTGGAACCGTGACGCAGCCA-3'
Integration of pAUL-A	*gfp*	*gfp*	r	5'-TTTGTAGAGCTCATCCATGCCA-3'
Integration of pAUL-A	*inlB*	*inlB*$^{3'}$	r	5'-CGCGGGAATGCAGGCATCTAC-3'
Reversion of pAUL-A	*inlA*	*inlA*$^{3'}$	f	5'-CGGCTCCGTAGACAGATTAGC-3'
Reversion of pAUL-A	*inlB*	*inlB*$^{3'}$	r	5'- CGCGGGAATGCAGGCATCTAC- 3'
Integration of pPL2	*tRNA*^{Arg}	PL 102	f	5'-TAACAGACCTAACCCAAACCTTCC-3'
Integration of pPL2	*int*	PL 95	r	5'-CAACATAATCAGTCCAAAGTAGATGC-3'
Integration of pPL2	*tRNA*^{Arg}	PL 103	r	5'-AATCGCAAAATAAAAATCTTCTCG-3'

2.4.6 Protein preparations for Western-blot analysis

Expression levels of InlA and InlB in complemented listerial strains were analyzed and compared with natural expression levels of unmodified bacteria. InlA functions mainly as cell wall associated protein, whereas InlB presumably acts in solution. Therefore proteins of cell-wall and culture-supernatant were independently analyzed.

An overnight culture of *L. monocytogenes* was inoculated into 50 ml fresh BHI-medium and grown at 37°C and 180 rpm until an OD = 1.0 was reached. The culture was centrifuged (30 min and 3500 x g) and the supernatant was transferred into a fresh 50 ml tube. 4.5 ml of 100 % (w/v) trichloroacetic acid (TCA) and 4 ml desoxycholate (1 mg/ml) were added. The mixture was incubated overnight at 4°C and centrifuged at 5500 g for 1 h. The supernatant

was removed and precipitated proteins were washed with 2 ml acetone, air dried, resuspended in 200 µl SDS-buffer and adjusted to neutral pH by adding 1 M Tris-HCl pH 8.0. To extract cell-wall associated proteins from bacterial cells the cell-pellet of the centrifuged 50 ml culture was resuspended in 1.4 ml PBS supplemented with 2% SDS and incubated at 37°C and 300 rpm for 1 h. Bacteria were sedimented by centrifugation (13000 g, 15 min) and the supernatant containing cell-wall associated proteins was transferred into a fresh 2 ml tube. 140 µl of 100 % (w/v) TCA and 140 µl of desoxycholate (1 mg/ml) were added. To precipitate proteins efficiently the mixture was incubated overnight at 4°C. Precipitated proteins were centrifuged (13000 g, 30 min), washed with 1 ml acetone, air dried, resuspended in 100 µl SDS-buffer and adjusted to neutral pH by adding 1 M Tris-HCl pH 8.0. Samples were analyzed on 10 % SDS-polyacrylamide gels. InlA and InlB were stained with monoclonal antibodies. Coomassie-stained gels served as loading control (total protein amount applied to the gel).

2.5 Adhesion and invasion assays

To enhance readability, the wild-type *Listeria monocytogenes EGD* serotype 1/2a (ATCC-number BAA-679) strain will henceforth be referred to as Lmo-EGD and its isogenic mutant strain (carrying the *inlA*^{m} gene) as Lmo-InlA^{m}.

Uptake of Lmo-EGD and Lmo-InlA^{m} were analyzed using the human colorectal epithelial cell line Caco2 (ATCC HTB-37) and the murine macrophage-like cell line J-774 (ATCC TIB-67). Caco2 cells were cultured in minimal essential medium (MEM) with Earle's salts (Invitrogen, Germany), supplemented with 20% FCS (PAA Laboratories, Austria), 2 mM glutamine, 1mM sodium pyruvate and 1% nonessential amino acids at 37°C / 7% CO_2. J774 cells were cultured in Dulbecco's modified Eagle's medium (DMEM, Invitrogen) supplemented with 10% FCS (PAA Laboratories, Austria) and 2 mM glutamine at 37°C / 7% CO_2. Two days prior to infection, $2 \bullet 10^6$ Caco2 cells or $2 \bullet 10^5$ J774 cells were seeded into 24-well plates. An overnight culture of *L. monocytogenes* was diluted 1:50 in BHI medium (Difco) and grown at 37°C till mid-log-phase. Bacteria were washed twice in medium without FCS and $8 \bullet 10^6$ (Caco2) or $2 \bullet 10^5$ (J774) bacteria were added to the monolayer (Caco2) or semiconfluent cells (J774) per well, centrifuged 5 min at 500 g and incubated for one hour. Cells were washed with PBS. Medium containing 100 µg/ml gentamicin was added to kill extracellular bacteria. After 1, 2, 3 and 4 h cells were washed with PBS and lysed using sterile water with 0.2%

Triton X-100. Serial dilutions of cell lysates were plated onto BHI agar plates and incubated 24 h at 37°C. Colonies were counted and the recovery per well determined. Each data point of one experiment was determined three times and experiments were independently repeated in triplicate.

Adhesion assays were performed like invasion assays without centrifugation after addition of bacteria to Caco2 cells. 30 min after infection cells were washed 5-fold with PBS and lysed with 0.2% Triton X-100. Bacterial numbers were determined as described.

2.5.1 Immunofluorescent staining of infected Caco-2 cells

Invasion assay were performed as described, but cells were seeded onto cover-slips 1 day prior to infection. After incubating cells with gentamicin, 4% paraformaldehyde in PBS was added for 30 min to fix cells. Cover-slips were washed with PBS, incubated in 0.2% Triton X-100 + PBS for 1 min to permeabilize cells and washed in PBS. Staining was performed with antibody-solutions (250 µg/ml) supplemented with 5% horse serum (PAA, Pasching) and 1% BSA in PBS for 1 h. Cover-slips were washed and incubated with secondary antibodies or phalloidin, labeled with fluorescence-dyes, for a further hour. After washing in PBS, cover-slips were embedded in moviol, containing 4% n-propyl gallate as bleaching protectant. E-cadherin and β-catenin monoclonal antibodies were purchased from BD-Transduction laboratories (No. 610182 and 610154, respectively). Fluorescent-dye labeled secondary antibodies (goat anti rabbit and anti mouse conjugates) and phalloidin were purchased from Molecular Probes. Images were acquired using an inverted microscope (Axiovert 135TV, Zeiss) equipped for epifluorescence microscopy, using 100 x / NA 1.4 plan-apochromatic objectives. Tungsten lamps were used for both transmitted and epi-illumination. Data were acquired using a back-illuminated, cooled charge-coupled-device camera (Princeton Research Instruments, New Jersey) driven by IPLab software (Scanalytics, Massachusetts) and with computer-controlled shutters (Optilas GmbH, Puchheim, Germany) in the transmitted and epi-fluorescence light paths to minimize radiation damage to the cells. Data were analyzed on a Power Macintosh G3 using IPLab and Adobe Photoshop 5.0 software.

2.6 Mouse infection experiments

All mouse experiments were performed in cooperation with Dr. Bastian Pasche and Dr. Andreas Lengeling in the Infection Genetics group, Department of Experimental Mouse Genetics, at the Helmholtz-Centre for Infection Research, Braunschweig, Germany. Experiments are presented and discussed in this work as they are constitute an integral part of the thesis.

Ten weeks old female C57BL/6J mice were purchased from Harlan-Winkelmann (Borchen, Germany) and housed for a further week in the specific pathogen-free (SPF) animal facility (Helmholtz Centre for Infection Research) prior to infection.

2.6.1 Oral infection

Lmo-EGD and Lmo-InlA^{m} were grown in BHI broth (BD-Difco, Heidelberg) until the end-log growth phase. After washing, bacteria were diluted in PBS. 0.2 ml of the desired inoculum of either strain were mixed with 0.3 ml PBS containing 50 mg $CaCO_3$ (Lecuit *et al.*, 2001). The suspension was inoculated intragastrically into mice starved overnight (water allowed) using a 21 gauge feeding needle attached to a 1 ml syringe. Animals were then either monitored daily to determine survival rates or sacrificed and dissected for histological analysis or to determine bacterial counts in organs at the time points indicated. All animal experiments were reviewed and approved by local authorities.

2.6.2 Intravenous infection

To infect C57BL/6J mice intravenously, the desired inoculum of Lmo-EGD or Lmo-InlA^{m} were diluted in 0.2 ml PBS and injected into the lateral tail vein (Pasche *et al.*, 2005). Survival rates and organ loads were determined as described for oral infections.

2.6.3 Infection of pregnant mice

BALB/c mice were purchased from Harlan-Winkelmann (Borchen, Germany). Couplings were carried out with 10-week-old BALB/c female mice. Mating was assessed by the appearance of a vaginal plug, denoting the first embryonic day of pregnancy. Pregnant mice were infected intragastrically or intravenously on day of gestation (E)13.5 or E14.5 as

described above. Animals were examined daily. At indicated time points after infection, mice were sacrificed and the abdominal cavity opened aseptically. Each placenta and fetus was independently dissected and analyzed by cfu determination or histopathology.

2.6.4 Bacterial counts in organs, placentae and embryos

Stomach and small intestine were removed and incubated for 2 h at 20°C in PBS supplemented with 100 µg/ml gentamicin (Gibco) to kill extracellular bacteria; other organs and embryos were sterilely dissected. Organs and embryos were homogenized and serial dilutions plated onto BHI-agar allowing a determination of bacterial counts per mg organ or per embryo.

2.6.5 Statistical analysis

Survival curves were statistically evaluated by Kaplan-Meier and Logrank (Mantel-Cox) analyses. Bacterial loads are listed as median ± 95% confidence intervals, statistically evaluated by the Mann-Whitney-U non-parametric test. Calculations were done using GraphPadPrism4 (GraphPad Software Inc., San Diego, USA). Differences were considered significant for P 0.05.

2.6.6 Histology and immunohistochemistry

Histological and immunohistochemical analysis was performed in cooperation with Prof. Dr. Achim Gruber, Department of Veterinary Pathology, Free University of Berlin.
Organs were fixed in 10% formalin, dehydrated and embedded in paraffin. 5 µm sections were cut and stained with hematoxylin-eosin or used for immunohistochemistry (IHC). For detection of *L. monocytogenes Listeria* O antiserum (Serotype 1 and 4; BD-Difco, Heidelberg) was used. For detection a secondary, peroxidase-coupled goat-anti-rabbit antibody was used. IHC sections were counterstained with hematoxylin.

3 Results

Human pandemics overwhelmingly result from mammalian or other animal pathogens suddenly adapting to humans. The molecular details underlying such changes in host specificity have been identified for a few cases including SARS and avian influenza. The mere documentation of molecular changes does, however, not fully illuminate the underlying processes nor the degree of change required in more complex systems such as bacterial pathogens to initiate a change in host tropism.

We have undertaken to investigate the concept of host tropism by identifying the minimal change required to modify the host range of the food-borne human pathogen *Listeria monocytogenes* to include the mouse. Using the crystal structure of the virulence factor InlA in complex with its human receptor E-cadherin (Schubert *et al.*, 2002), we infer novel amino acid substitutions in InlA that potentially increase its binding affinity for the human receptor E-cadherin. We confirm the anticipated effects at the molecular level by solving the high resolution crystal structures of InlA-variant/hEC1 complexes. The binding affinities of InlA-variants for hEC1 were determined using ITC. A combination of two substitutions, introduced into InlA, increases the affinity for hEC1 by three orders of magnitude and extends the binding specificity to include previously incompatible mEC1. The newly created interaction of reengineered $InlA^m$ and mEC1 was analyzed structurally by solving the high resolution crystal complex structure as well as biophysically using ITC. By introducing these two mutations into the genome of Lmo-EGD the isogenic mutant strain Lmo-$InlA^m$ has been created and was analyzed for its invasion potential into human cells *in vitro*. Altered host tropism of Lmo-$InlA^m$ was analyzed using mouse infection experiments including survival experiments, determination of organ loads after oral and intravenous infection as well as histological and immunohistochemical analyses of infected organs.

3.1 Rationale for individual point mutations

The crystal structure of the InlA/hEC1 recognition complex combined with biophysical analysis using analytical ultracentrifugation (Schubert *et al.*, 2002) revealed important information on the interaction interface, binding affinity, atomic details of direct or water mediated contacts, and their contribution to complex formation. Despite the large interaction interface the binding affinity is rather weak (K_D = 8 ± 4 µM) and depends on the presence of Ca^{2+} (K_D = 50 ± 30 µM in Ca^{2+}-free buffer, Schubert *et al.*, 2002). Whereas structural and biophysical data consistently explain this result, the question of biological relevance of the weak affinity remains. To solve this question, the binding affinity of InlA was to be increased. Protein-protein interactions have previously been modified using several techniques. Computer-based methods, for example, calculate sophisticated force-fields to identify amino acid substitutions that increase binding affinity or change binding specificity (Kortemme and Baker, 2004). Random approaches creating large libraries of protein variants, often by error-prone PCR, have been used to alter protein properties (Hoess, 2001) including their target recognition potential. In this work, rational protein interface design has been used to identify regions of low surface complementarity of InlA and hEC1. Mutations in InlA that would potentially increase the binding affinity by increasing surface complementarity have been proposed and introduced into InlA.

3.1.1 InlA Tyr369Ala (Y369A)

In uncomplexed InlA, the aromatic side chain of Tyr369 forms a well-ordered stacking interaction with Tyr347 (Figure 3.1-1). In the complex InlA/hEC1, the position of Ty369 is occupied by Asn27 of hEC1. As a result, Tyr369 adopts two alternate side chain conformations. The first is similar to that of free InlA resulting in an unfavorably close contact between $Tyr369_{InlA}$ and Asn27 of hEC1. In the second, $Tyr369_{InlA}$ swings away around the χ_1-angle, abrogating the stacking interaction to $Tyr347_{InlA}$, and displaces $Asn370_{InlA}$ and $His392_{InlA}$ from a similar stacking interaction with $Phe348_{InlA}$. By replacing Tyr369 by alanine, the need for both of these alternate conformations would be eliminated.

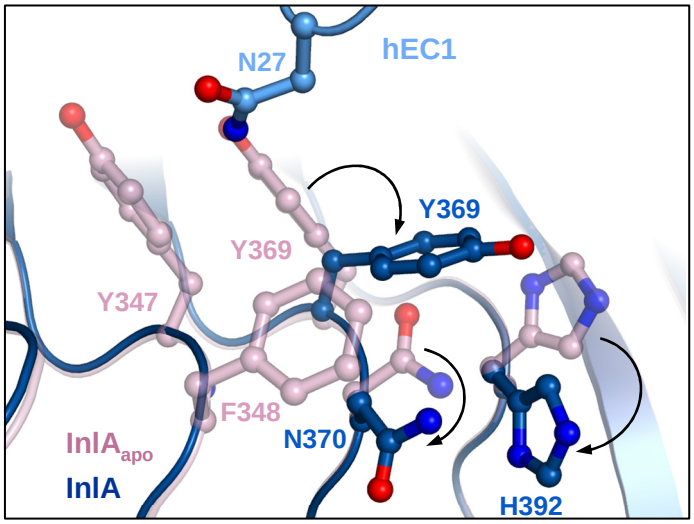

Figure 3.1-1: Tyr369$_{InlA}$-induced side chain rearrangements during complex formation. Superposition of uncomplexed InlA (pink) and InlA/hEC1 (blue). On complex formation Ans27$_{hEC1}$ (light blue, top) causes Tyr369$_{InlA}$ (pink) to flip to an alternative, less favorable conformation (dark blue), displacing Asn370 and His392 from their stacking interaction with Phe348 (black arrows).

3.1.2 InlA Tyr369Ser (Y369S)

While an alanine at position 369 eliminates the two conformations of Tyr369 (above), its small size and the lack of hydrogen bonding donors or acceptors presumably prevent direct interactions to hEC1. By placing a small hydrophilic amino acid such as serine at this position, direct or water-mediated hydrogen bonds to hEC1 should be possible.

3.1.3 InlA Ser192Asn (S192N)

Ser192 of InlA adopts two equally occupied conformations, both of which hydrogen bond a water molecule that itself bridges InlA and hEC1 in the complex (Figure 3.1-2). Such a water-mediated hydrogen bond is presumably less stable than a direct hydrogen bond between proteins. Additionally, disordered side chains indicate a degree of flexibility mostly caused by weak interactions to neighboring atoms. We thus replaced Ser192$_{InlA}$ by asparagine, the next largest hydrophilic, yet uncharged side chain, extending its length slightly and potentially allowing for a direct hydrogen bond to hEC1. Overall only two (heavy) atoms C and N are introduced.

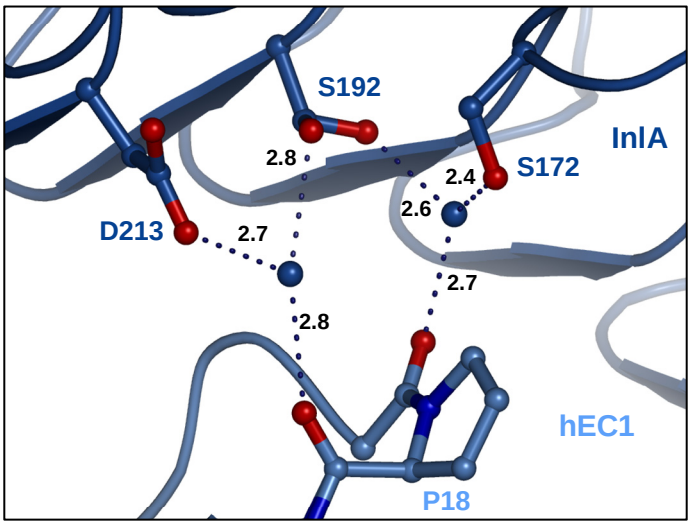

Figure 3.1-2: Water mediated contacts of Ser192$_{InlA}$ with hEC1-backbone atoms. Ser192 adopts two equally occupied conformations. In either orientation it forms hydrogen bonds to two water molecules (blue spheres) held in position by Asp213$_{InlA}$-Oδ1 and Pro18$_{hEC1}$-O (left water molecule), or Ser172$_{InlA}$-Oγ and Phe17$_{hEC1}$-O (right water molecule).

3.1.4 InlA Gly194Ser-i194Ser (G194S+S)

Compared to all other LRRs of InlA, repeat 6 is shorter by one residue consisting of 21 residues instead of the canonical 22.

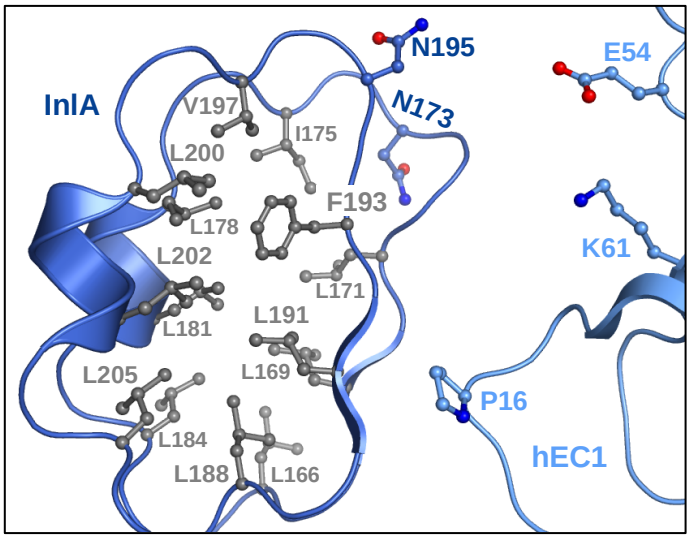

Figure 3.1-3: InlA LRR5 and 6 and their interactions with hEC1. The deletion in LRR6 creates a large cavity to hEC1, preventing direct or water mediated contact formation with Glu54 or Lys61 of hEC1. The rigid hydrophobic core (gray amino acids) maintains stacking of the secondary structure elements (cartoon representation). Due to the shorter loop of LLR6, Asn195 of InlA is excluded from the hydrophobic core (Asn173 of LRR5), disrupting the Asn-ladder. Note: crucial Pro16 of hEC1 is in close proximity to the LRR6-cavity.

Removal of this residue disrupts the regular LRR-geometry of InlA, shortens the loop that

follows the LRR β-strand (Schubert *et al.*, 2002), discontinues the asparagine ladder characteristic of LRR-proteins (Kobe and Deisenhofer, 1994) and creates a 7.5 Å, hydrophobic, water-filled cavity on the surface of InlA (Figure 3.1-3). To restore the regular LRR architecture, an additional serine (i194S) was introduced after residue 194 and Gly194 was replaced by serine, the most common residue at this position in other repeats of InlA.

3.2 Structural verification of predicted atomic-scale changes

InlA-mutant/hEC1 complexes were analyzed by X-ray crystallography at 2.0 Å resolution or better. For data collection and refinement statistics see Table 3.2-1. Superimposing all complexes indicates that single substitutions in InlA do not affect the overall structure of InlA itself, nor the geometry of the complex (r.m.s.-deviations 0.65 Å). This allows atomic changes in the immediate vicinity of the mutation to be analyzed, especially as regards hydrogen bond networks and water-mediated interactions.

3.2.1 Y369A and Y369S

Replacing sterically demanding tyrosine with alanine or serine allows $Asn370_{InlA}$ and $His392_{InlA}$ to maintain their stacking interaction with $Phe348_{InlA}$ as in uncomplexed InlA (Figure 3.2-1). Thus no conformational changes in the vicinity of Ala369 or Ser369 were induced upon E-cadherin binding, as postulated. In the wild-type complex $Tyr369_{InlA}$ shields a cavity form the environment, bearing three water molecules (black spheres in Figure 3.2-1). These water molecules are located adjacent to hydrophobic surfaces of InlA and hEC1, indicating that they are rotationally restrained. In the complexes Y369A/hEC1 and Y369S/hEC1 the cavity is opened, allowing exchange of solvent molecules with the environment. Water molecules within this cavity, however, occupy identical positions to the wild-type complex, indicating that the weak interactions suffice to position them precisely. One such water molecule, hydrogen bonded to $Asn27_{hEC1}$-Nδ2 in all complexes, forms a second hydrogen bond to $Ser369_{InlA}$-Oγ in Y369S/hEC1, bridging $InlA^{Y369S}$ and hEC1 by an additional hydrogen bond. In the mutant complexes, tyrosine is substituted by two further water molecules (red spheres in Figure 3.2-1) bound by $Asn370_{InlA}$ and $His392_{InlA}$. They replace a water molecule from the second solvation shell of InlA/hEC1 (blue).

Table 3.2-1: Data collection, refinement statistics and structural characteristics of InlA-mutant/hEC1 complexes.

	$InlA^{Y369A}$/ hEC1	$InlA^{G194S+S}$/ hEC1	$InlA^{S192N}$/ hEC1	$InlA^{S192N-Y369S}$/ hEC1	$InlA^{S192N-G194S+S}$/ hEC1	$InlA^{G194S+S-Y369S}$/ hEC1
Data collection[1]						
Space group	$P2_12_12_1$	$P2_12_12_1$	$P2_12_12_1$	$P2_12_12_1$	P1	P1
Cell constants						
a, *b*, *c* (Å)	55.3, 84.6, 108.3	55.2, 88.5, 110.5	55.5, 68.9, 132.4	55.4, 87.4, 111.0	44.9, 54.1, 68.6	45.0, 54.3, 68.6
α, β, γ (°)	90.0, 90.0, 90.0	90.0, 90.0, 90.0	90.0, 90.0, 90.0	90.0, 90.0, 90.0	74.7, 80.7, 67.7	75.0, 80.8, 67.4
Resolution (Å)	40-1.6 (1.63-1.60)	40-2.0 (2.1-2.0)	40-1.7 (1.76-1.70)	50-1.9 (1.97-1.90)	50-1.7 (1.77-1.70)	50-1.8 (1.86-1.80)
R_{merge} (%)	5 (29)	12 (37)	6 (28)	8 (42)	6 (52)	6 (51)
I / σ_I	29 (6)	9 (4)	20 (4)	17 (3)	16 (2)	12 (2)
Completeness (%)	99 (95)	96 (92)	99 (95)	97 (86)	91 (77)	94 (75)
Redundancy	8 (8)	5 (4)	6 (6)	12 (4)	5 (4)	5 (4)
Refinement						
Resolution (Å)	1.6	2.0	1.7	1.9	1.7	1.8
No. reflections	60684	37285	50104	43193	56061	47450
R_{work} / R_{free} (%)	15 / 19	19 / 28	16 / 21	15 / 22	17 / 22	16 / 22
No. atoms						
Protein	4645	4524	4704	4630	4797	4691
Ca^{2+}/Cl^-	0 / 0	1 / 1	2 / 4	2 / 2	1 / 1	1 / 1
Water	801	605	697	845	723	783
B-factors mean	11	18	10	18	14	18
Wilson	16	23	14	21	19	15
R.m.s deviations						
Bond lengths (Å)	0.022	0.024	0.025	0.022	0.024	0.022
Bond angles (°)	1.8	2.1	2.0	1.7	2.0	1.9
Analysis[2]						
r.m.s.d. (InlA)	0.43	0.39	0.59	0.30	0.32	0.24
r.m.s.d. (hEC1)	0.47	0.28	0.46	0.24	0.42	0.41
r.m.s.d. (complex)	0.64	0.30	0.61	0.31	0.50	0.57

[1] Numbers in parenthesis correspond to values of the highest resolution shell.
[2] r.m.s.d. values were calculated using main chain atoms.

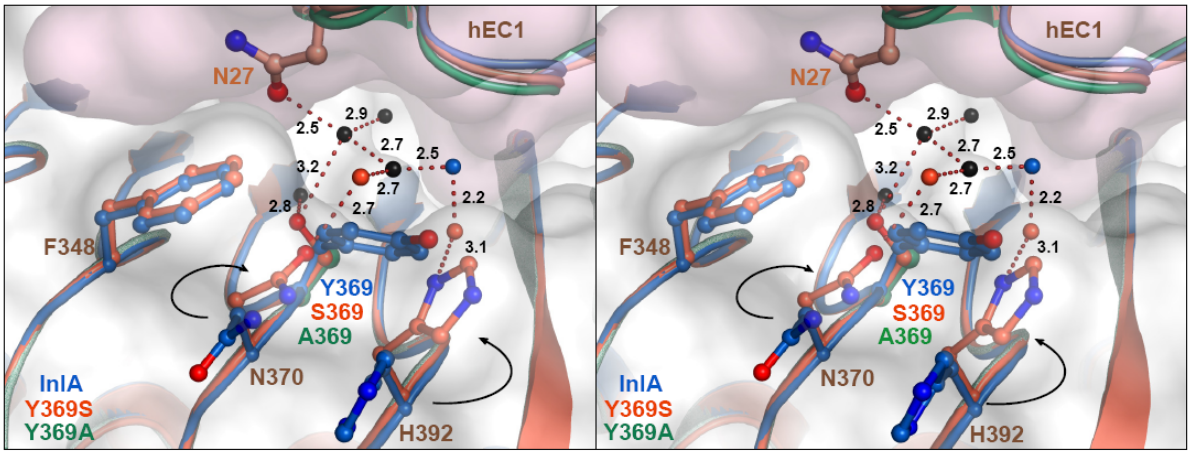

Figure 3.2-1: Stereo view of structural details of InlA, Y369A, and Y369S in complex with hEC1. The interface near Y369 of InlA is compared for the wild-type complex (blue), Y369A/hEC1 (green) and S192N-Y369S/hEC1 (dark orange), respectively. Variants of InlA (bottom) are rendered in dark colors, hEC1 (top) in corresponding lighter shades; the molecular surfaces of Y369A and the matching hEC1 in grey and light-purple. Side chains, involved in Tyr369-centrered rearrangement, are shown for the wild-type complex (blue) and S192N-Y369S/hEC1 (dark orange). Spheres represent water molecules: Grey - conserved in all complexes, blue - present only in the wild-type complex, orange - present in both variant complexes. The removal of the bulky side chain of Tyr369 prevents its disruptive re-orientation during complex formation but exposes an otherwise unaffected, water-filled cavity. Changes in the solvation pattern at the cavity entrance include hydrogen bonds from Ser369-Oγ to two conserved water molecules. One of the water molecules is bound to Asn27-Oδ1 (hEC1) in all complexes introducing an additional water-bridged contact between Y369S and hEC1.

3.2.2 S192N

In $InlA^{wt}$/hEC1, $Ser192_{InlA}$ adopts two distinct, equally occupied conformations, each involved in a water-mediated hydrogen bond to the main-chain oxygens of $Phe17_{hEC1}$ or $Pro18_{hEC1}$ (Figure 3.1-2). Each water molecule additionally interacts with a second residue of InlA, Asp213 and Ser172. Replacing $Ser192_{InlA}$ by asparagine allows the latter to fill the intermolecular space, eliminating one of the two water molecules coordinated by $Ser192_{InlA}$ in the wild type complex and introducing a direct hydrogen bond from $Asn192_{InlA}$-Nδ2 to $Phe17_{hEC1}$-O. The second water molecule (dark red sphere in Figure 3.2-2) is, however, retained, maintaining its bridging interactions with $Asp213_{InlA}$Oδ1 and $P18_{hEC1}$-O. Only one of two water-bridged interaction is thus replaced by a direct H-bond. The low temperature-factor of the $Asn192_{InlA}$-coordinated water indicates a much tighter interaction of $Asn192_{InlA}$, $Pro18_{hEC1}$ and $Asp213_{InlA}$ in S192N/hEC1 than in InlA/hEC1. The Oδ1 atom of $Asn192_{InlA}$ is involved in an intramolecular H-bonds to the backbone of the neighboring repeat. Though this interaction ensures H-bond saturation for this atom, it prevents additional contacts to hEC1.

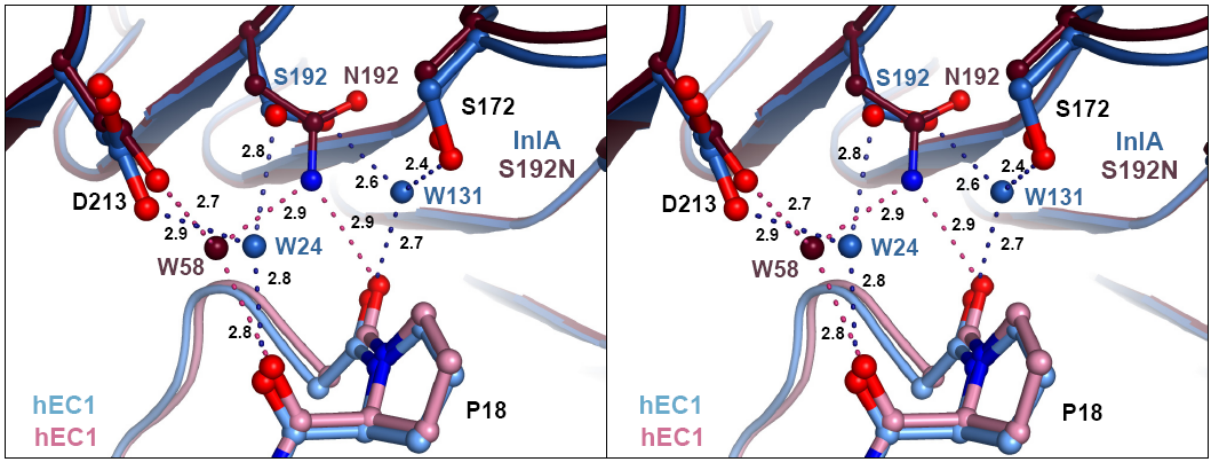

Figure 3.2-2: Stereo view of superimposed complexes InlA/hEC1 and S192N/hEC1. The vicinity of $Ser192_{InlA}$ is compared for wild-type complex (blue) and S192N/hEC1 (purple). In the wild-type complex, Ser192 adopts two alternate conformations each of which creates a water-bridged hydrogen bond to the carbonyl oxygen of $Phe17_{hEC1}$ and $Pro18_{hEC1}$, respectively. The water molecules involved are additionally hydrogen bonded by Asp213 and Ser172 of InlA. Replacing Ser192 by asparagine displaces one water and introduces a hydrogen bond between $Asn192_{InlA}$-Nδ2 and $Pro18_{hEC1}$-O. The second water maintains the hydrogen bonding pattern of the wild-type complex.

3.2.3 G194S+S

Replacing $Gly194_{InlA}$ by serine and inserting a second serine after Ser194 (+S), allows LRR6 to adopt a backbone geometry similar to that of all other repeats (Figure 3.2-3A). The compact, unaltered packing of aliphatic residues within the hydrophobic core (gray in Figure 3.2-3A) ensures that structural changes are limited to the immediate neighborhood of the inserted residue. As part of these changes, $Asn195_{InlA}$ flips into the hydrophobic core complementing the asparagine ladder. As a result, the hydrophobic water-filled cavity between wild-type InlA and hEC1 (Figure 3.2-3B) is eliminated, reducing the distance between the two proteins from ~10 to ~4 Å (Figure 3.2-3C). In the wild-type complex, the water molecules between LRR6 and hEC1 are poorly defined (weak electron density), indicating weak interaction with the hydrophobic surfaces of both proteins resulting in high positional variability. In the complex G194S+S/hEC1 at least four water molecules are displaced from the interaction interface (light-blue spheres in Figure 3.2-3A). The narrow cavity between both proteins increases the distinct localization of water molecules, leading to more distinct electron density. The residue +S hydrogen bonds a water molecule that additionally forms a long range interaction (4.0 Å) to $Glu54_{hEC1}$. A second water molecule, held in position by hydrogen bonds of 3.0 Å to both $Glu54_{hEC1}$ and $Lys61_{hEC1}$, similarly forms a long range interaction of 4.2 Å to +S (Figure 3.2-3A).

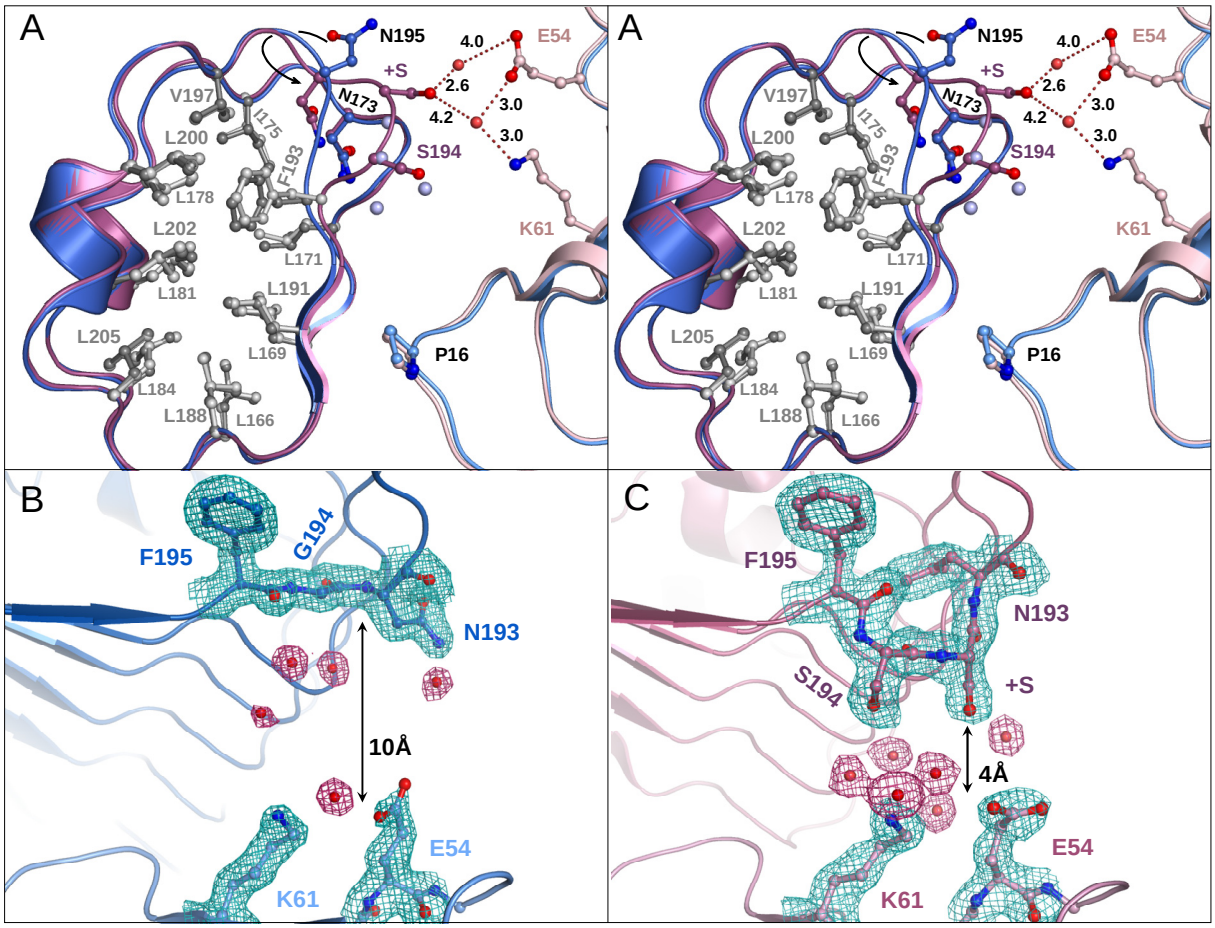

Figure 3.2-3: Structural details of G194S+S/hEC1 complex. The interaction of LRR5 and 6 (InlA) with hEC1 are compared for wild-type InlA/hEC1 (blue) and G194S-i194S/hEC1 (purple/salmon). (**A**) Stereographic view. The mutation G194S and the insertion of an additional serine (i194S) restores the canonical LRR-repeat geometry in LRR6. Asn195 flips into the hydrophobic core of InlA (dark-grey: wild-type, light-grey: mutant) in G194S-+S (arrow) creating a continuous asparagine-ladder. A large, water-filled cavity is removed. (**B**) Electron density ($2F_O$-F_C, contoured at 1σ) of the 21-residue LRR6 in wild-type InlA/hEC1 complex. Electron density of protein and water is colored dark green and dark red, respectively. The shortened LRR6 creates a hydrophobic cavity between Gly194 of InlA and Glu54 and Lys61 of hEC1. Waters, filling the gap, are poorly defined (weak electron density). (**C**) The equivalent view of (**B**) in the mutant complex G194S-i194S/hEC1. The gap between interaction partners is narrower, yielding a well-defined yet unsaturated water cluster.

3.2.4 InlA double substitutions

Taking advantage of the small and distinct structural changes within the InlA/hEC1 interface introduced by single substitutions in InlA, combinations were created to analyze their structural and biophysical interdependence. They include S192N-Y369A, S192N-Y369S, S192N-G194S+S, and G194S+S-Y369S. The latter three combinations were co-crystallized with hEC1 and complex structures were solved at 1.9 Å resolution or better. Although most InlA-variant/hEC1 complexes crystallized in the same space group as the wild-type complex (orthorhombic, $P2_12_12_1$), the combinations S192N-G194S+S and G194S+S-Y369S

crystallized in the triclinic space group P1 with one complex in the asymmetric unit. Crystal contacts in the orthorhombic wild-type packing are predominantly mediated by InlA. Only one minor contact involves hEC1. Packing of complexes in the triclinic lattice is entirely unrelated. The convex face of LRR7-10 is packed against the solvent exposed face of hEC1 of a symmetry related molecule (Figure 3.2-4). Despite different crystal lattices, the overall structures of complexes are identical (rmsd < 0.6, see Table 3.2-1).

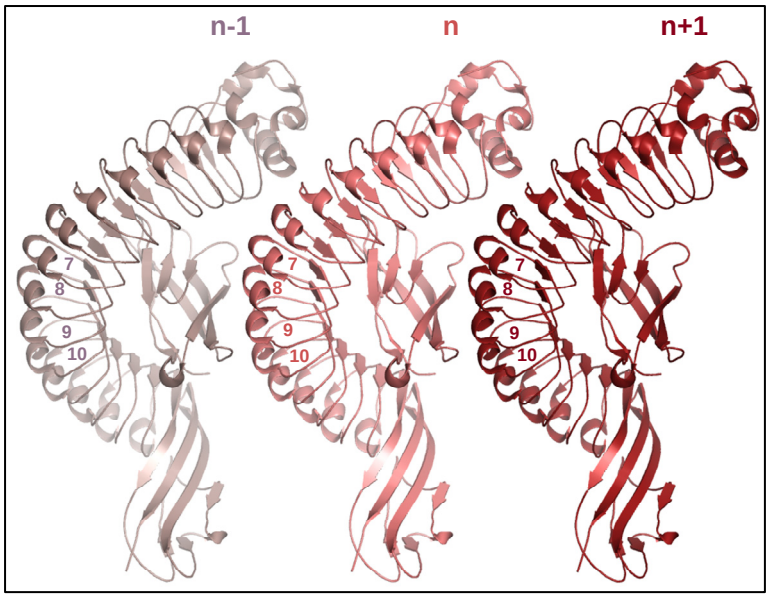

Figure 3.2-4: Crystal contacts of G194S+S-Y369S / hEC1 and S192N-G194S+S / hEC1 complexes. LRRs seven to ten of molecule n (n+1) are packed against hEC1 of the symmetry related molecule n-1 (n) creating a large crystal contact. Both complexes crystallized in contrast to the wild-type complex and all other InlA-variant complexes in P1 (triclinic space group, see Table 3.2-1).

The physically distant double substitutions S192N-Y369S and G194S+S-Y369S combine structural modifications of the individual single substitutions. Differences in side chain conformations are not obvious so that structural changes appear to be strictly additive. Combining the physically adjacent mutations S192N and G194S+S, however, results in structural interference (Figure 3.2-5). The side chain of $Asn192_{InlA}$ is locked into a tight intramolecular hydrogen bond to the backbone nitrogen of $Ser194_{InlA}$ (Figure 3.2-5B-C). The additional H-bond of $Asn192_{InlA}$ to the carbonyl oxygen of $Phe17_{hEC1}$ is preserved, but no water is excluded from the interaction interface (Figure 3.2-5D). One of the water-mediated hydrogen bonds of the inserted serine residue (+S) to $Glu54_{hEC1}$ appears shorter in the S192N-G194S+S complex structure (4.2 Å in the single mutant vs. 2.3 Å in the double mutant), indicating that an additional water-mediated H-bond has been introduced. In the complex structure of the related double mutant G194S+S-Y369S the same shortened H-bond

is present, excluding the possibility that the combination of physically adjacent mutations S192N and G194S+S causes this extra stabilization. Instead, both InlA-variants crystallize in space group P1 in a packing arrangement unrelated to the wild-type complex characterized by extensive crystal contacts between hEC1 and the LRR-domain of a symmetry related molecule (Figure 3.2-4). Analyzing both crystal structures and comparing them with the structure of G194S+S/hEC1 (without this extended inter-complex interface) indicates that a crystallization artifact may be responsible for the shorter distance of $Glu54_{hEC1}$ to the bridging water molecule. The neighboring residue $Arg55_{hEC1}$ is in close contact to residues of LRR9 of a symmetry related complex, displacing $Glu54_{hEC1}$ towards InlA.

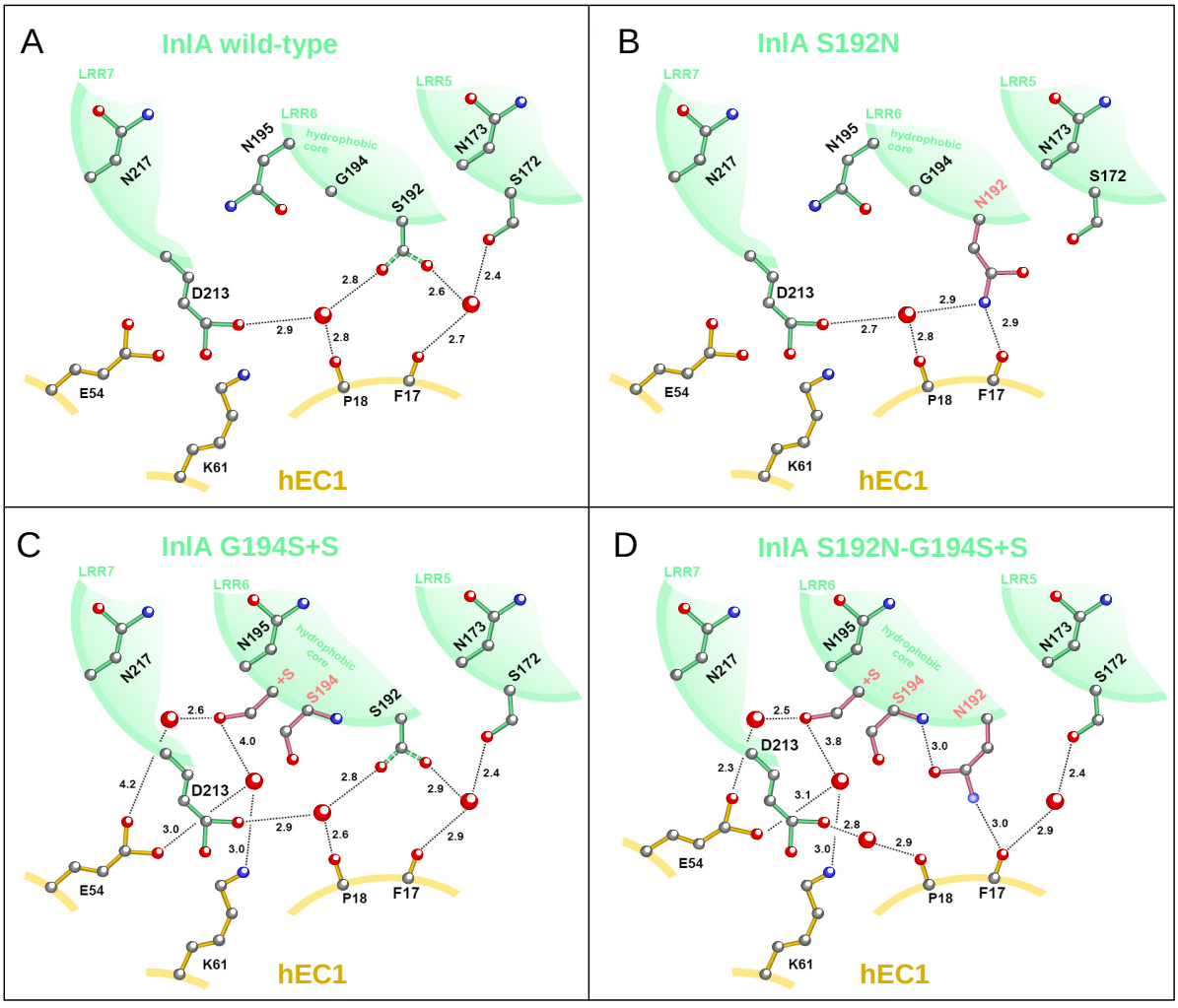

Figure 3.2-5: Schematic representation of local rearrangements in InlA-variants. LRR 5-7 of InlA-variants are shown in green, interacting residues of hEC1 in yellow. Amino acid substitutions are highlighted in red. (**A**) InlA/hEC1: disordered $Ser192_{InlA}$ and its water-mediated interactions to hEC1. (**B**) $Asn192_{InlA}$ creates a direct hydrogen bond to $Phe17_{hEC1}$. (**C**) G194S+S: Restoring the canonical LRR-architecture reduces the distance to $Glu54_{hEC1}$ and $Lys61_{hEC1}$. (**D**) Combination of substitutions S192N and G194S+S (**B** and **C**). $Asn192_{InlA}$ forms an intramolecular hydrogen bond to $Ser194_{InlA}$-N while retaining the direct hydrogen bond to $Phe17_{hEC1}$. As a result Asn192 no longer excludes a second water molecule (see **B**). A shorter hydrogen bond from $Glu54_{hEC1}$ to bridging water molecules may indicate tighter interaction with the inserted serine +S. Alternatively, these shorter distances may result from a different crystal packing.

3.3 Biophysical analysis of protein interactions

To analyze whether the atomic adjustments of InlA-variants increase the interaction strength with hEC1, we analyzed the binding affinity of all complexes with ITC. The wild-type interaction previously analyzed by analytical ultracentrifugation was additionally investigated by ITC to allow comparison with InlA-variants. ITC, furthermore, allows changes in binding affinity to be separated into enthalpic and entropic contributions.

3.3.1 Wild-type InlA/hEC1 complex formation is enthalpy and entropy driven

The dissociation constant for wild-type InlA and hEC1 was determined to be 8 ± 4 µM by analytical ultracentrifugation (Schubert *et al.*, 2002). Using isothermal titration calorimetry (ITC), this has been narrowed down to 3 ± 1 µM.

Analyzing the association of $InlA^{wt}$ and hEC1 in different buffers, indicates that the apparent enthalpy (H_{app}) of complex formation is dependent on the ionization enthalpy (H_{ion}) of the buffer (Christensen *et al.*, 1976), implying that complex formation is associated with an exchange of protons. H_{app} is found to be -6.7 ± 0.3 kJ/mol in cacodylate buffer (H_{ion} = -2,5 kJ/mol), -1,8 ± 0.2 kJ/mol in Hepes buffer (H_{ion} = 23.9 kJ/mol), and 3.5 ± 0.2 kJ/mol in Tris buffer (H_{ion} = 47.7 kJ/mol). Plotting H_{app} against H_{ion} (Figure 3.3-1) indicates that 0.2 ± 0.1 protons (gradient) are taken up during complex formation. The side chain involved remains unclear. Nevertheless, the binding enthalpy may be corrected for H_{ion} and is found to be –6.2 kJ/mol (y-axis intercept, H_{ion}=0). The binding entropy (T S) is 25 kJ/mol. Complex formation of InlA and hEC1 is thus both entropy and enthalpy driven.

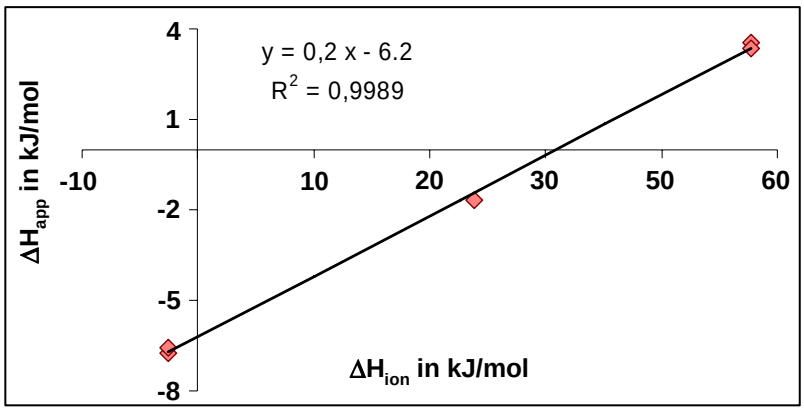

Figure 3.3-1: Plot of apparent enthalpy (ΔH_{app}) against ionization enthalpy of the buffer (ΔH_{ion}). The precise enthalpy of binding may be revealed by plotting the apparent enthalpy against the ionization enthalpy of the buffer. The y-axis intercept (ΔH_{ion}=0) corresponds to ΔH_{bind} whereas the gradient reveals the number of protons taken up (positive number) or being released (negative number) during complex formation.

3.3.2 Divergent thermodynamic behavior of InlA-variants

ITC experiments for InlA-mutants were all performed in Hepes buffer in the presence of $CaCl_2$. As a result, H-values comparing complex formation for mutant and wild-type InlA with hEC1 are independent of H_{ion}. The small, structural changes introduced within the binding interface by the mutation of InlA result in surprisingly large and divergent changes in thermodynamic behavior. The titration curves (Y369A and G194S+S shown in Figure 3.3-2) indicate that while both improve binding affinity (see below), Y369A reduces the enthalpy of binding (Figure 3.3-2A, favorable) while G194S+S results in a dramatic increases (Figure 3.3-2B, unfavorable), resulting in an endothermic reaction.

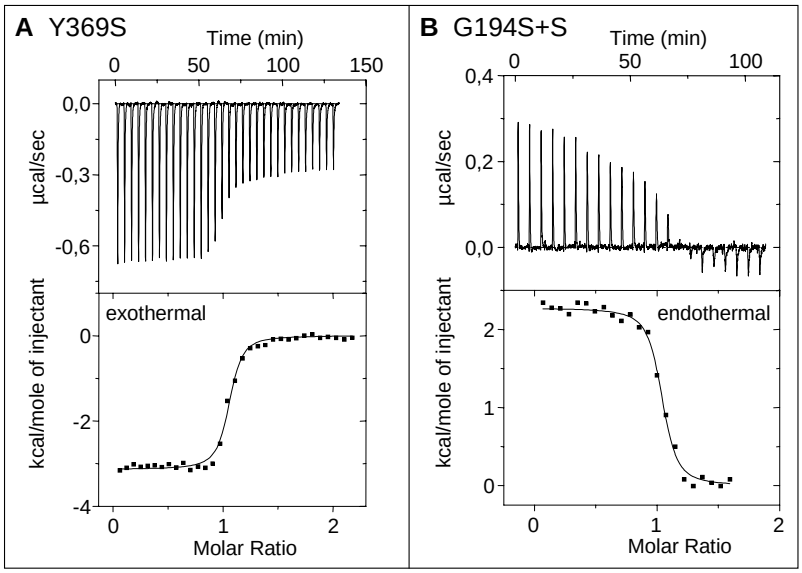

Figure 3.3-2: Isothermal titration curves. (**A**) The titration curve of hEC1 against Y369S demonstrates the association to be exothermal. 8 µl aliquots of Y369A (0.43 mM) were successively injected into a 0.04 mM solution of hEC1. The association affinity constant and the binding enthalpy were derived by curve fitting using the single set of independent sites model. (**B**) Titrating hEC1 (0.035 mM) against G194S-i194S (0.66 mM) using 5 µl injections reveals an unusual endothermal association reaction. Both titrations yield a binding stoichiometry of 1 ± 0.1.

Figure 3.3-3 summarizes thermodynamic data including binding affinities, binding enthalpy, and binding entropy. Delta-delta values compare changes in binding enthalpy ($\Delta\Delta H$), entropy ($\Delta T\Delta S$) or binding affinity (in multiples) of the wild-type complex (at the top of Figure 3.3-3A and B) with those of InlA single substitutions (middle row). They are systematically marked by colored arrows and boxes. Equivalent substitutions are highlighted by identical colors. Furthermore, thermodynamic data of double substitution variants of InlA (bottom row)

are either compared to the wild-type complex (orange labels) or to its constitutive single substitution complexes. Colors again highlight individual substitutions.

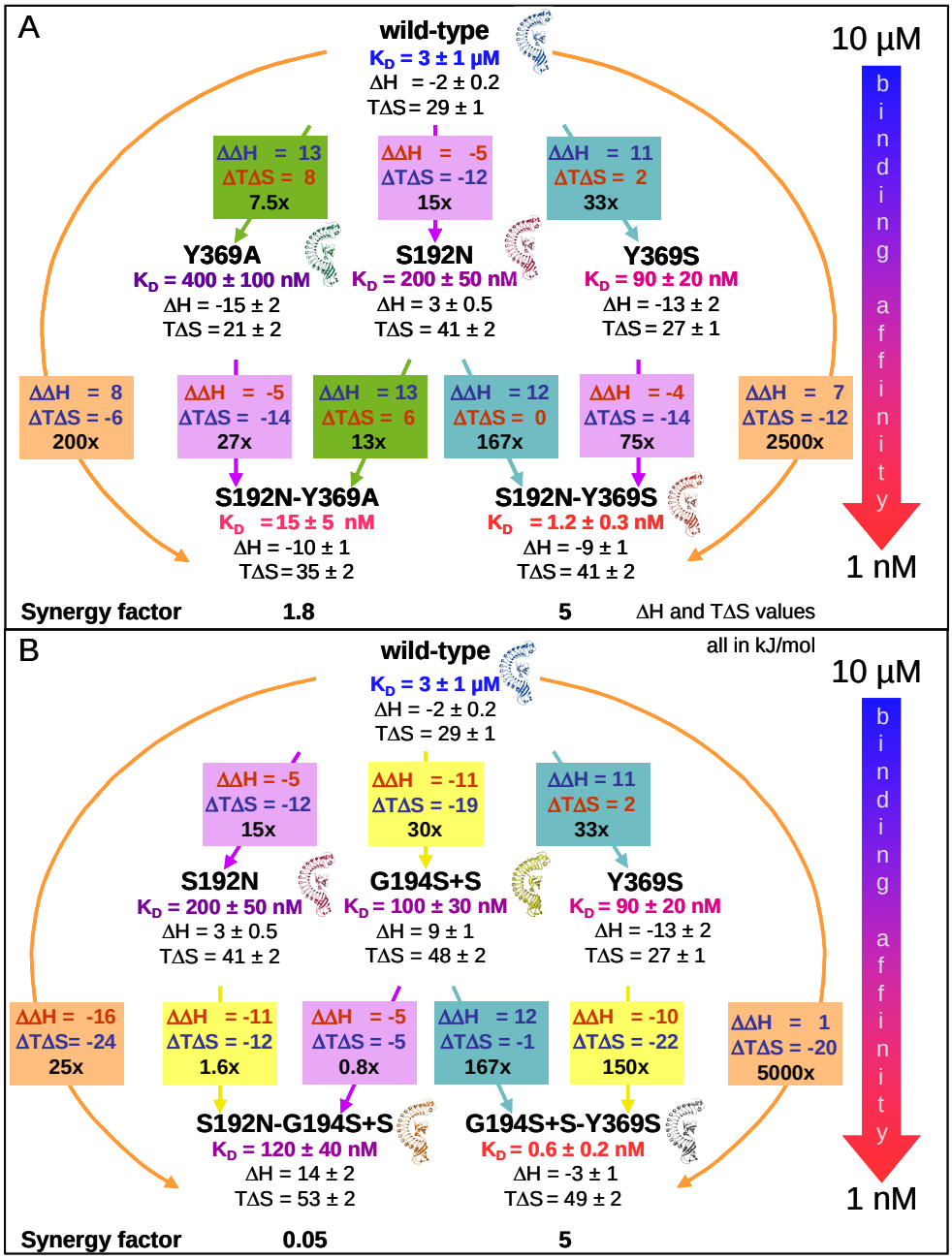

Figure 3.3-3: Thermodynamic network. Binding affinities (K_D) derived by isothermal titration calorimetry (ITC), as well as binding enthalpies (H) and entropies (T S) are summarized for complexes of wild-type and variant InlA with hEC1. Substitutions and associated changes in binding enthalpies (H = H_{wt} - H_{mut}) and entropies (T S = T S_{wt} – T S_{mut}) are listed in color-coded boxes: green - Y369A, magenta - S192N, blue - Y369S, yellow - G194S+S. Blue and red fonts respectively denote thermodynamically favorable and unfavorable changes. Note the excellent reproducibility for identical substitutions introduced into different backgrounds. Combining substitutions results in non-additive strengthening of corresponding complexes (orange-colored arrow). Synergy factors indicate positive (>1) as well as negative (<1) cooperativity between combined substitutions. Complexes for which crystal structures have been solved are indicated by ribbon pictograms. Color-graded arrows indicate binding affinities of InlA-variants: blue µM and red nM affinities.

3.3.3 Y369A and Y369S

Both substitutions, Y369A and Y369S, contribute enthalpically to complex formation: ΔΔH = 13 kJ/mol for Y369A (green boxes in Figure 3.3-3A) and 11 kJ/mol for Y369S (turquoise in Figure 3.3-3, Figure 3.3-2A). In Y369A the favorable enthalpy is counteracted by an unfavorable entropic contribution, an apparent case of "enthalpy/entropy compensation" (Dunitz, 1995). Compared to $InlA^{wt}$, Y369A therefore increases binding affinity (K_D = 400 ± 100 nM) to hEC1 only 7.5-fold. In Y369S (blue labels in Figure 3.3-3) a much smaller entropic compensation results in the highest binding affinity for hEC1 (K_D = 90 ± 20 nM) of any single InlA-mutant investigated in this study.

3.3.4 S192N and G194S+S

In contrast to Y369A and Y369S, complex formation is observed to be endothermal (Figure 3.3-2B) for both S192N (magenta labels in Figure 3.3-3, ΔΔH = -5 kJ/mol) and G194S+S (yellow labels in Figure 3.3-3B, ΔΔH = -11 kJ/mol). The unfavorable change in enthalpy is, however, more than compensated by a large increase in binding entropy ($\Delta T\Delta S_{S192N}$ = -12 kJ/mol, $\Delta T\Delta S_{G194S+S}$ = -19 kJ/mol) resulting in a significantly higher binding affinity for hEC1 than that of $InlA^{wt}$. The substitutions S192N and G194S+S thus improve surface complementarity of InlA/hEC1 allowing the entropically favorable elimination of one and four constrained water molecules from the interface, respectively.

3.3.5 Thermodynamics of long-range cooperativity between combined mutations

To achieve a higher binding affinity, the described amino acid substitutions were combined to yield the four InlA-variants S192N-Y369A, S192N-Y369S, G194S+S-Y369S and S192N-G194S+S (bottom row, Figure 3.3-3A and B). Note the excellent consistency of the thermodynamic data: H (T S)-values differ by no more than 1 (3) kJ/mol for each substitution, whether introduced into $InlA^{wt}$ (upper row of colored boxes in Figure 3.3-3A and B) or combined with another substitution (same color, lower row).

Combining physical distant single mutations dramatically increases the binding affinity for hEC1. Thus the binding affinities of S192N-Y369A, S192N-Y369S, and G194S+S-Y369S are 200, 2500, and 5000-fold (orange boxes, Figure 3.3-3A and B) that of $InlA^{wt}$. Though the

sites of substitution are separated by ~34 Å, binding energies of individual substitutions are not merely additive but indicate positive cooperativity instead. 'Synergy factors' were calculated by dividing the increase in binding affinity of the doubly substituted variant (lower colored box in Figure 3.3-3A and B) by that of the single substitution variant (upper box of identical color). For S192N-Y369A this amounts to 13/7.5 ≈ 27/15 ≈ 1.8, while S192N-Y369S and G194S+S-Y369S both yield a value of ~5 (Figure 3.3-3A and B). The synergy is invariably entropic in nature, as $T\Delta S$ is always 2-3 kJ/mol lower for double substitution variants than for corresponding single substitution variants (boxes of identical color in upper and lower rows of Figure 3.3-3A and B).

The tightest binding affinity of an InlA-variant for hEC1 is that of G194S+S-Y369S, K_D = 0.6 ± 0.2 nM. Only two rationally chosen substitutions in InlA thus suffice to transform the weak binding affinity of the wild-type complex, K_D = 3 ± 1 µM, to a tight fit comparable to that of typical proteinase/proteinaceous-inhibitor complexes (Stites, 1997) - one of the highest increases in binding affinity (5000-fold) reported for any protein-protein interaction (Cho *et al.*, 2005).

In contrast to the synergy for S192N-Y369A, S192N-Y369S, and G194S+S-Y369S, the substitutions of the fourth double variant S192N-G194S+S are anti-cooperative. The synergy factor is 0.8/15 ≈ 1.6/30 ≈ 0.05 (Figure 3.3-3B) resulting in a binding affinity that is similar to that of the individual substitution variants rather than ~10-fold stronger as expected if the effects were additive. A reduction of $T\Delta S$ by ~7 kJ/mol indicates this to be an entropic effect.

3.4 Biological consequence of improved affinity

Using minimal, structure derived modifications the weak binding affinity of the invasion protein InlA for its human receptor hEC1 was dramatically improved. Affinities in the lower nanomolar range were obtained by exchanging only two amino acids of the wild-type protein. To determine the biological consequences of improved binding affinity, listerial strains expressing full-length InlA-variants – instead of the C-terminally truncated versions used for structural and biophysical analysis – had to be generated. The shuttle vector pPL2 that integrates into the listerial genome was used to stably complement the *inlA*-deletion of the *L. monocytogenes* Δ*inlA*2 strain with full-length *inlA* or its variants (see Methods, 2.4 page 25). Integrating a single copy of the entire *inlA* locus including promoter and terminator regions

into the listerial genome leads to stable expression levels without the need for any selection pressure.

3.4.1 Genomic integration of pPL2-constructs bearing full-length *inlA*-variants

The pPL2 integration vector (Lauer *et al.*, 2002) carries the PSA attachment site along with the PSA-integrase gene (*int*), allowing for efficient integration into the listerial genome. The vectors pPL2-*inlA*, pPL2-*inlA*^{Y369A}, and pPL2-*inlA*^{m} (= *inlA*$^{S192N-Y369S}$) were transformed into *L. monocytogenes* Δ*inlA*2 to complement the in-frame *inlA*-deletion. Disruption of the bicistronically transcribed *inlAB* locus is known to dramatically affect expression levels of *inlA* and *inlB* (Lingnau *et al.*, 1995). To normalize results for altered expression levels, a reference strain bearing pPL2-*inlA* (unmodified) was used.

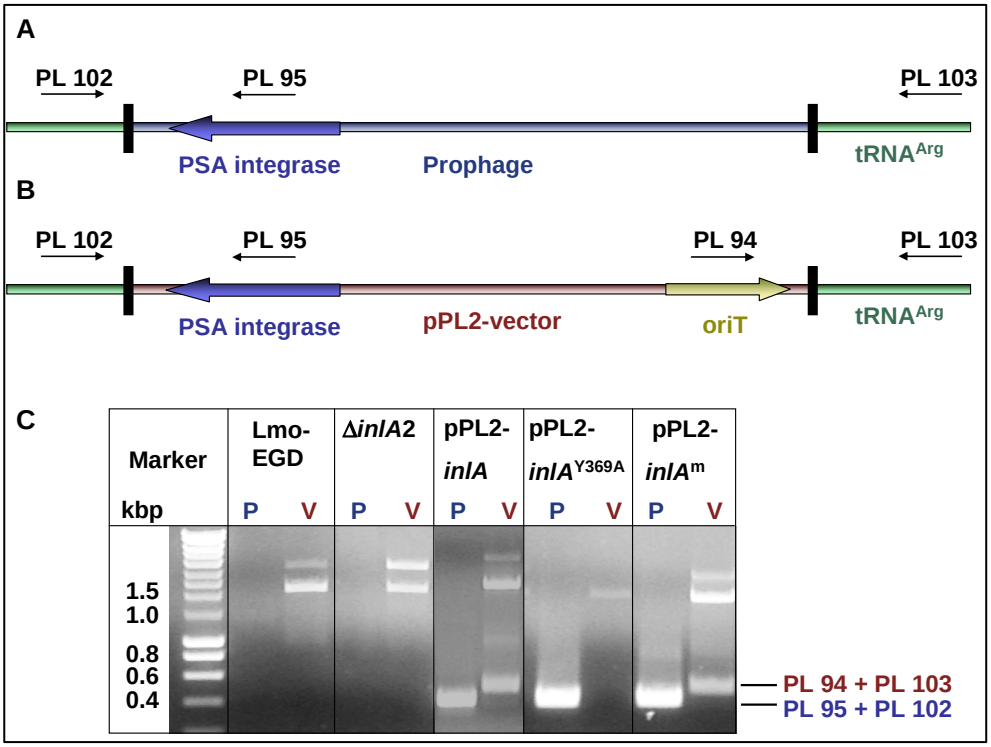

Figure 3.4-1: Colony PCR to verify proper integration of pPL2-constructs into *L. monocytogenes*-Δ*inlA*2 strains. (A) The presence of the PSA-prophage within the listerial genome was analyzed using primer pairs PL 102 and PL 95. Phage and vector borders are indicated by black bars, tRNA^{Arg} = natural PSA-phage attachment site, also used by pPL2. **(B)** Once the vector pPL2 has been integrated, two PCR products are obtained when using primer-pairs PL 102 and PL 95 (same as in **A**) or PL 94 and PL 103 (unique for pPL2). (**C**) Colony-PCR products of wild-type *L. monocytogenes* (Lmo-EGD), the in-frame deletion mutant *L. monocytogenes*-Δ*inlA*2 (Δ*inlA*2) and the strains with respective pPL2-vector integrations. P = Prophage- or non-integrated vector is detected, V = integrated vector is exclusively detected.

To ensure proper and stable integration of pPL2-constructs, the absence of the ubiquitously distributed listerial PSA pro-phage has to be confirmed. Genomic integration of this phage is schematically illustrated in Figure 3.4-1A. In unmodified *L. monocytogenes* (Lmo-EGD) or its derivative *L. monocytogenes* Δ*inlA*2 no phage-specific PCR-product was amplified (Figure 3.4-1C, left two panels denoted Lmo-EGD and Δ*inlA*2, respectively), indicating that the PSA pro-phage is absent in these strains. Integration of the pPL2-constructs could therefore be performed as described. Colony PCR of strains Lmo-pPL2-*inlA* and Lmo-pPL2-*inlA*^{m} resulted in appropriate PCR-products for both primer pairs, confirming a proper integration of the vectors into the genome. The absence of PCR-product PL 94 + PL 103 in Lmo-pPL2-*inlA*^{Y369A} could indicate that the PSA pro-phage is present and the vector itself has not been integrated. However, the presence of the pro-phage was excluded for the starting strain *L. monocytogenes* Δ*inlA*2, used to integrate the vector. Therefore the single PCR-product of Lmo-pPL2-*inlA*^{Y369A} suffices to confirm the correct vector integration.

3.4.2 Expression analysis of Lmo-pPL2-*inlA*-variant strains

Complementing the *inlA*-deletion with different *inlA*-variants should result in detectable InlA-variant and InlB-protein levels, expressed by different strains. Because InlA functions as anchored protein, whereas InlB works in solution, TCA-precipitated cell wall extracts and culture supernatants were independently analyzed on SDS-gels and stained with monoclonal antibodies against InlA or InlB (see 2.4.6 on p.29).

Analyzing the complemented strains reveals that full-length InlA-variants are expressed (82 kDa band in Figure 3.4-2). InlA and its variants were detectable in the supernatant as well as in cell-wall extracts, indicating that they are secreted and attached to the cell-wall as in Lmo-EGD. The amount of InlA in the supernatant appears to exceed that of the cell-wall extract. However, because cell-wall extracts and supernatants were processed differently (see 2.4.6 on p.29) the amount of protein in both samples can not be compared directly. Comparing expression levels of InlA and InlB for the wild-type strain (Lmo-EGD, Figure 3.4-2) and its deletion-derivative *L. monocytogenes* Δ*inlA*2 confirms that InlA is absent (no band visible in αInlA blot), but additionally demonstrates that the InlB-expression level is strongly reduced in the Δ*inlA*2-strain. The same is true for all complemented strains, as complementation does not reconstitute the *inlAB* locus, required for natural expression levels. Compared to Lmo-EGD, expression levels for InlA in complemented strains are significantly reduced (5-10-fold),

while the amount of InlA is comparable in all complemented strains when corrected for total protein levels. The strain Lmo-pPL2-*inlA* may thus be used as reference in biological assay.

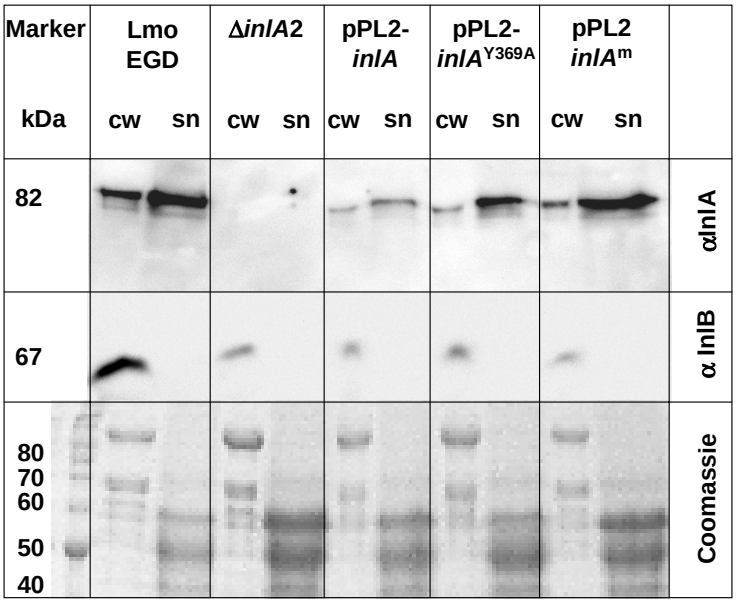

Figure 3.4-2: Expression analysis of InlA and InlB in reconstituted *L. monocytogenes* strains. Western blots with monoclonal antibodies against InlA (αInlA) or InlB (αInlB) were performed to detect these proteins in TCA-precipitated cell-wall extracts (cw) or culture supernatants (sn). Names of strains as in Figure 3.4-1. Coomassie-stained SDS-gel is used as a loading control (total amount of proteins loaded onto the gel).

3.4.3 Genomic integration of pPL2-constructs carrying the entire *inlAB*-locus

The strongly reduced expression levels of InlA-variants and InlB in *inlA*-complemented strains probably result from the disruption of the *inlAB*-locus. Complementing the entire *inlAB*-locus of an *inlAB*-deletion strain (*L. monocytogenes* Δ*inlAB*2) with respective *inlA*-variants could be an option to circumvent reduced expression levels.

The constructs pPL2-*inlAB*, pPL2-*inlA*^{Y369A}*inlB*, and pPL2-*inlA*^{m}*inlB* were integrated into *L. monocytogenes* Δ*inlAB*2 (Lingnau *et al.*, 1995) as described for the pPL2-*inlA* constructs. To confirm proper integration of the plasmids within the listerial genome a single PCR-reaction with primer pair PL 102 and PL 95 was used (Figure 3.4-1A). Analyzing the in-frame deletion strain *L. monocytogenes ΔinlAB* confirms the absence of the listerial pro-phage PSA. Colony-PCR products with expected size for listerial strains carrying respective pPL2-constructs demonstrated their correct integration (Figure 3.4-3A).

3.4.4 Expression analysis of Lmo-pPL2-*inlA*-variant *inlB* strains

Expression of InlA-variants and InlB in *inlAB*-deletion strains complemented with the entire *inlAB*-locus were analyzed as described for the Lmo-pPL2-*inlA* variants (Figure 3.4-3B).

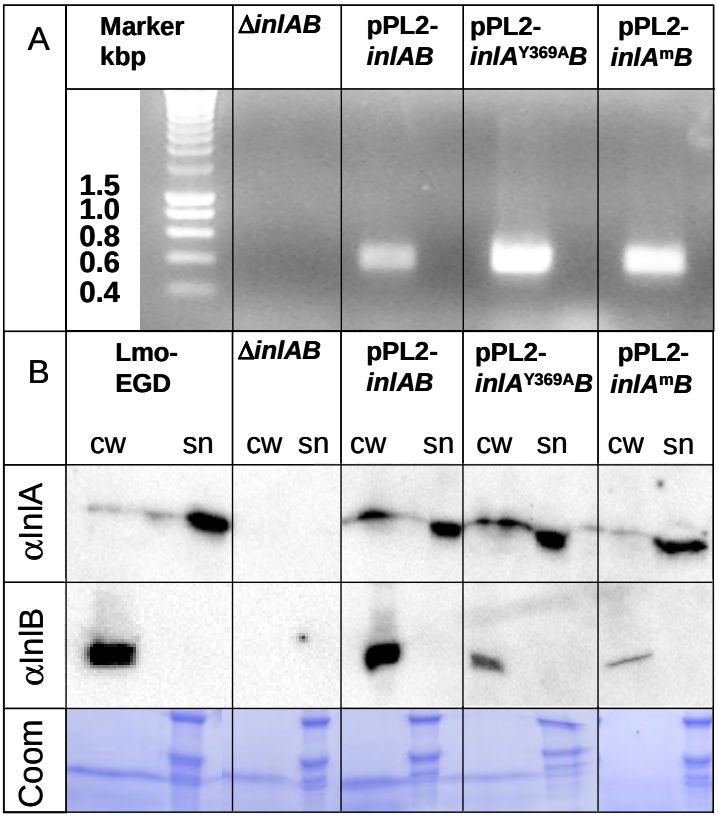

Figure 3.4-3: Analysis of reconstituted *L. monocytogenes* pPL2-*inlAB* strains. (**A**) Colony-PCR of *strains L. monocytogenes* Δ*inlAB* (Δ*inlAB*) and its derivatives Lmo-pPL2-*inlAB*, Lmo-pPL2-*inlA*^{Y369A}*inlB*, and pPL2-*inlA*^{m}*inlB* with primers PL 95 and PL 102. (**B**) Western blots with monoclonal antibodies against InlA (αInlA) or InlB (αInlB) of TCA-precipitated cell-wall extracts (cw) or culture supernatants (sn). Names of strains as in (**A**). Coomassie-stained SDS-gel (Coom) is used as a loading control (total amount of proteins loaded onto the gel).

Equal protein amounts were extracted and analyzed from culture-supernatants. InlA-expression is, correspondingly, observed to be comparable in all InlA-variant strains. More importantly, the amount of InlA produced by re-engineered strains is comparable to that of Lmo-EGD. Surprisingly, InlB is not detectable in the supernatant of the wild-type strain, nor in that of re-engineered strains (Figure 3.4-3B).

The total protein amount in cell-wall fractions is not as constant as that observed for the supernatant fraction. As a result, InlA and InlB amounts appear to differ in each strain. Correcting for total protein amounts, however, confirms InlA- and InlB-amounts to be comparable for re-engineered strains and, in the case of InlB, for the wild-type strain. While

the cell-wall extract of Lmo-EGD appears to contain lower amounts of InlA than the re-engineered strains, a comparison of InlA- and InlB-expression levels for Lmo-EGD in Figure 3.4-2 and Figure 3.4-3B, indicates the latter to underestimate the amount of InlA.

Overall, we may conclude that complementation of the entire *inlAB*-locus allows expression levels of both invasion proteins InlA and InlB to be maintained – in contrast to the dramatically reduced expression of InlA in strains with disrupted *inlAB*-locus.

3.4.5 Invasion of pPL2-complemented listerial strains into Caco2 cells

The invasion protein InlA binds its receptor human E-cadherin and induces uptake of *L. monocytogenes* into non-phagocytotic cells of the host. To clarify whether improved affinity of InlA would induce uptake more efficiently or interfere with phagosomal release after uptake, listerial strains expressing re-engineered InlA-variants with increased affinity for E-cadherin (hEC1) were analyzed using gentamicin-protection invasion assays (see 2.5 on p. 30).

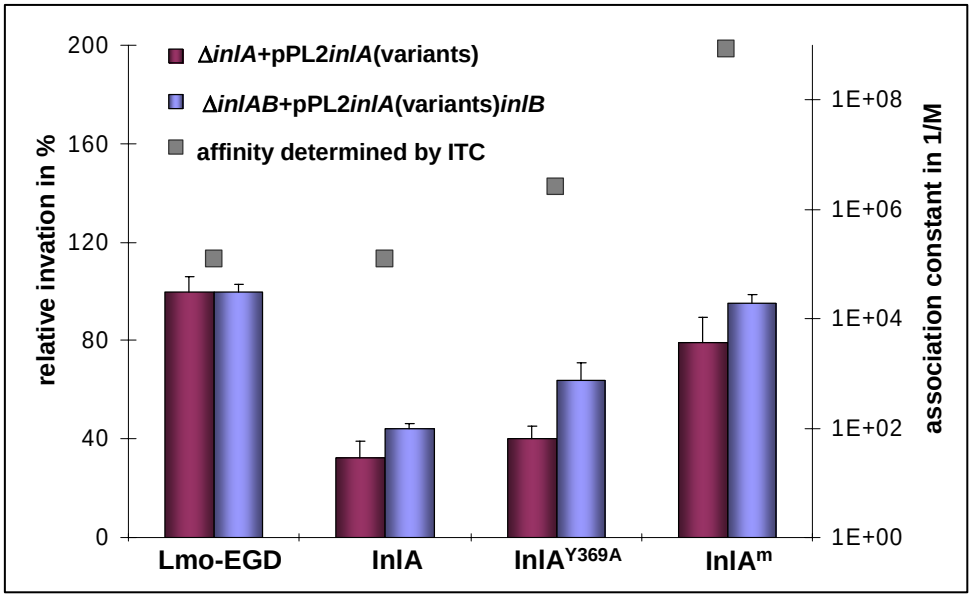

Figure 3.4-4: Uptake of transgenic listerial strains into Caco2 cells. Uptake of *L. monocytogenes* Δ*inlA*2-pPL2-*inlA*-variant strains (violet) and *L. monocytogenes* Δ*inlAB*2-pPL2-*inlA*-variant-*inlB* strains (blue, mutations for both as indicated) are compared with that of unmodified wild-type bacteria (Lmo-EGD). Invasion is plotted relative to that of Lmo-EGD (100%). Grey boxes and right-hand y-axis: the association constant ($1/K_D$) in l/mol (1/M) is plotted, greater values correspond to tighter binding. Affinity of the InlA-variant for its receptor hEC1 correlates with invasion efficiency of the respective strain.

Most cell-lines down-regulate E-cadherin expression during transformation, increasing the invasiveness through weaker or absent cell-cell-adhesion (Navarro *et al.*, 1991). The human epithelial cell line Caco2 expresses E-cadherin in amounts, comparable to those of

untransformed cells. The effect of improved affinity could therefore optimally be analyzed using this cell-line.

Lmo-EGD induces uptake into Caco2 cells efficiently. Complementing the deletion strains *L. monocytogenes* Δ*inlA* and *L. monocytogenes* Δ*inlAB* with unmodified *inlA* and *inlAB* restores invasion but reduces invasion rates to 32% and 44% of wild-type levels (100%), respectively (Figure 3.4-4). Reduced expression levels of InlA and InlB, observed for the complementation of *L. monocytogenes* Δ*inlA* (Figure 3.4-2) are presumably responsible for this decreased invasiveness. Complementing the deletion strain with the entire *inlAB*-locus restores expression levels of both proteins to levels indistinguishable from the wild-type (Figure 3.4-3B). Correspondingly, invasion rates of this strains are found to be significantly increased compared with the *inlA*-complementation. Invasion rates comparable to those of Lmo-EGD were, however, not observed (Figure 3.4-4).

Transgenic strains, expressing either $InlA^{Y369A}$ or $InlA^{m}$ ($InlA^{S192NY369S}$) invade Caco2 cells more efficiently than the corresponding $InlA^{wt}$ strains, indicating that invasiveness correlates with the affinity of InlA for its receptor human E-cadherin. Although a correlation of affinity and invasiveness is obvious, the relationship is non-linear. A 2500-fold increase in binding affinity of $InlA^{m}$ for hEC1 only results in a two-fold increase of invasion efficiency (Figure 3.4-4). These results indicate that the weak affinity of InlA did not evolve to circumvent interference with release of bacteria from the phagosome. In fact $InlA^{wt}$ seems to be largely optimized, at least under *in vitro* conditions using Caco2 cells where the amount of apically exposed E-cadherin is drastically increased, compared to the *in vivo* situation.

3.4.6 Creating the isogenic listerial strain Lmo-$InlA^{m}$

To circumvent limitation in expression levels of invasion proteins (see above) a listerial strain carrying only the two substitutions S192N (TCT → AAC) and Y369S (TAT → TCG) in an otherwise unmodified genome was created. The pAUL-A-*inlA*^{m}-*inlB*$^{5'}$-*gfp* integration vector, bearing full-length *inlA*^{m} and the 5' part of *inlB* fused to *gfp*, was transformed into the in frame *inlA* deletion strain *L. monocytogenes* Δ*inlA*2. The vector integrates into the genome via homologous recombination either upstream of the Δ*inlA* gene (vector attachment site: Δ*inlA*, Figure 3.4-5A) or in between Δ*inlA* and full-length *inlB* (vector attachment site: 5' part of *inlB*, Figure 3.4-5B). Selection of integrated clones was achieved by growth at 42°C where no

extra-chromosomal replication of the vector occurs using the temperature sensitive origin of replication of pAUL-A (Figure 3.4-5C).

After purification, one clone of either integration site (clones 5_1 and 8_2 in Figure 3.4-5C) was used to perform reversion via homologous recombination as described (see 2.4.4 on page 27). Several reversed clones were obtained and one of them (clone 2 in Figure 3.4-5D, derived from clone 8_2 in Figure 3.4-5C) was further analyzed and characterized to establish correct reversion.

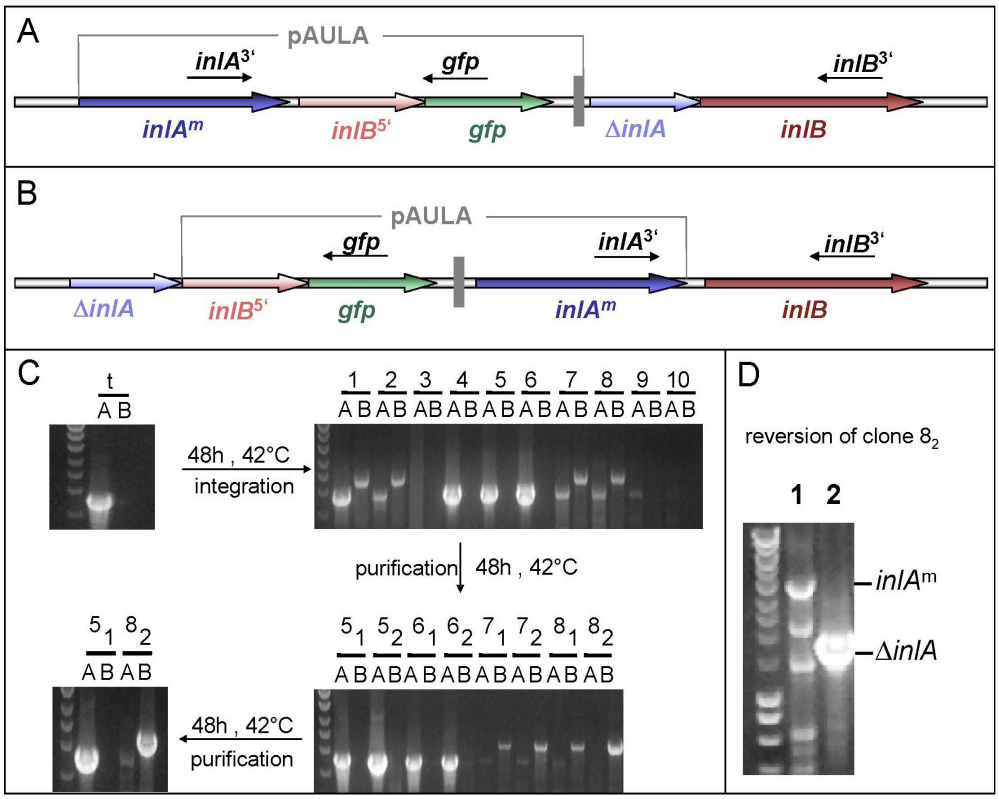

Figure 3.4-5: Creation of the isogenic mutant strain Lmo-InlA^m. Schematic representation of the two possible integration scenarios via homologous genomic sequences of Δ*inlA* (light blue, **A**) or *inlB* (brown, **B**). pAUL-A vector (grey bar and grey lines) bearing full-length *inlA*^{m} (dark blue) and the 5'part of *inlB* (light red) fused to gfp (green) is either integrated upstream of the genomic Δ*inlA*-*inlB* locus (**A**) or in between Δ*inlA* and *inlB* (**B**). PCR product of primer pair *inlA*$^{3'}$ and *gfp* (**A**) indicates the presence of unintegrated vector or vector, integrated via *inlA*-homology (**A**). The PCR product of the *inlA*$^{3'}$ and *inlB*$^{3'}$ primer pair is specific for the vector, integrated via *inlB*-homology (**B**). (**C**) The vector was transformed into Lmo-Δ*inlA*2 (t, PCR product with primer pair *inlA*$^{3'}$ and *gfp*, denoted A). Clones with integrated vectors were selected by growth at 42°C. Ten potential candidate clones were analyzed; numbers 1, 2, 7 and 8 carry the vector integrated via *inlB* as shown in **B** and numbers 4, 5, 6 and 9 either the non-integrated vector or vector integrated via Δ*inlA* as shown in **A**. Purification of clones 5 to 8 by growth at 42°C, two subclones were analyzed as indicated. Clone 5_1 and 8_2 were further purified by growth at 42°C. (**D**) Reversion of the vector yield either the original strain Lmo-Δ*inlA*2 (2) or the isogenic strain Lmo-InlA^m (1). PCRs were performed with primers *inlA*$^{3'}$ and *inlB*$^{3'}$ and yield characteristic fragment sizes for *inlA*^{m}-*inlB* (4.0 kbp) and Δ*inlA*-*inlB* (1.8 kbp) as indicated.

3.4.7 Expressional analysis of Lmo-InlA^m

The correct reversion of pAUL-A to create Lmo-InlA^m was confirmed by sequencing the entire *inlAB*-locus. Expression levels of InlA and InlB in Lmo-InlA^m were semi-quantitatively analyzed using Western-blots and ActA as loading control. ActA-expression, like that of InlA and InlB, is regulated by the transcriptional activator PrfA. The chemo-luminescence intensities of bands corresponding to InlA, InlB, or ActA were integrated and the relative protein amount was calculated with respect to the ActA-intensity (relative amount = 1). Both strains, Lmo-EGD and Lmo-InlA^m, express equivalent amounts of the two invasion proteins InlA and InlB. Reconstituting the *inlAB* locus avoids changes in expression levels so that reliable conclusions can be drawn from the experimental data using the isogenic mutant strain.

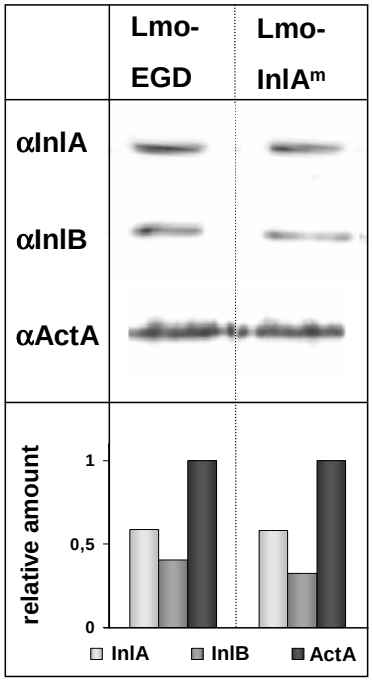

Figure 3.4-6: Western blot of whole cell lysates of Lmo-EGD and Lmo-InlA^m. Both invasion proteins were stained with monoclonal antibodies against InlA (αInlA) and InlB (αInlB), respectively. PrfA-regulated ActA was stained with a monoclonal antibody against ActA (αActA) and served as loading control. The diagram shows a semiquantitative analysis of chemiluminescence-intensity (Fujifilm LAS-3000 imager and Aida image analyzer software). Intensities of InlA and InlB are normalized against ActA-intensity (relative amount = 1). Equivalent amounts of both invasion proteins were expressed by Lmo-EGD and Lmo-InlA^m. The results confirm the reconstitution of the *inlAB* locus of the isogenic mutant after vector reversion (see 2.4.4 on page 27).

3.4.8 Adhesion and invasion of Lmo-InlA^m

Binding of InlA to human E-cadherin induces listerial uptake into human epithelial cells by the zipper mechanism (Cossart and Sansonetti, 2004), requiring localized rearrangements of the cytoskeleton as well as a physically tight interaction between bacterium and eukaryotic cell membrane. To establish whether improved affinity of InlA^m for its receptor results in stronger adhesion of Lmo-InlA^m, its adhesion to the E-cadherin expressing human epithelial cell line Caco2 was analyzed. A two-fold increase in adhesion efficiency of Lmo-InlA^m, compared to wild-type bacteria (Figure 3.4-7A) was observed.

To investigate the link between improved adhesion of Lmo-InlA^m and bacterial uptake gentamicin protection invasion assays (Elsinghorst, 1994) were used. A doubling in the number of internalized bacteria when expressing InlA^m compared to InlA^{wt} (Figure 3.4-7B) indicates that invasion is predominantly caused by improved adhesion of Lmo-InlA^m to Caco2 over Lmo-EGD.

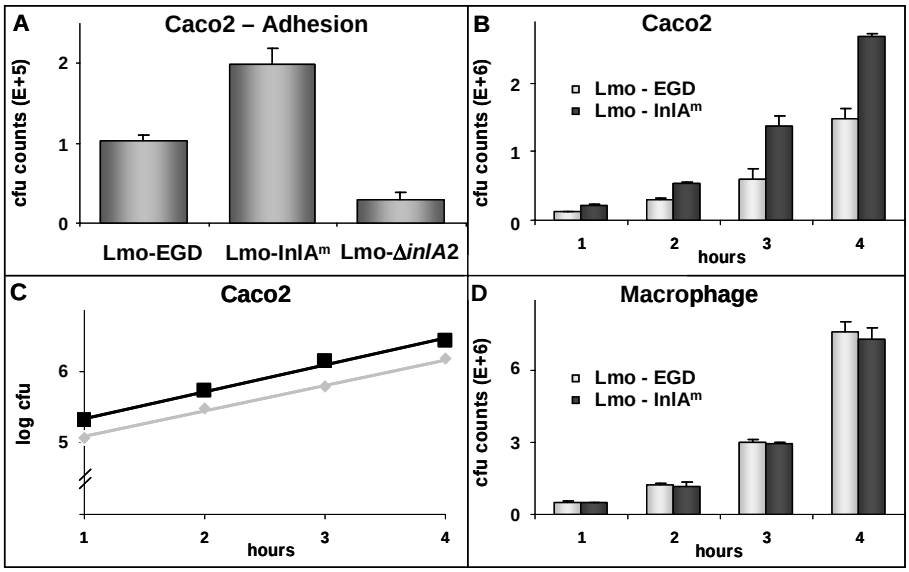

Figure 3.4-7: Adhesion and invasion of Lmo-InlA^m and Lmo-EGD with InlA-dependent and –independent mechanisms. (**A**) Adhesion assay. Confluent layers of Caco2 cells were infected with Lmo-EGD, Lmo-Δ*inlA*2 or Lmo-InlA^m for 30 min. Cells were washed extensively and lysates were plated onto BHI-agar plates. (**B-C**) Intracellular growth curve of Lmo-EGD and Lmo-InlA^m in Caco2 cells. Extracellular bacteria were killed after one hour by gentamicin. Intracellular bacteria were quantified after 1 to 4 hours by plating cell lysates onto BHI agar plates. (**B**) Observed cfu-values. (**C**) The mean bacterial doubling time is 50 ± 4 min (gradient of the linear log cfu plotted against time). (**D**) Intracellular growth curve of Lmo-EGD and Lmo-InlA^m in the macrophage-like cell line J774 were uptake is InlA-independent. Cells were infected for 30 min and intracellular bacteria were quantified after 1 to 4 hours. All observed cfu-values were corrected for differences in the starting inoculum. Data show one representative of three independently performed experiments.

Following phagocytosis, bacteria need to escape from the phagosome to avoid lysosomal degradation. To rule out that factors after phagocytosis affect the observed increase in

intracellular bacteria, intracellular growth-rates of Lmo-EGD and Lmo-InlA^m were analyzed. A plot of cfu against time (Figure 3.4-7B) indicates a similar exponential increase for both Lmo-EGD and Lmo-InlA^m. A logarithmic plot (Figure 3.4-7C) reveals the replication time of both strains to be 50 ± 4 min (gradient). The re-engineering of InlA therefore predominantly affects the process of listerial adherence, while uptake, phagosomal escape, intracellular replication rates and cell-to-cell spread appear unaltered.

As a control, intracellular growth curves of both strains in the professionally phagocytic, macrophage-like cell-line J774 were analyzed. Uptake into these cells is InlA-independent (Dramsi *et al.*, 1997). Correspondingly, indistinguishable invasion efficiencies and intracellular replication times of 46 ± 3 min for both strains (Figure 3.4-7D) were observed. InlA-independent pathophysiological characteristics of Lmo-EGD thus remain unaltered in Lmo-InlA^m.

3.4.9 Immunofluorescent staining of intracellular Lmo-EGD and Lmo-InlA^m

To analyze the intracellular phase of Lmo-EGD and Lmo-InlA^m in more detail, immunofluorescent stainings of infected Caco-2 cells were performed. To establish, whether a co-localization between InlA^{wt} or InlA^m and E-cadherin is detectable, invading bacteria were incubated with antibodies specific for each protein and stained with secondary antibodies, labeled with fluorescence-dyes. Different infection times were analyzed, but even as early as 30 min post infection co-localization could not be detected (Figure 3.4-8A and B). This would indicate that InlA is rapidly turned over, releasing the biophysically stable InlA^m/E-cadherin complex from the surface of bacteria. Surprisingly, all infected cells revealed altered E-cadherin distributions independent on the bacterial strain. Normally, E-cadherin is confined to cell-cell-junctions creating sharp rim-like fluorescence at the cell membrane (Figure 3.4-8I) associated with β-Catenin (Figure 3.4-8J). In infected cells, E-cadherin is delocalized and accumulates at sites of bacterial invasion (Figure 3.4-8A-D and I-J). Co-staining E-cadherin and F-actin (using fluorescent phalloidin) confirmed E-cadherin to be associated with the actin-network at cell-cell-contacts (Figure 3.4-8C-D). In infected cells, however, the re-arrangement of E-cadherin similarly influences the distribution of F-actin (Figure 3.4-8C-D). Staining of InlA and actin (Figure 3.4-8E-F) revealed a co-localization of actin and InlA near *L. monocytogenes*, demonstrating that InlA is still expressed after ActA expression has been

initiated and F-actin accumulates at the surface. As a control, we co-stained ActA and actin and observed a co-localization as expected (Figure 3.4-8G-H).

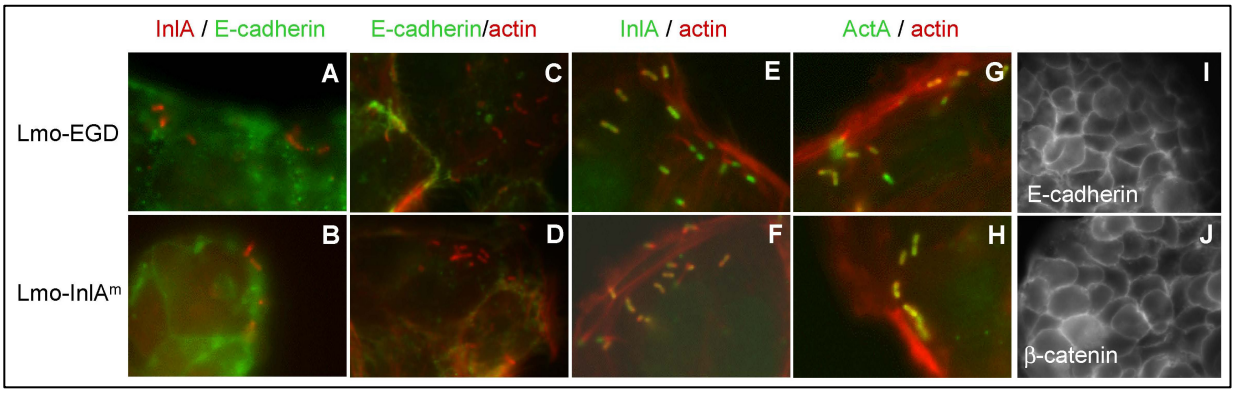

Figure 3.4-8: Immunofluorescent staining of Caco2 cells infected with Lmo-EGD or Lmo-InlA^m. Infected cells were stained as indicated with mono- or polyclonal antibodies against InlA, E-cadherin, ActA or with phalloidin to stain F-actin. Images were merged to identify co-localization of indicated molecules (A-F). Colors of labels correlate with colors of images (A and B staining of InlA and E-cadherin; C-D: E-cadherin and actin; E-F: InlA and actin; G-H: ActA and actin; I: E-cadherin and J: β-catenin. Cells in I-J are not infected).

3.5 Modifying binding specificity

The dramatic increase in binding affinity of InlA^m for hEC1 may potentially not only affect the invasiveness of *L. monocytogenes* into cells expressing human E-cadherin. Instead an improved affinity could compensate structural limitations in recognition of E-cadherins from other species. Mapping amino acids of available E-cadherin sequences that deviate from the human sequence onto the InlA/hEC1 complex could indicate those most likely to be responsible for preventing recognition by InlA. A sequence alignment and a phylogenetic tree of E-cadherin sequences of different species (Figure 3.5-1) confirms that the EC1 domain is highly conserved, but that some residues involved in InlA-recognition have been substituted. Rabbit EC1 is most similar to hEC1 (Figure 3.5-1) with no substitutions in residues required in InlA-recognition. Increased affinity of InlA^m for hEC1 therefore presumable applies to rabbit EC1 as well.

Bovine, mouse and rat EC1 belong to one subtree, whereas the crucial Pro16Glu mutation that efficiently prevents binding by InlA in murine EC1 (Lecuit *et al.*, 1999) is only present in mouse and rat EC1 domains. In bovine EC1, Asn20$_{hEC1}$ is replaced by serine. As Asn20$_{hEC1}$ is involved in water mediated H-bonds to InlA, serine can presumably substitute for asparagine without affecting binding affinity for InlA significantly. A more critical substitution, also

present in mouse and rat EC1, is the replacement of $Glu64_{hEC1}$ by glutamine. In InlA/hEC1 $Glu64_{hEC1}$ forms a water-solvated salt-bridge to $Arg85_{InlA}$, stabilizing the complex. Replacing glutamate by glutamine changes the salt-bridge into a hydrogen bond, potentially reducing the binding affinity. Additionally, $Asp29_{hEC1}$ involved in Ca^{2+}-coordination is exchanged against glutamate in bovine EC1. As $Asp29_{hEC1}$ is only involved in water-mediated interactions with Ca^{2+}, this substitution could allow for direct Ca^{2+}-coordination, potentially strengthening the affinity for InlA. Correspondingly, cattle are found to be susceptible for orally acquired listeriosis (Pohl *et al.*, 2006), indicating that these three mutations together reduce binding affinity of InlA to a lesser extent.

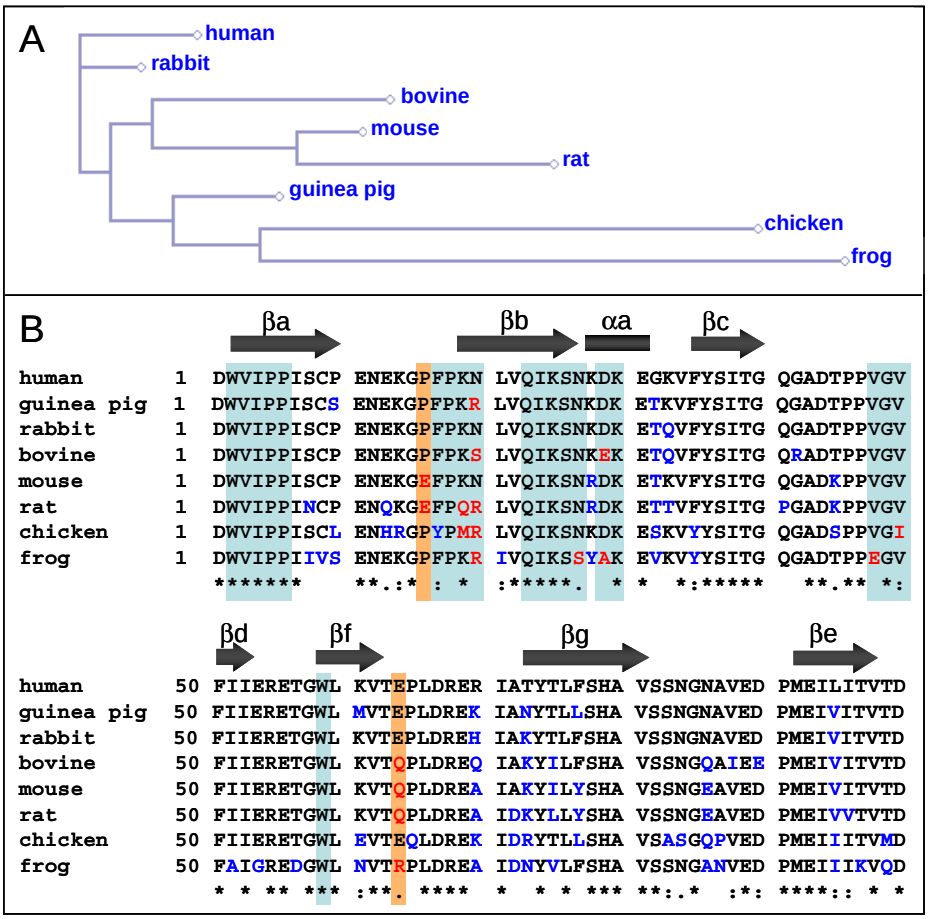

Figure 3.5-1: Sequence alignment of EC1-domains from different species. (A) Based on the sequence alignment derived phylogenetic tree. Rabbit EC1 is most similar to hEC1. **(B)** Sequence alignment. Blue background color: regions involved in InlA recognition, orange: key residues for InlA recognition but frequently substituted in non-human species. Red / blue characters: mutations within regions involved / not involved in InlA recognition. Symbols beneath alignment: ★ conserved residues, **:** and **.** indicate conservative and semiconservative substitution, respectively. No symbol indicates non-conservative substitutions.

In guinea pig EC1 only one residue involved in InlA recognition, $Asn20_{hEC1}$, is replaced by unrelated arginine. $Asn20_{hEC1}$ only creates water-mediated contacts to InlA leaving space to

accommodate the larger side chain of arginine without steric clashes. In fact, this substitution could be advantageous in terms of binding affinity to InlA because arginine matches a corresponding negative charge to $Asp279_{InlA}$, potentially creating a direct salt bridge.

Chicken and frog EC1 domains are evolutionarily remote from human EC1 and carry a number of mutations involved in InlA-recognition. As in bovine EC1, the substitution Asn20Arg is also present in chicken EC1. In addition, $Lys19_{hEC1}$, involved in coordination of the bridging Cl^- ion in the vicinity of the stabilizing Ca^{2+} ion is replaced by methionine. This substitution may interfere with stabilization of these two bridging ions and potentially decreases complex stability. Frog EC1, evolutionarily most distant from hEC1 includes numerous substitutions of key-residues of InlA-recognition. These would be certain to prevent complex formation.

An extended $InlA^m$ specificity allowing recognition of formerly incompatible EC1-domains requires amino acids targeted by newly created contacts from $InlA^m$, including the backbone of Phe17-Pro18 and Asn27, to be conserved. The substitution of $Pro16_{hEC1}$ by glutamate in murine EC1 potentially changes the width of the loop bearing Phe17 and Pro18 interfering with the interaction of the modified residue Asn192 of $InlA^m$. The second target site involving Asn27 is conserved in EC1 domains. Only frog EC1 carries a serine at position 27, weakening or preventing stabilization via $Ser369_{InlA}$.

Taken together the alignment confirms that guinea pig, rabbit and cattle are susceptible to orally acquired listeriosis due to EC1-variants that are recognized by $InlA^{wt}$, whereas the other species analyzed are not. Improved affinity of $InlA^m$ may be expected for all non-permissive and permissive species. A change of host tropism, however, needs to be investigated for each species. We have restricted our analysis to murine E-cadherin, due to the widespread interest in a murine model of human listeriosis.

3.5.1 Recognition of murine E-cadherin by $InlA^m$

The most striking effect of re-engineered $InlA^m$ would be a changed binding specificity of $InlA^m$, resulting in recognition of previously incompatible murine EC1 (mEC1), thereby extending the host range of *L. monocytogenes* to create a versatile model of orally acquired listeriosis *in vivo*. To analyze this, mEC1 (residues 1-105) was cloned from a c-DNA library into the pGEX-expression vector (see 2.1.1 on p. 19) and the protein was expressed and purified as described (see 2.1.2 on p. 20).

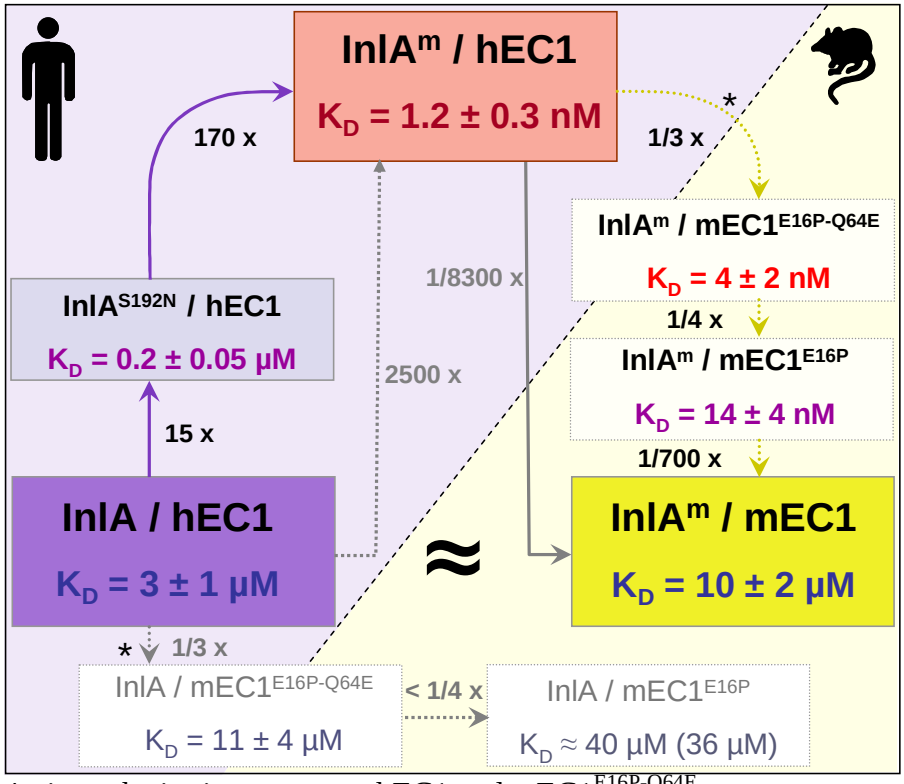

Figure 3.5-2: Re-engineering the interaction of InlA and E-cadherin. Colored boxes represent protein complexes and their dissociation constants (K_D). Shades of violet to red indicate complexes involving human E-cadherin (hEC1), shades of yellow and white complexes involving murine E-cadherin (mEC1). Two substitutions in InlA generate $InlA^{S192N}$ and $InlA^{S192N-Y369S}$ ($InlA^m$) increasing binding affinity for hEC1 15- and 170-fold (together 2500-fold), while the eleven substitutions separating hEC1 and mEC1 reduce binding affinity of $InlA^m$ 8300-fold. Coincidentally, binding affinities of InlA/hEC1 (dark violet) and $InlA^m$/mEC1 (yellow) are similar. Substituting Pro16 by glutamate ($mEC1^{E16P}$) results in weaker binding affinity by $InlA^m$ and wild-type InlA than for hEC1, while doubly substituted $mEC1^{E16P-Q64E}$ is recognized with an affinity more closely resembling that of InlA and hEC1, indicating improved humanization of mEC1 (white boxes).

Analyzing the affinity of the $InlA^m$/mEC1 complex reveals the dissociation constant to be K_D = 10 ± 2 µM (Figure 3.5-2). Though weak, the binding affinity closely matches the K_D = 3 ± 1 µM for $InlA^{wt}$/hEC1. By introducing two additional contacts to EC1, unfavorable interactions of $Glu16_{mEC1}$ and the hydrophobic pocket of $InlA^m$ are entirely compensated. Apart from the previously identified substitution of $Pro16_{hEC1}$ by glutamate (Lecuit *et al.*, 1999) and its role in restricting host tropism of *L. monocytogenes*, the sequence alignment (Figure 3.5-1) indicated a second substitution in mEC1 that could potentially interfere with InlA-recognition. The exchange of $Glu64_{hEC1}$ by glutamine replaces a salt-bridge to $Arg85_{InlA}$ by a hydrogen bond (see above). To determine the contributions of either substitution to loss of binding affinity we analyzed dissociation constants of both $InlA^{wt}$ and $InlA^m$ for the mEC1-variants $mEC1^{E16P}$ and $mEC1^{E16P-Q64E}$, respectively (Figure 3.5-2).

3.5.2 A second determinant of binding affinity

The substitution of $Pro16_{hEC1}$ by $Glu16_{mEC1}$ clearly dominates the host tropism of *L. monocytogenes* (Lecuit *et al.*, 2001). Genetically replacing $Glu16_{mEC1}$ by proline in mice has been proposed as a route to create a new animal model rendering all E-cadherin expressing cells susceptible to InlA-mediated entry (Lecuit, 2005). Analyzing the affinity of InlA for $mEC1^{E16P}$ biophysically, we find the interaction to be exceedingly weak ($K_D \approx 40$ µM) preventing its unambiguous quantification. Using the high affinity variant $InlA^m$ we estimate the binding affinity as follows: $InlA^m$ binds $mEC1^{E16P}$ with a $K_D = 14 \pm 4$ nM (Figure 3.5-2) confirming the dominant effect (factor of 700) of the Glu16Pro substitution. The ten remaining substitutions in mEC1 (Figure 3.5-1) contribute a factor of ~12 (Figure 3.5-2). Provided the changes are largely additive, the K_D for InlA/$mEC1^{E16P}$ would be ~12 x K_D = 3 µM (InlA/hEC1) or ~36 µM (Figure 3.5-2), demonstrating the upper level revealed by ITC (40 µM) to be correct.

The second substitution in mEC1, involved in $InlA^m$ recognition is the substitution of $Glu64_{hEC1}$ by glutamine which replaces a salt bridge to $Arg85_{InlA}$ by a hydrogen bond. Reverting this substitution in $mEC1^{P16E}$ produces $mEC1^{P16E-Q64E}$ with an affinity of $K_D = 4 \pm 2$ nM for re-engineered $InlA^m$ (Figure 3.5-2) or $K_D = 11 \pm 4$ µM for $InlA^{wt}$ – similar to that of InlA/hEC1 (K_D = 3 µM). A transgenic mouse bearing both the substitutions Glu16Pro and Gln64Glu in murine E-cadherin could therefore represent a system more closely resembling the human situation than the singly substituted protein.

The binding affinity of humanized $mEC1^{E16P-Q64E}$ for $InlA^{wt}$ or $InlA^m$ is, however, three-fold weaker than that of the hEC1-complexes, respectively, indicating that other substitutions may interfere with InlA-recognition. The nine remaining substitutions, discriminating $mEC1^{E16P-Q64E}$ from hEC1, are solvent exposed in the recognition complex, excluding the possibility that they directly interfere with InlA recognition. To exclude, that these substitutions impede InlA recognition structurally we solved the structure of the rationally created recognition complex $InlA^m$ / mEC1.

3.5.3 Atomic view on host specificity

Having identified biophysical contributions of single amino acid substitutions between hEC1 and mEC1 on InlA recognition, their structural influence remains unclear. To analyze the

structural homology to InlA/hEC1 we solved the high resolution crystal structure of the InlA^{m}/mEC1 complex. Data collection and refinement statistics are shown in Table 3.5-1. Superimposing, the InlA^{m}/mEC1 structure with the previously solved InlA/hEC1 structure (Schubert *et al.*, 2002) revealed the overall complex architecture to be essentially unchanged (r.m.s.d. for main-chain atoms ~0.7 Å). In addition, the hydrogen bonds introduced to strengthen the interaction of InlA/hEC1 (see above) are retained in InlA^{m}/mEC1, explaining the altered specificity of InlA. Differences between InlA/hEC1 and InlA^{m}/mEC1 most noticeably involve residues 16 of hEC1 and mEC1 and their immediate neighborhood. Pro16$_{hEC1}$ adopts a strained cis-conformation optimally positioning its side chain within a hydrophobic binding pocket of InlA (Figure 3.5-3C). Glu16$_{mEC1}$ of the engineered complex, by contrast, adopts a relaxed trans-conformation permitting the backbone to move aside to accommodate the longer glutamate side chain.

Table 3.5-1: Data collection and refinement statistics of the InlA^{m}/mEC1 complex. Numbers in parenthesis correspond to values of the highest resolution shell.

	InlA$^{S192N-Y369S}$/mEC1
Data collection[1]	
Space group	$P2_1$
Cell constants	
a, *b*, *c* (Å)	55.4, 113.0, 55.7
α, β, γ (°)	90.0, 101.3, 90.0
Resolution (Å)	50-1.85 (1.92-1.85)
R_{merge} (%)	7 (33)
I / σ_I	14 (3)
Completeness (%)	94 (85)
Redundancy	4 (3)
Refinement	
Resolution (Å)	1.85
No. reflections	50581
R_{work} / R_{free} (%)	17 / 20
No. atoms	
Protein	4784
Ca^{2+}/Cl^-	4 / 1
Water	893
B-factors mean	19
Wilson	22
R.m.s deviations	
Bond lengths (Å)	0.016
Bond angles (°)	1.7

Compact Pro16$_{hEC1}$ binds into a pre-shaped binding groove of InlA creating one of the key interactions between these two proteins (Schubert *et al.*, 2002). Unexpectedly, the carboxylate of Glu16$_{mEC1}$ occupies the same hydrophobic pocket of InlA as Pro16$_{hEC1}$ in InlA/hEC1 (Figure 3.5-3C).

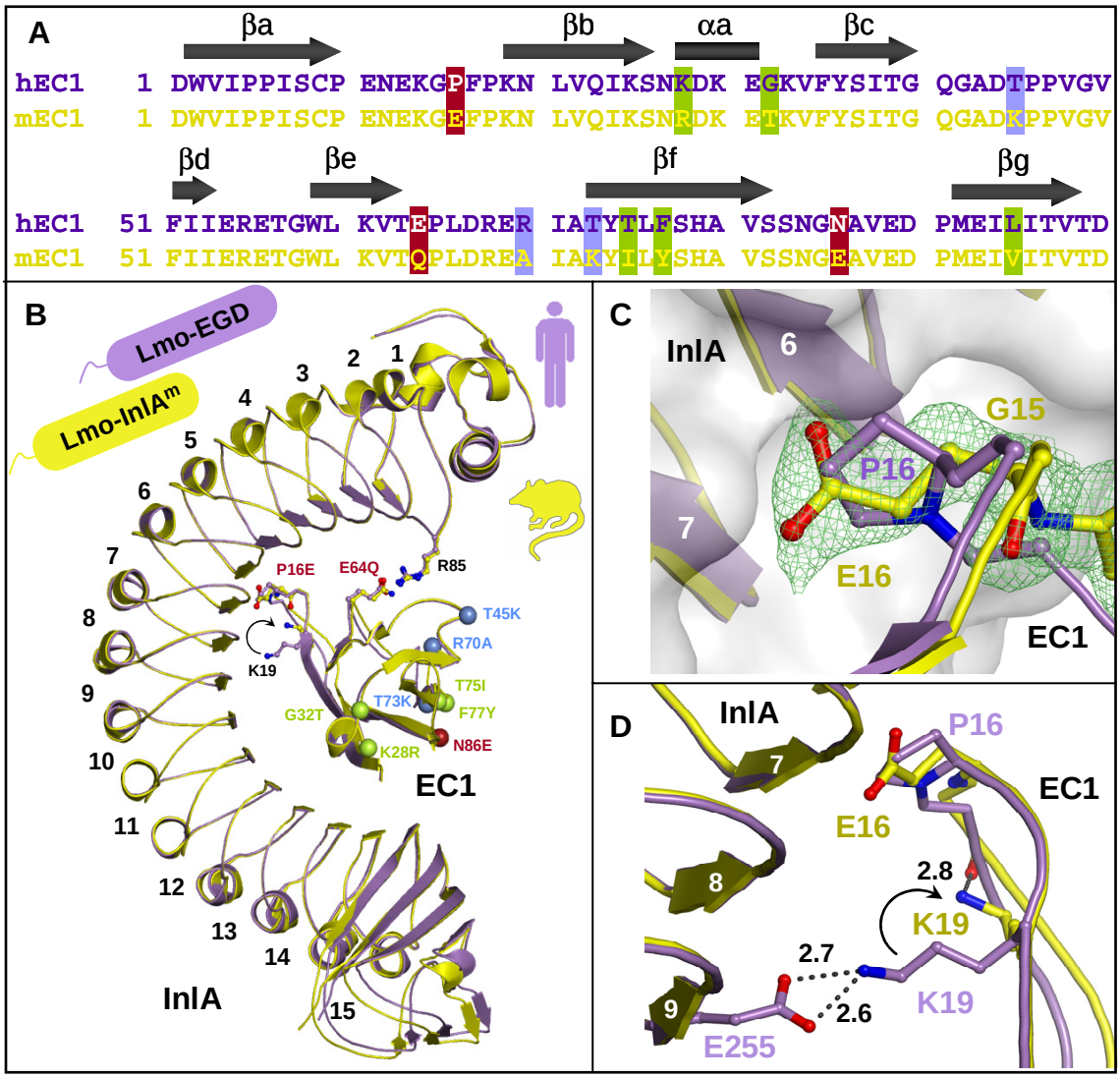

Figure 3.5-3: Comparison of InlA/hEC1 (human, violet) and InlAm/mEC1 (murine, yellow) complexes. (**A**) Sequence alignment of the N-terminal, extracellular domains (EC1) of human (hEC1, violet) and murine (mEC1, yellow) E-cadherin. Sequence differences involving charged residues are marked in red and blue, all others in green. (**B**) Superposition of both protein complexes. LRRs are numbered. Critical residues are shown as ball-and-stick, solvent-exposed substitutions as spheres (colors as in **A**). (**C**) Hydrophobic $Pro16_{hEC1}$ (violet) is accommodated in a hydrophobic pocket of InlA. The carboxylate of $Glu16_{mEC1}$ (yellow), well defined in the $2F_O$-F_C difference electron density (green, contoured at 1σ), is forced to occupy the same pocket. (**D**) $Lys19_{hEC1}$ forms a favorable salt bridge to InlA. Trans-$Glu16_{mEC1}$ repositions $Lys19_{mEC1}$, trapping its side chain through an intramolecular H-bond (arrow).

Disrupting the optimal fit of $Pro16_{hEC1}$ and its binding pocket alone would reduce the binding affinity significantly. Forcing a charged carboxylate into this low dielectric environment, however, exponentially increases the unfavorable effect of the lost surface complementarity, even if the carboxylate is protonated during binding. $Glu16_{mEC1}$ additionally induces a local re-arrangement involving $Lys19_{mEC1}$ repositioning it away from a salt bridge to $Glu255_{InlA}$ observed in InlA/hEC1 (Schubert *et al.*, 2002). The 700-fold reduced binding affinity for InlA

is thus not exclusively due to the disparate physical properties of glutamate and proline but also due to local adjustments within EC1 (Figure 3.5-3D).

Although weakening the interaction of $InlA^m$ and mEC1, $Gln64_{mEC1}$ adopts the same conformation as $Glu64_{hEC1}$, replacing the ionic interaction to $Arg85_{InlA}$ of the wild-type complex by a hydrogen-bond (Figure 3.5-3B). The other nine mutations (Figure 3.5-3A and B), solvent exposed during complex formation, have no influence on the structure or spatial orientation of residues, involved in InlA recognition.

3.5.4 *In vitro* analysis of changed host tropism

To see, whether recognition of the functional domains $InlA^m$ and mEC1 permits Lmo-$InlA^m$, isogenetically expressing full-length $InlA^m$ in an otherwise unmodified genetic background, to induce uptake into murine E-cadherin expressing cells, gentamicin protection invasion assay were performed (see 2.5 on p. 30). As mentioned previously, most cell-lines down-regulate E-cadherin expression during immortalization. The number of cell-lines expressing sufficient amounts of E-cadherin to investigate InlA-dependent entry is therefore severely limited. MCA-3D, derived from epidermal tissue of BALB/c mice (Navarro *et al.*, 1991), is the only murine cell line currently available that expresses appreciable amounts of murine E-cadherin.

Analyzing the invasion potential of wild-type bacteria (Lmo-EGD) in MCA-3D cells revealed that uptake is surprisingly efficient, despite InlA being non-functional (Figure 3.5-4). Correspondingly, the invasion efficiency of Lmo-Δ*inlA*2 is found to be indistinguishable from that of wild-type bacteria (Figure 3.5-4). Only the deletion of both invasion proteins (Lmo-Δ*inlAB*2) or LLO (Lmo-Δ*hly*), which is essential for release of bacteria from the phagosome, reduces invasion efficiency significantly. To quantify unspecific uptake of MCA-3D cells, the invasion of apathogenic *Listeria innocua* expressing LLO under the control of PrfA (*L. innocua + prfA + hly*) and hence permitting release of bacteria from the phagosome as in *L. monocytogenes*, was analyzed. Bacteria were unable to enter MCA-3D cells, indicating that unspecific uptake is absent in MCA-3D cells (Figure 3.5-4).

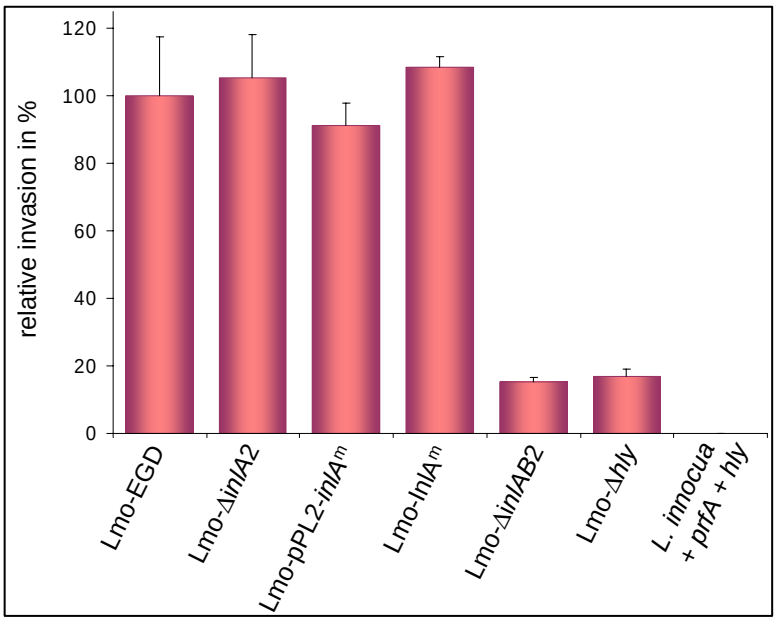

Figure 3.5-4: Invasion assays into murine E-cadherin expressing MCA-3D cells. Relative invasion compares invasion rates of different strains with that of the wild-type strain Lmo-EGD (= 100% invasion). Invasion rates of the in-frame deletion strains for InlA (Lmo-Δ*inlA*2), InlA and InlB (Lmo- Δ*inlAB*2) or LLO (Lmo-Δ*hly*) were analyzed. Additionally, the non-pathogenic strain *Listeria innocua* expressing PrfA and LLO (*L. innocua + prfA + hly*) was tested to determine the amount of unspecific uptake. Neither the complementation of the InlA-deletion with pPL2-*inlA*^{m} (Lmo-pPL2-*inlA*^{m}) nor isogenic expression of InlA^m (Lmo-InlA^m) improved uptake efficiency into MCA-3D cells.

Introducing functional InlA^m by either complementing the deletion with pPL2-*inlA*^{m} (Lmo-pPL2-*inlA*^{m}) or using the isogenic strain Lmo-InlA^m should increase uptake of bacteria by making a second route of invasion available. The invasion efficiency is, however, not increased in either strain. The significantly reduced invasiveness of the complemented strain Lmo- pPL2-*inlA*^{m}, presumably results from reduced expression levels of InlB, indicating InlB to be the dominant invasion protein.

To increase the sensitivity of the invasion assay for InlA-mediated bacterial uptake, murine fibroblast-like cells (L-cells), stably transfected with murine E-cadherin, have been used (Ozawa *et al.*, 1989). Endogenous E-cadherin expression is down-regulated in these cells, but due to the transfection with E-cadherin c-DNA they over-express E-cadherin, presumable enhancing their susceptibility for InlA-mediated uptake. However, the same problem arises, and invasion rates were almost identical as in MCA-3D cells.

3.6 Altered host tropism *in vivo*

To establish whether increased binding affinity of InlA^m for murine E-cadherin will allow infection of the murine intestine in a manner comparable to that of humans, C57BL/6J mice were infected intragastrically with both Lmo-EGD and Lmo-InlA^m. Because the bacterium is adapted to its murine receptor, any mouse strain could, in theory have been used for infection experiments.

In this work inbred C57BL/6J mice were chosen as these mice are known to be highly resistant to oral challenge with Lmo-EGD. Other, more susceptible mice (Cheers *et al.*, 1979; Munder *et al.*, 2005) are frequently used in other studies to decrease bacterial loads, necessary to establish systemic infections via the oral route (Czuprynski *et al.*, 2003). The reason for enhanced susceptibility of these mice is not known but presumably involves deficiencies in components of the innate immune response, mimicking an immunocompromized situation (Poltorak *et al.*, 1998).

Challenging C57BL/6J mice with $5•10^7$ to $5•10^{10}$ Lmo-InlA^m result in dose-dependent mortality rates (Figure 3.6-1). The median lethal dose is inferred to be ~$5•10^7$. By contrast, the highest achievable inoculum of $5•10^{10}$ of Lmo-EGD is lethal only for ~30% of infected mice (Figure 3.6-1, grey line). Lmo-InlA^m is thus at least three orders of magnitude more virulent in mice than wild-type Lmo-EGD.

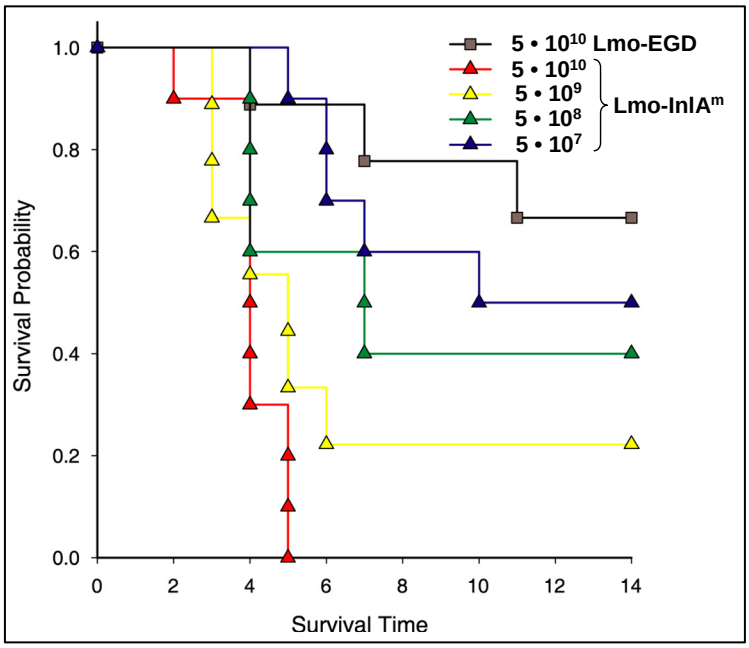

Figure 3.6-1: Survival curves of female C57BL/6J mice inoculated intragastrically with Lmo-EGD or Lmo-InlA^m. The highest achievable inoculum of $5 • 10^{10}$ cfu resulted in 30% or 100% lethality of Lmo-EGD (grey curve) or Lmo-InlA^m (red curve) infected mice. The LD_{50} of Lmo-InlA^m is inferred to be $5 • 10^7$ cfu. Lmo-InlA^m exhibit more than 1000-fold higher virulence than Lmo-EGD (n = 20 for each experiment).

To establish the route of infection of Lmo-InlA^m in mice, we analyzed the load of Lmo-InlA^m and Lmo-EGD in affected organs, following intragastric challenge with $1•10^{10}$ bacteria (Figure 3.6-2). In stomach and intestine, loads of Lmo-InlA^m and Lmo-EGD (Figure 3.6-2A-B) are largely comparable until day 2 post infection (p.i.). Thereafter Lmo-InlA^m loads increase strongly, while loads of Lmo-EGD remain constant.

In mesenteric lymph nodes, spleen and liver, bacterial loads of both strains increase until day 2 p.i. (Figure 3.6-2C-E). Lmo-EGD counts then stabilize in mesenteric lymph nodes, spleen and liver (infection controlled). In Lmo-InlA^m-infected mice, by contrast, stabilization of bacterial numbers is not observed. Instead bacteria loads increase exponentially in spleen and liver until day 4 p.i. (solid lines, Figure 3.6-2D-E) resulting in 1.000-fold higher bacterial numbers in spleen and liver in Lmo-InlA^m than Lmo-EGD on day 4 p.i. Bacterial counts in mesenteric lymph nodes diverge after day 2 p.i. but loads of Lmo-InlA^m increase more slowly than in liver and spleen.

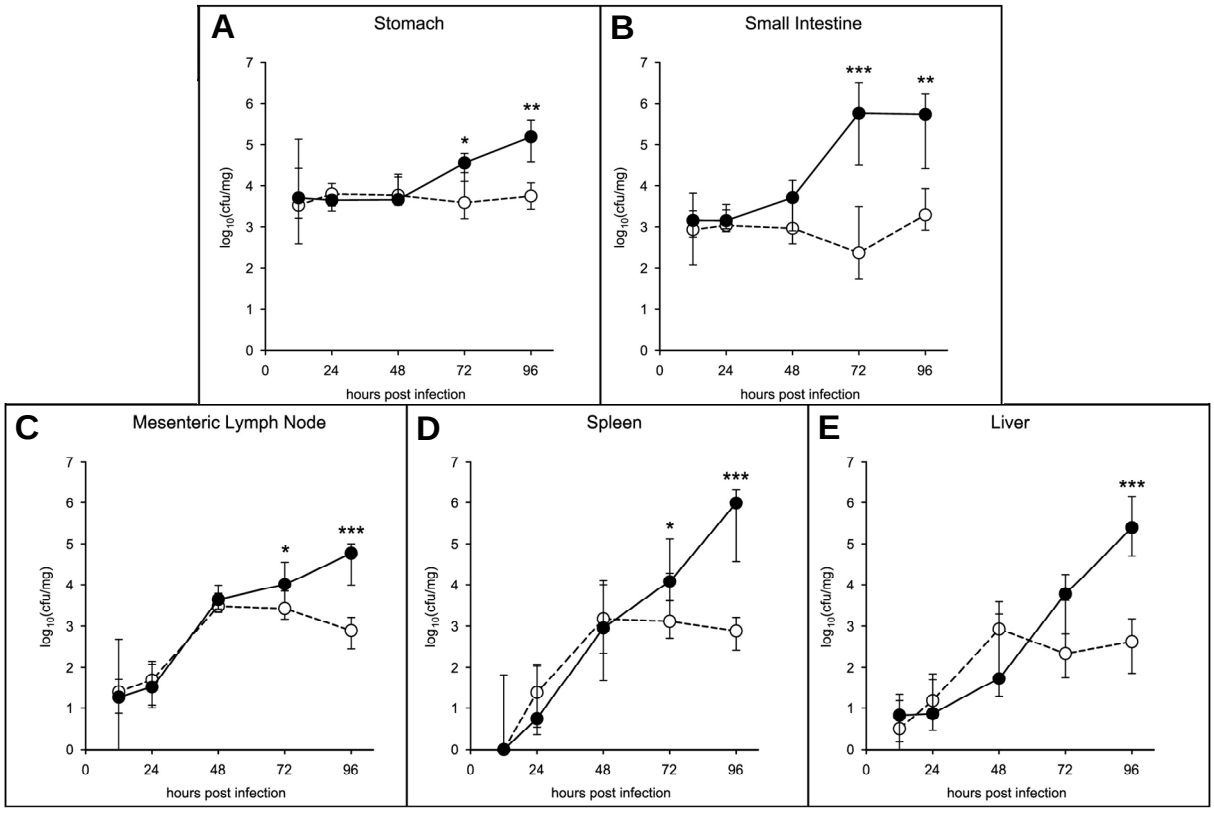

Figure 3.6-2: Organ loads of female C57BL/6J mice inoculated intragastrically with Lmo-EGD (dashed curve, ○) or Lmo-InlA^m (solid curves, ●). $1•10^{10}$ bacteria of either strain were administered intragastrically to analyze kinetics of bacterial growth (n = 6 for 24h p.i. and n = 12 for all others). Organ loads were ascertained at 5 time points in stomach (**A**), small intestine (**B**), mesenteric lymph nodes (**C**), spleen (**D**) and liver (**E**). All data are from two independent experiments. The bar represents the median for each time point and genotype, 95% confidence intervals are indicated. Statistical significance by Mann-Whitney-U non-parametric test: * P<0.05, ** P<0.01, *** P<0.001.

3.6.1 Histological analysis of InlA-dependent infection mechanisms

Histological and immunohistochemical studies of Peyer's patches of infected mice indicate that both Lmo-EGD and Lmo-InlA^m remain restricted to the dome and germinal centers inducing neutrophil infiltration and necrosis (Figure 3.6-3) with gradually increasing severity along the small intestinal axis. Colonization is, however, essentially indistinguishable until day 4 p.i. While the Lmo-EGD infection subsides after day 4 p.i., no such remission is observed for Lmo-InlA^m.

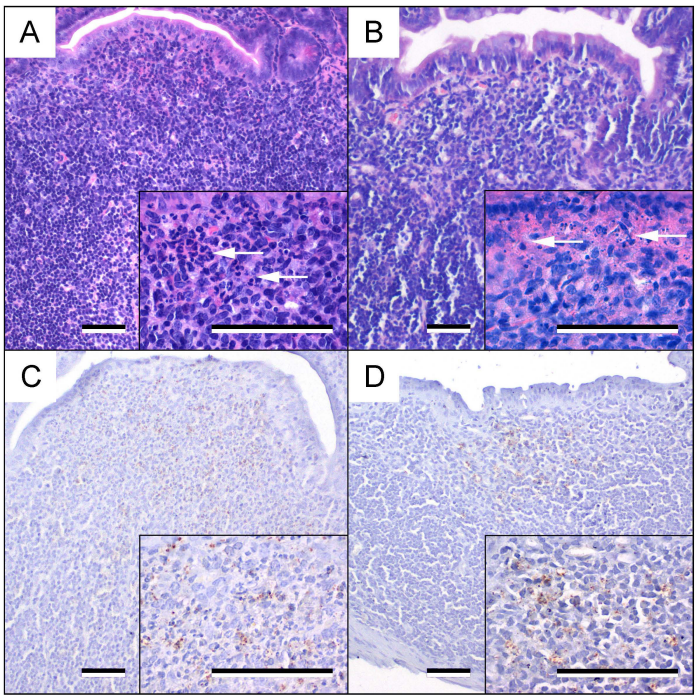

Figure 3.6-3: Histological and immunohistochemical analyses of Peyer's patches of either Lmo-EGD (left column) or Lmo-InlA^m (right column) infected mice. Mice were infected with $1.5 \bullet 10^{10}$ cfu of either strain and sacrificed 48 hours post infection. Necrosis and influx of granulocytes (**A**-**B**, H&E staining, arrows in **A** pointing to granulocytes, in **B** to necrotic cells) were comparable in Peyer's Patches of Lmo-EGD and Lmo-InlA^m infected mice. Similarly, colonization (**C**-**D**, anti Lmo-staining) of Peyer's patches by Lmo-EGD is indistinguishable from Lmo-InlA^m. Size bar (for all) = 100 µm.

Immunohistochemical analyses of the intestinal mucosa clearly demonstrate that Lmo-EGD do not invade epithelial tissue (Figure 3.6-4). Instead, bacteria are exclusively observed in the lumen or occasionally adhere to the surface of individual villi (Figure 3.6-4B, F, J) as late as day 4 p.i. (Figure 3.6-4N). Similarly, the intestinal tissue is fully intact without any signs of inflammation until day 3 p.i. (Figure 3.6-4A, E). Transient inflammatory response with enhanced mucus secretion and mild, local erosion of epithelium is present at day 4 p.i. (Figure 3.6-4I). The inflammation, however, subsides by day 5 p.i. (Figure 3.6-4M).

In Lmo-InlA^m infected mice, colonization of epithelia at villous tips are observed 24 h p.i. in the ileum (Figure 3.6-4D), rapidly spreading to extended areas of the epithelium and accumulating within the lamina propria (subepithelial tissue, Figure 3.6-4H, L, P). On day 4 p.i. high bacterial loads cause erosion of the epithelium and fusion of villi (Figure 3.6-4K, O). Lesions are more pronounced in the ileum than in the duodenum and jejunum.

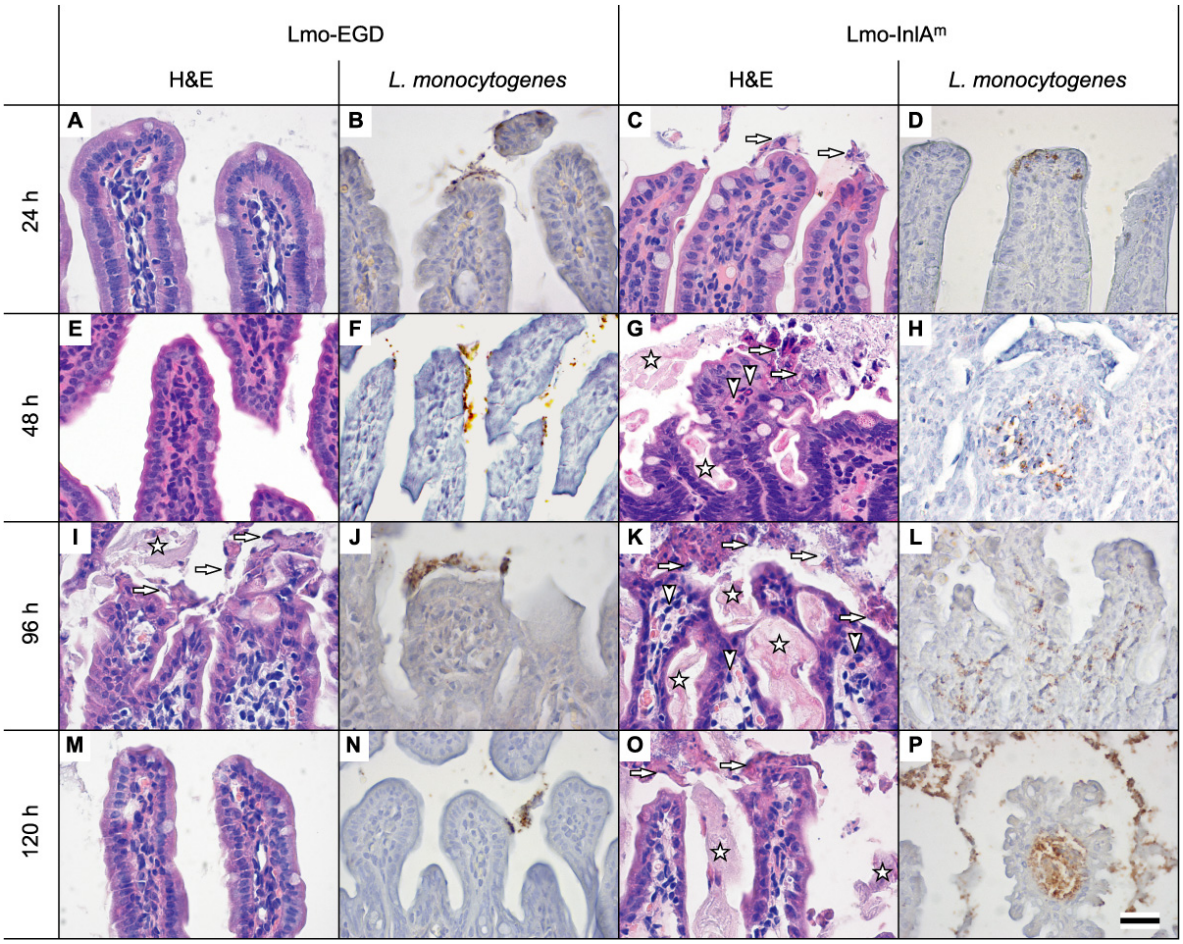

Figure 3.6-4: Histology and immunohistochemical detection of *L. monocytogenes* in the distal part of the small intestine of C57BL/6J mice 24, 48, 96 and 120 h after intra-gastric inoculation with $1.5 \bullet 10^{10}$ Lmo-EGD or Lmo-InlA^m. The intestinal epithelium was analyzed by H&E staining or anti-*Listeria* immunohistochemistry. (**A**) No lesions and no inflammatory response are seen 24 h p.i. in Lmo-EGD infected mice. (**I**) 96 h p.i., moderate inflammation is visible with mild apical epithelial cell necrosis (⇨) and increased secretion of mucus (☆). (**M**) 120 h p.i., the intestinal epithelium is fully regenerated. This correlates with anti-*Listeria* staining, where Lmo-EGD are located in the intestinal lumen, occasionally associated with villi surfaces, without detectable invasion (**B**, **F**, **J**, **N**). (**C**-**D**) 24 h p.i., Lmo-InlA^m infected mice reveal mild erosion of epithelial cells exclusively seen at tips of the villi (⇨). (**G**, **K**) 48 and 96 h p.i., widespread necrosis, loss of villous epithelial cells (⇨) and massive secretion of mucus (☆) are clearly visible. Neutrophils and lymphocytes (∇) infiltrate the villi. (**H**, **L**) These observations coincide with extensive colonization of the epithelium and deeper tissues (lamina propria) of villi by Lmo-InlA^m. (**O**) 120 h p.i., necrotic enterocytes are shed into the intestinal lumen (⇨). Overproduction of mucus (☆) and distortion of villous structures are also apparent. (**P**) This corresponds to extensive growth of Lmo-InlA^m in the epithelium and lamina propria. Size bar (for all) = 50 µm.

3.6.2 Role of InlA in systemic spread

To analyze the role of $InlA^m$ in systemic infections of internal organs independent of intestinal uptake, we inoculated mice intravenously (i.v.) with both low ($5•10^3$) or high ($2.4•10^4$) doses of Lmo-EGD or Lmo-$InlA^m$. In contrast to the oral route of infection, the survival rates for both strains are found to be indistinguishable for both bacterial doses (Figure 3.6-5A-B). Similarly, bacterial loads in mesenteric lymph nodes, spleen and liver at different time points after i.v. inoculation demonstrates comparable virulence of Lmo-EGD and Lmo-$InlA^m$ (Figure 3.6-5C-E).

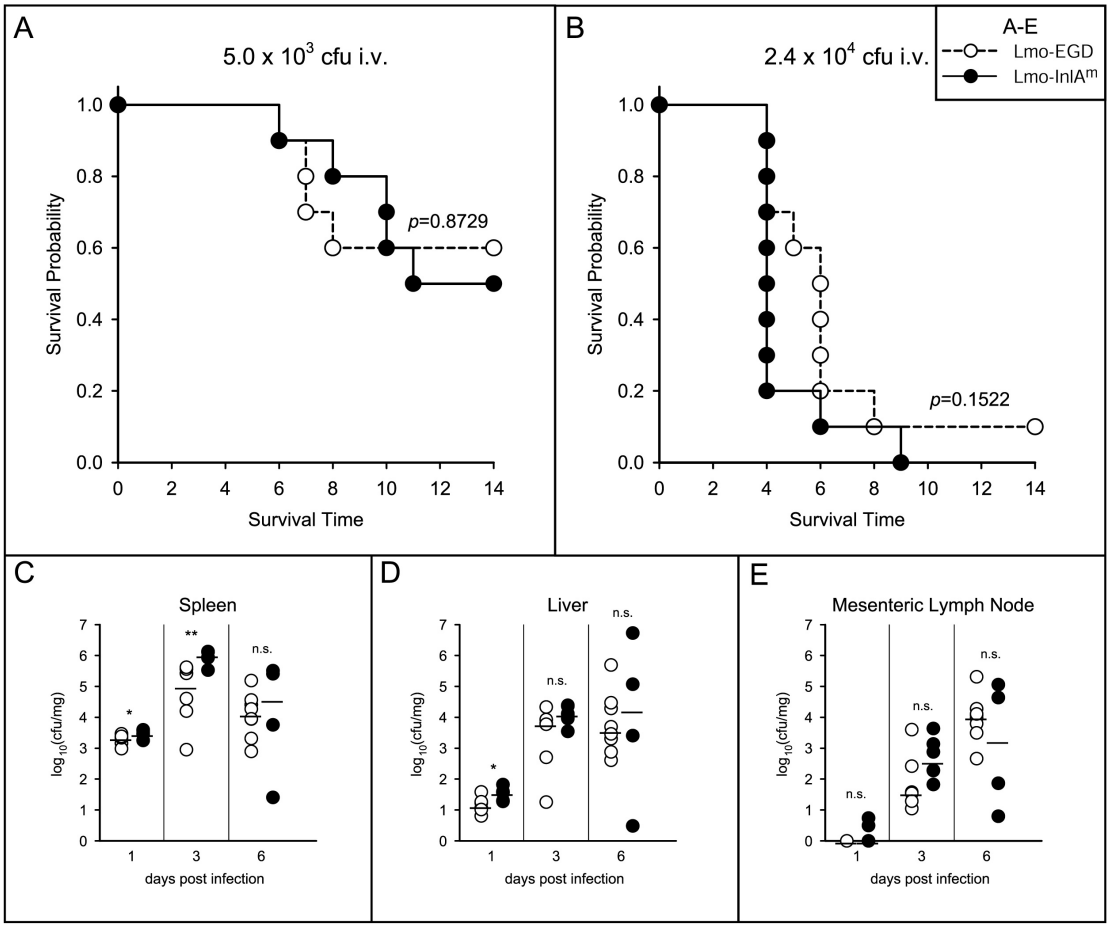

Figure 3.6-5: Survival curves (A-B) and organ loads (C-E) of female C57BL/6J mice infected intravenously with either Lmo-EGD (dashed curves, ○) or Lmo-$InlA^m$ (solid curves, ●). (A-B) The Lmo-$InlA^m$ strain exhibits no significantly higher virulence, compared to wild-type Lmo-EGD strain at low ($5.0•10^3$ cfu; **A**) and high ($2.4•10^4$ cfu; **B**) infection doses (n = 10). (**C**-**D**) Both strains were inoculated i.v. with $9•10^3$ bacteria to analyze entry of bacteria in deeper tissues without crossing the intestinal barrier. Organ loads (n = 6) were analyzed at 3 different time points in spleen (**C**), liver (**D**) and mesenteric lymph nodes (**E**). No appreciable enhanced virulence of the mutant strain Lmo-$InlA^m$ could be detected. Note, however, that a statistically insignificant trend to higher virulence of Lmo-$InlA^m$ is detectable in survival experiments, as well as in organ counts at days 3 and 6 p.i. Statistic evaluation as in Figure 3.6-2.

3.6.3 Blood-placental barrier

Lmo-EGD remains problematic to humans *inter alia* because of its ability to cross the blood-placental barrier, leading to sepsis or miscarriage. *Ex-vivo* experiments have shown that InlA-mediated entry into human placental trophoblasts is important in placental infection (Lecuit *et al.*, 2004). Studies of Lmo-EGD infected pregnant BALB/c mice (functional InlB, non-functional InlA, Le Monnier *et al.*, 2007) and guinea pigs (functional InlA and non-functional InlB, Bakardjiev *et al.*, 2004) indicate that InlA and InlB individually are insufficient to induce vertical transmission *in vivo*. They, however, confirm trophoblasts to be the primary target of Lmo-EGD.

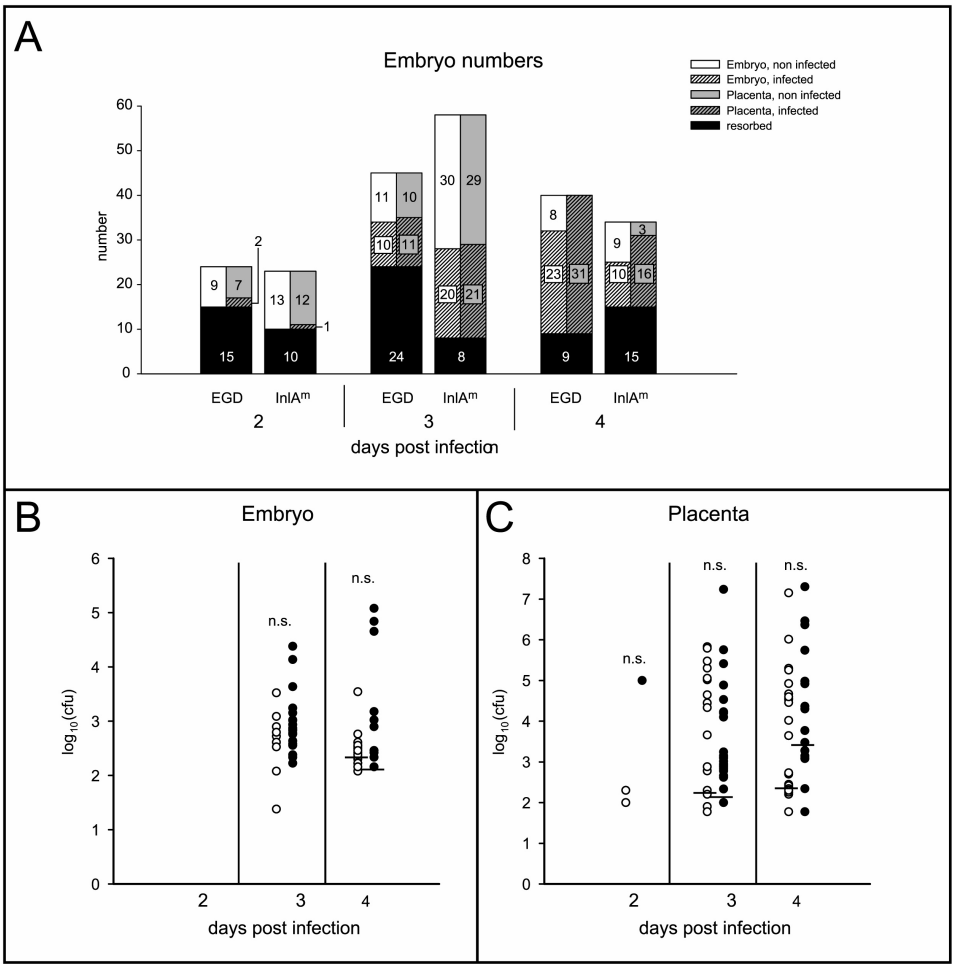

Figure 3.6-6 Infection of pregnant mice with *L. monocytogenes*. BALB/c mice were infected intragastrically with $5 \bullet 10^9$ cfu Lmo-EGD and Lmo-InlA^m. (**A**) Number of resorbed, infected, and non-infected embryos as well as of infected and noninfected placentae as indicated. (**B**) Bacterial loads of embryos from (**A**) at days 2, 3, and 4 p. i. (**C**) Bacterial loads in placentae from (**A**) at different time points as indicated. n.s. = statistically indistinguishable. Statistical analysis: Mann-Whitney U nonparametric test. Note, due to uninfected placentae/embryos (see **A**, not plotted), medians are either zero (**B**, day 3) or lower than apparent from the plotted data.

To ascertain whether the combination of functional InlA and InlB facilitates vertical transmission, we analyzed the ability of Lmo-InlA^{m} to breach the murine blood-placental barrier. Pregnant BALB/c mice were infected orally with $5•10^{9}$ cfu of Lmo-EGD or Lmo-InlA^{m} at embryonic day (E)13.5 or E14.5 of gestation. We find bacterial loads of fetal-placental units at day 2, 3 and 4 p.i. to be indistinguishable (Figure 3.6-6). Equivalent bacteria loads were also observed in fetal-placental units in female mice challenged with $5•10^{4}$ cfu Lmo-InlA^{m} and Lmo-EGD intravenously at day E14.5 (data not shown). Crossing of the blood-placenta barrier is thus not InlA-dependent in BALB/c mice.

4 Discussion

Using minimal, structure-derived modifications of a single pathogenicity factor, we have rationally redesigned the interface of InlA/hEC1 to increase its binding affinity and, in the process, modify the binding specificity of InlA to include murine E-cadherin. Incorporating these modifications into the original bacterium, we create a new listerial strain that mimics the uptake of wild-type Lmo-EGD in the human intestine in the mouse instead (Figure 4-1).

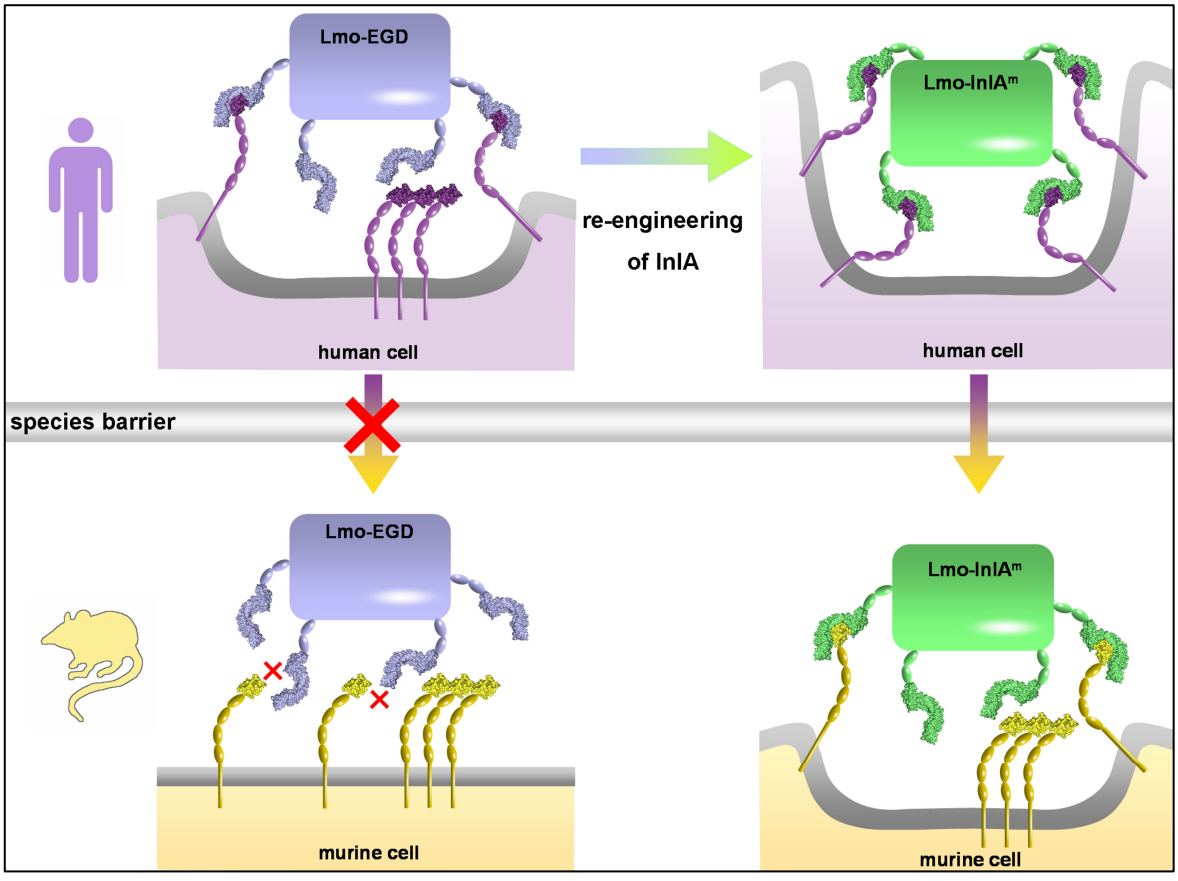

Figure 4-1: Schematic presentation of the experiment. (**A**) To breach the human intestinal barrier, wild-type Lmo-EGD (blue) binds human E-cadherin (violet, surface representation of hEC1) through its invasion protein InlA (blue, functional domain as surface representation). The low affinity of the complex InlA/ is symbolized by incomplete complex formation. (**B**) Murine E-cadherin (mEC1) differs from its human counterpart by twelve amino acid substitutions. These interfere with InlA recognition of mEC1 preventing Lmo-EGD from invading murine epithelial cells. (**C**) The rationally-chosen amino acid substitutions $S192N_{InlA}$ and $Y369S_{InlA}$, improve surface complementarity and increase binding affinity of hEC1 2500-fold (blue-green arrow). Lmo-$InlA^m$ (green) is more efficiently taken up into human intestinal epithelial cells (more complexes formed). (**D**) Re-engineered $InlA^m$ also recognizes mEC1 with an affinity, similar to that of InlA/hEC1. Lmo-$InlA^m$ hence breaches the murine intestinal barrier. Species barrier (grey bar) between human and mice (violet and yellow pictograms) exists only for Lmo-EGD, whereas Lmo-$InlA^m$ efficiently infects both hosts.

Our approach circumvents the limitations of existing models of listeriosis, in that both early and late responses are accessible, and by uniquely providing a system in which both InlA and the second invasion protein InlB are fully functional and expressed at wild-type levels. As intestinal uptake depends only on murine E-cadherin, all mouse strains may be analyzed using Lmo-InlA^{m}. It should furthermore allow both host responses to food-borne pathogens crossing the intestinal barrier and the role of individual listerial factors during infection to be analyzed in an *in vivo* setting. This is the first time that a virulence factor has been rationally modified, without relying on known mutations from related strains, or that a novel strain of a pathogen has been created with an extended host range.

4.1 Rational protein interface design

Protein-protein interactions are mediators of almost all biological processes. Influencing or specifically regulating these processes requires the protein-protein interaction itself to be controlled. Two basic techniques have been used to achieve this goal. On the one hand, error-prone PCR is used to generate a large set of protein variants from which the variant most closely conforming to the anticipated properties is selected by appropriate assays (Wang *et al.*, 2006). By repeating the process for a number of cycles, highly specific binding may be achieved – without the structural reason for improved binding necessarily being known. A more rational approach is based on computational algorithms to specifically modify single amino acids or to re-design entire interaction interfaces (Kortemme and Baker, 2004). This process, however, requires all biological and chemical "rules" of protein-protein interactions to be translated into mathematical formulations to allow their integration into software applications. The average protein-protein interface buries around 800 Å^2 of solvent accessible area of each interaction partner (Wodak and Janin, 2002) and generally involves hydrophobic interactions, salt bridges and hydrogen bonds to fine-tune complex stability and binding specificity (Sharma *et al.*, 2002). To quantify or merely understand this complex set of interactions is dependent upon highly precise structural data as Coulombic (or van der Waals) forces are inversely proportional to the square (or the sixth power) of the distance separating the atoms involved (Murphy, 1995). Even at high resolution, the average error in atomic coordinates of protein complex crystal structures is fairly large (~0.2 Å) limiting precise quantification.

By rationally substituting two amino acids in InlA, the binding affinity of the recognition complex InlA/hEC1 is increased 5000-fold, demonstrating that 'rational protein interface design' may represent an alternative to non-directed and computational techniques to modify the interaction of two proteins. Rationally designing an interface, however, requires structures of uncomplexed components and of the complex to be elucidated at high resolution – a condition that had been met for the protein complex InlA/hEC1. Another major advantage of the InlA/hEC1 is the inherent rigidity of both proteins. Mutations within the LRR-domain of InlA do not induce complex rearrangements within the domain itself or within the entire protein. Such a structural rigidity is not the norm for most proteins. Complex formation of InlA and hEC1 may therefore be described as an interaction between rigid bodies.

Apart from a change in binding affinity, the rational redesigning of InlA also changes its binding specificity allowing it to recognize previously incompatible murine E-cadherin. Rather than calculating precise contributions of individual amino acids to the binding energy, rational protein interface design relies on conscious appraisal of surface-noncomplementarity. This approach may in suitable instances reduce the experimental overhead compared to the established computational (Rosenberg and Goldblum, 2006) or non-directed techniques (Schimmele and Plückthun, 2005), that are routinely used in rational drug design based on known protein-ligand complexes (Hopkins *et al.*, 2006). The system under investigation, however, needs to fulfill most of the prerequisites discussed above, to increase the likelihood of success. This restriction, however, similarly also applies to computational modeling techniques.

4.2 Thermodynamics of complex formation

The crystal structure of the InlA/hEC1 complex and its biophysical characterization using analytical ultracentrifugation (Schubert *et al.*, 2002) revealed important information on complex assembly and function. In addition to the binding affinity, an in-depth biophysical characterization would, however, also call for the quantification of its enthalpic and entropic contributions. Isothermal titration calorimetry is the biophysical method of choice, in this regard, as it is able to reliably and precisely quantify binding affinity as well as the enthalpy and entropy of complex formation (Leavitt and Freire, 2001).

The thermodynamic analysis of complex formation for InlA and hEC1 indicates that this process is both enthalpically and entropically favored. Similarly the large apparent interaction

surface for the complex would generally indicate a tight interaction. Nevertheless, the binding affinity of the complex is weak. Thermodynamically, binding entropy at T S = 25 kJ/mol is seen to outweigh binding enthalpy at H = -6 kJ/mol. Despite the large interface, only two hydrophobic contact areas, centered on $Val3_{hEC1}$ and $Pro16_{hEC1}$, would appear to dominate the entropic stabilization (exclusion of water molecules). The smaller enthalpic contribution implies that relatively few hydrophilic interactions stabilize the interaction of InlA and hEC1. Enthalpically favorable direct contacts between the proteins correspondingly include only seven hydrogen bonds, three salt bridges, and eight water bridged interactions (Schubert *et al.*, 2002). Compared to tighter protein complexes (Levy and Onuchic, 2006), the overall low surface complementarity between InlA and hEC1 allows significantly more water molecules to be retained within the interface, giving rise to the observed moderate entropic and weak enthalpic stabilization.

The low binding affinity and poor surface complementarity of InlA/hEC1, however, provides an optimal system to study the crucial role of water in complex formation. By increasing the number of water molecules excluded during complex formation, the interaction can be stabilized entropically. Alternatively, water molecules enthalpically contribute to binding affinity if their hydrogen bonding potential is optimized to bridge hydrophilic interfaces (Levy and Onuchic, 2006). The available high resolution structural data on complexes of InlA-variants with hEC1 coupled to their precise thermodynamic analysis allows the two sets of data to be correlated and may be used to describe small structural changes in terms of their thermodynamic effect.

4.2.1 Y369A and Y369S

Compared to InlA/hEC1, the substitutions Y369A and Y369S dramatically improve the enthalpy of binding ($\Delta\Delta H$ = 13 or 11 kJ/mol; green and turquoise labels in Figure 3.3-3), but lead to a reduced entropic contribution ($\Delta T\Delta S$ = 2 or 8 kJ/mol). The gain in enthalpy appears to be due to the enthalpically favorable stacking (Meyer *et al.*, 2003) of Phe348, Asn370 and His392 being retained in the variant complexes as in uncomplexed InlA (transparent, pink residues in Figure 3.1-1) rather than being disrupted as in InlA/hEC1 (blue in Figure 3.1-1).

The entropic loss of Y369A structurally correlates with the exposure of a hydrophobic patch of InlA solvated by two rotationally restrained water molecules (orange spheres in Figure 3.2-1). A neighboring water-filled cavity that is opened by the loss of Tyr369 appears not to

affect the entropy significantly as the water structure within the cavity largely remains undisturbed (black spheres).

In Y369S/hEC1, the entropically unfavorable hydrophobic patch is partly eliminated by the addition of a hydrophilic Oγ atom of $Ser369_{InlA}$ reducing the loss in entropy of Y369A (6 kJ/mol). Ser369 binds two conserved water molecules (black spheres), increasing their entropy as well as that of the complex. Complex formation of Y369S/hEC1 (turquoise boxes, Figure 3.3-3) is thus entropically favored over that of Y369A/hEC1 (green boxes).

4.2.2 S192N

Ser192 adopts two alternate conformations in $InlA^{wt}$/hEC1 (Figure 3.1-2 and Figure 3.2-5) each of which hydrogen bonds a bridging water molecule (see above). Replacing Ser192 by asparagine displaces one of these water molecules. Excluding a single water molecule from a protein interface leads to a gain in entropy of ~6-9 kJ/mol (Dunitz, 1994), largely accounting for the observed 12 kJ/mol increase in binding entropy of S192N/hEC1 (magenta boxes in Figure 3.3-3). The loss of the water-mediated hydrogen-bond $Ser172_{InlA}$–$Phe17_{hEC1}$ in turn explains the observed enthalpic loss of 5 kJ/mol, resulting in complex formation being endothermal.

4.2.3 G194S+S

G194S+S fills a large depression on the surface of InlA (compare Figure 3.2-3 B and C) excluding four rotationally restrained water molecules from the interface and dramatically increasing binding entropy ($\Delta T\Delta S$ = -19 kJ/mol). Why though does the binding enthalpy increase to such an extent as to make complex formation endothermic? In the $InlA^{wt}$/hEC1 complex, a distance of 10 Å between InlA and hEC1 is sufficiently large to allow bulk solvent to fill the cavity between the two independently solvated surfaces (Figure 3.2-3B). In G194S+S/hEC1, the distance is reduced to ~4 Å. This distance appears too narrow to allow independent solvation of each surface yet too wide for a single bridging layer of solvent. Instead the inter-protein hydrogen-bonding network is found to be discontinuous and hence enthalpically unfavorable. The exclusion of water molecules from the interface would improve entropy of complex formation while imperfect solvation of both proteins would impair the enthalpy.

4.2.4 Synergy of combined mutations

Strikingly, our study indicates that changes in binding affinity of single substitutions are never simply additive when substitutions are combined in a single protein.

Combining S192N and G194S+S results in anti-cooperative behavior characterized by a synergy factor of 0.05. Binding affinity of $InlA^{S192N\text{-}G194S+S}$/hEC1 is thus weaker than the combination of individual substitutions would imply. The effect is largely entropic, with $T\,S \approx 7$ kJ/mol (e.g. $T\,S_{S192N \rightarrow S192N\text{-}G194S+S}$ - $T\,S_{InlA \rightarrow G194S+S,}$ Figure 3.3-3) indicating that roughly one water molecule less is displaced by S192N-G194S+S than by S192N and G194S+S together. Correspondingly, the crystal structure of S192N-G194S+S/hEC1 indicates that the side chain of $Asn192_{InlA}$ is locked into a tight intramolecular hydrogen bond to the physically adjacent backbone nitrogen of Ser194 (Figure 3.2-5D), preventing Asn192 from displacing a water molecule as described for S192N/hEC1 (compare Figure 3.2-5B-C with D).

Potentially more interesting are variants S192N-Y369A, S192N-Y369S and G194S+S-Y369S, all of which are characterized by synergy factors above one, indicating individual substitutions to be cooperative. All of these InlA-variants combine individual substitutions physically separated by more than 30 Å. For example, S192N-Y369S combines S192N in LRR6 with Y369S in LRR14, spanning a distance of 34 Å (Figure 4.2-1A). Previously, studies on large datasets of protein-complexes had indicated synergy to be limited to clustered residues (Keskin *et al.*, 2005), whereas spatially distant improvements were strictly additive (Reichmann *et al.*, 2007). Only recently has this view been challenged following the report of positive cooperativity for substitutions in the T-cell receptor variable domain separated by 20 Å (Moza *et al.*, 2006).

Structurally, the observed long-range synergy in InlA-variants appears to be due to a physical link in the form of a β-strand between two sites of mutation (or mutational "hot spots"). The variants S192N and Y369A/S increase binding affinity of hEC1 through favorable interactions to $Phe17_{hEC1}$ and $Asn27_{hEC1}$, respectively. The latter two residues are located at either end of β-strand **b** (β**b**, residues 19-26) of hEC1 (Figure 4.2-1). While interactions of β**b** to InlA in InlA/hEC1 are restricted to two water-mediated contacts, β-strand β**a** (residues 2-10) and loop β**a**-β**b** (residues 10-19) constitute the major part of the InlA/hEC1-interface. By stabilizing either end of β**b**, substitutions S192N and Y369A/S stabilize the interface as a

whole, resulting in the observed synergistic increase in binding affinity (Figure 4.2-1 and Figure 3.3-3).

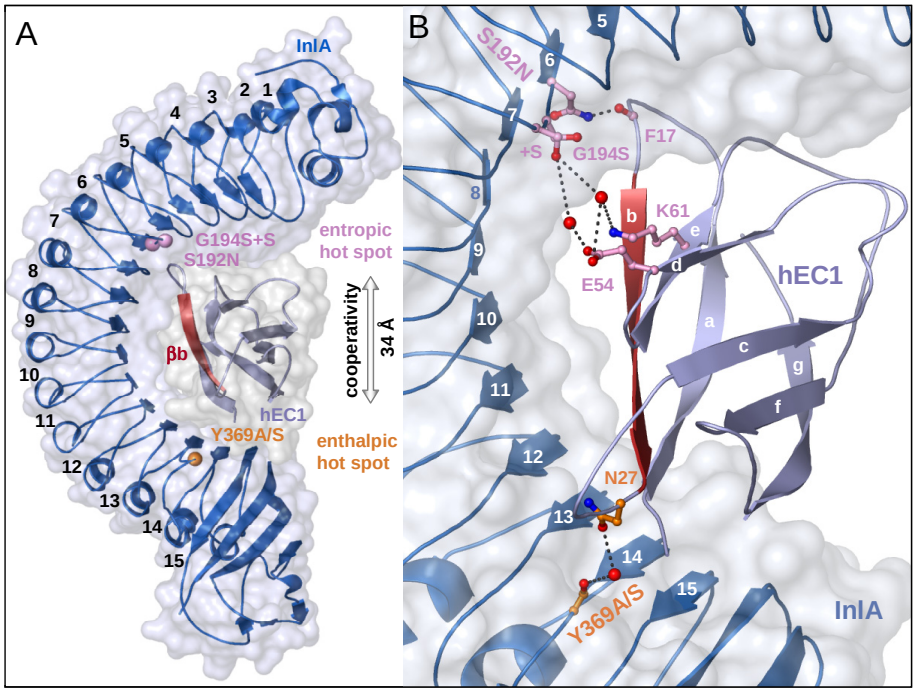

Figure 4.2-1: Cooperativity of re-engineered substitutions in InlA / hEC1 (dark / light blue). (**A**) Re-engineered residues are indicated by spheres. Though separated by 34 Å, combinations of substitutions from entropically (violet) and enthalpically (orange) dominated "hot spots" act synergistically by stabilizing β-strand **b** of hEC1 (red). (**B**) Close-up view of the interaction interface. S192N and Y369A/S (ball-and-sticks) stabilize opposite ends of β**b**. G194S+S shortens the distance to residues $Glu54_{hEC1}$ and $Lys61_{hEC1}$ (ball-and-stick) in β**d** and β**e**, respectively. Stabilization is transmitted through β-sheet **bde** to the N-terminus of β**b**.

Compared to Y369S, Y369A binds the C-terminal end of β**b** less tightly (see above). As a result, the synergy factor of Y369A when combined with S192N is only 1.8, compared to a factor of 5 for Y369S. A single water-mediated hydrogen bond, introduced through Y369S, thus appears to noticeably increase the degree of synergy between two proteins.

In the case of G194S+S-Y369S, the insertion of serine (+S) restores the canonical LRR-architecture (Figure 3.2-3A and Figure 3.2-5C) and stabilizes the residues $Glu54_{hEC1}$ and $Lys61_{hEC1}$ by excluding unfavorably restrained intervening water molecules. Glu54 and Lys61 are, however, part of β**d** and β**e** of hEC1, (Figure 4.2-1B) that form a β-sheet with strand β**b**. The partial stabilization of β-strands β**d** and β**e** may thus be transmitted through β-sheet **bde** to the N-terminus of β**b** and still give rise to a measurable positive cooperativity. This mechanism of long-range cooperativity resembles the intra-molecular, allosteric effects frequently observed in multimeric protein complexes (Changeux and Edelstein, 2005).

Depending on the number of active site carrying subunits, multimeric enzymes bind a specific number of substrate molecules. Frequently, binding of one substrate facilitates binding of further substrate molecules due to a conformational change or induced fit upon binding of the first substrate (McCammon, 2005) that is transmitted to another subunit (Yu and Koshland, Jr., 2001). A variety of enzymes have been analyzed both, structurally and functionally, to characterize cooperativity of substrate binding in terms of conformational changes. Examples include extensively studied hemoglobin (Perrella, 1999) as well as the ACT-domain of enzymes involved in amino acid biosynthesis (Aravind and Koonin, 1999; Liberles *et al.*, 2005). Flexible hinge regions, required to induce movement after ligand-binding, and α-helices that transmit movements between hinge regions were found to be crucial to cooperativity (Liberles *et al.*, 2005).

In the recently analyzed complex of the T-cell receptor variable domain and the superantigenic toxic shock syndrome toxin 1 with positive cooperativity between "hot spots" of recognition (Moza *et al.*, 2006), a β-strand was observed to connect both stabilizing protein-protein contacts. The β-strand was assumed to be responsible for cooperativity as its stabilization leads to a stabilization of the entire interaction interface. Secondary structure elements thus seem important to connect regions involved in cooperative behavior both in enzymes and protein-protein complexes. Presumably their rigidity allows favorable interactions to be transmitted or combined resulting in improved recognition, either of ligands in enzymes or of interaction partners in protein-protein complexes.

Apart from secondary structure, it appears that tertiary structural elements such as β-sheets may also be crucial in transmitting such conformational changes across long distances. Analyzing the G194S+S-Y369S / hEC1 complex reveals a β-sheet as potentially responsible for synergistic strengthening of hEC1-recognition. This mechanism bears some resemblance to signal transduction events of transmembrane proteins, where extracellular binding of ligands is transmitted across the membrane by a ligand-induced conformational change and initiating cytosolic signaling cascades (Ottemann *et al.*, 1999). Transmembrane signaling appears to depend on a change in orientation of α-helices within the membrane. The participation of a β-sheet in connecting two "hot spots" of recognition have not been reported previously. The analysis of other protein-protein or protein-ligand interactions will, we believe, confirm that β-sheets are generally able to transmit conformation change signals.

The "entropic bonus" responsible for positive cooperativity in the InlA-variant/hEC1 complexes is generally quite small, lying in the range of 2-3 kJ/mol. This represents about a

third of the energy associated with the exclusion of a single water molecule from a protein-protein-interface. Despite the noticeable synergy, the structural changes accounting for this small change in energy are difficult to localize. However, as an increase in entropy indicates an increase in degrees of freedom, we assume that the tighter interaction of β**b** with InlA results in a small increase in solvation entropy, stabilizing the complex. The change in flexibility of β**b** is not directly observed in the crystal structures, possibly because crystal packing forces the complex in one conformation suppressing structural variations that would occur outside of a crystal. In solution, where association and dissociation of proteins happen continuously, the stabilization of β**b** by the two substitutions could decrease the dissociation rate constant resulting in an extra strengthening compared to the single substitutions accounting for the observed synergy.

4.3 Implications of InlA affinity for EC1

To induce uptake into epithelial cells by the zipper-mechanism, *L. monocytogenes* must adhere tightly to the eukaryotic cell membrane. Accordingly, tighter adherence of Lmo-InlA^{m} to Caco2 cells increases the efficiency of uptake compared to wild-type Lmo-EGD. Surprisingly, however, the 2500-fold increased binding affinity merely causes a doubling in bacterial adhesion (Figure 3.4-7A). As low binding affinity may be counteracted by high protein concentration, the efficient adhesion of Lmo-EGD to Caco2 cells is probably due to the high concentration of E-cadherin molecules on these cells.

In the intestinal epithelium *in vivo*, the amount of E-cadherin accessible to *L. monocytogenes* apically is limited by its basolateral localization. Multicellular junctions in epithelial monolayers transiently expose E-cadherin (Pentecost *et al.*, 2006) providing *L. monocytogenes* with a point of attachment. The low abundance of such junctions and the low affinity of InlA for its receptor E-cadherin would severely limit uptake of *L. monocytogenes in vivo*. By increasing binding affinity, the available E-cadherin could be utilized more efficiently allowing a higher proportion of Lmo-InlA^{m} to invade the intestinal epithelium. While pathogenicity would potentially be increased, higher rates of uptake of InlA^{m} may prove advantageous therapeutically as in oral vaccination (Guimaraes *et al.*, 2005), bacterial gene therapy (Dietrich *et al.*, 1998) or drug delivery (Sleator and Hill, 2006). As regulation of E-cadherin is, furthermore, intimately linked to cell transformation and to the development of

cancer (Wheelock and Johnson, 2003), $InlA^m$ may prove useful in studying E-cadherin mediated signal transduction.

4.3.1 The advantage of functional InlA

L. monocytogenes differs from the genomically closely related non-pathogenic soil bacterium *Bacillus subitilis* in that it contains the virulence cluster LIPI-1 (*Listeria* pathogenicity island 1) that encodes almost all virulence factors including PrfA, LLO, ActA, and the two PLCs (Glaser *et al.*, 2001). Perhaps not surprisingly, this virulence cluster is also present in *L. ivanovii* (Gouin *et al.*, 1994), explaining in part the virulence of this species with respect to animal hosts (Hof and Hefner, 1988). Pathogenicity in humans and/or other susceptible species, additionally requires the presence of a second virulence associated locus, known as the *inlAB* locus in case of *L. monocytogenes* (Dussurget *et al.*, 2004) and potentially a related, though as yet uncharacterized locus in *L. ivanovii*. Consequently, LIPI-1 alone appears to be insufficient to render *Listeriae* pathogenic as it is also present in the nonpathogenic species *L. seeligeri*. A simple explanation may be that bacteria are not able to access host cells if the *inlAB* locus or homologous loci encoding for invasion proteins are missing. The invasion proteins of *L. monocytogenes*, InlA and InlB, promote bacterial uptake into normally non-phagocytic host cells such that the absence of either factor severely reduces the virulence of *L. monocytogenes in vivo* (Lingnau *et al.*, 1995). In this work, the role of InlA has been further clarified by revealing its contribution in causing extensive infections in intestinal tissues of susceptible hosts – the first and crucial step in systemic listeriosis. The importance of InlA to listerial pathogenicity is reflected by the high ratio of clinical isolates of *L. monocytogenes* expressing functional InlA (Nightingale *et al.*, 2005b). This is also true of animal hosts, susceptible to orally acquired listeriosis (Orndorff *et al.*, 2006).

The ability of *L. monocytogenes* to breach the blood-brain-barrier is documented by the high prevalence of rhombencephalitis in infected ruminants, which leads to the well documented circling disease syndrome (Charlton and Garcia, 1977) and to meningoencephalitis (Cordy and Osebold, 1959). The coincidence of ruminant infections, of functional InlA in isolates of these infected ruminants, and of infections of the central nervous system (CNS) during severe listeriosis was suggested to indicate a link between CNS infections and functional InlA (Lecuit, 2005). As infection of placentas and embryos in mice appear to be independent of InlA (see 3.6.3 on p. 74), the role of InlA may, in fact, be restricted to overcoming the

epithelial barrier of the hosts intestine. Transport to deeper and well-protected tissues would instead be mediated by macrophages and other immune cells as proposed by the "Trojan horse" theory (Dramsi *et al.*, 1998).

Although InlA and InlB appear to induce listerial uptake with highly disparate efficiencies, the two proteins presumably serve distinct, possibly non-overlapping functions. InlB appears uninvolved in inducing listerial uptake into the intestinal epithelium *in vivo* (Khelef *et al.*, 2006), highlighting the necessity of InlA-mediated uptake during the intestinal phase of infection.

The evolution of InlA, though disadvantageous to humans, is presumably the result of the fecal-oral enrichment cycle of domestic ruminants (Weis and Seeliger, 1975). It creates an evolutionary selection pressure for *L. monocytogenes*, favoring efficient listerial uptake into the intestinal epithelium. Colonization of the intestinal epithelium is, however, not necessarily associated with systemic listeriosis. Instead, it facilitates fecal shedding of bacteria and hence its further distribution. This assumption is supported by the observation that gastroenteritis is the major manifestation of human listeriosis in healthy individuals (Hof, 2001). Severe manifestations of listeriosis possibly occurs as "side effect" in immunocompromized individuals, driven by the efficient and fine-tuned action of virulence factors, produced by *L. monocytogenes*. Human listeriosis may thus have evolved due to the high homology of human receptors to those of ruminants.

4.3.2 Evolutionary view on InlA^{wt}-affinity

The initial question of the biological implication of weak affinity of InlA^{wt} for its receptor human E-cadherin can not finally be answered. On the one hand we observed a dramatic increase in molecular binding affinity *in vitro* through the substitution of only two residues. Even a range of single substitutions suffice to transform the weak micromolar affinity of the InlA^{wt}/hEC1 complex into a tight fit with a dissociation constant in the upper nanomolar range. Single amino acid changes are evolutionary frequently observed. Assuming such a change to be advantageous, as presumed for an improved affinity of InlA for E-cadherin, positive selection should have allowed *L. monocytogenes* to evolve higher affinity InlA-variants. Several *inlA*-genes from various isolates have been sequenced (Nightingale *et al.*, 2005b). Analyzing these sequences indicates that only residues not involved in E-cadherin recognition are exchanged; those residues in direct contact to E-cadherin are generally highly

conserved (Figure 4.3-1). Loss of InlA is clearly disadvantageous to *L. monocytogenes*, as strains expressing nonfunctional InlA are frequently isolated from environmental habitats but not from clinical samples (Olier *et al.*, 2003). As contact residues are conserved, improved affinity is either not sufficiently advantageous to induce positive selection or it is simply disadvantageous.

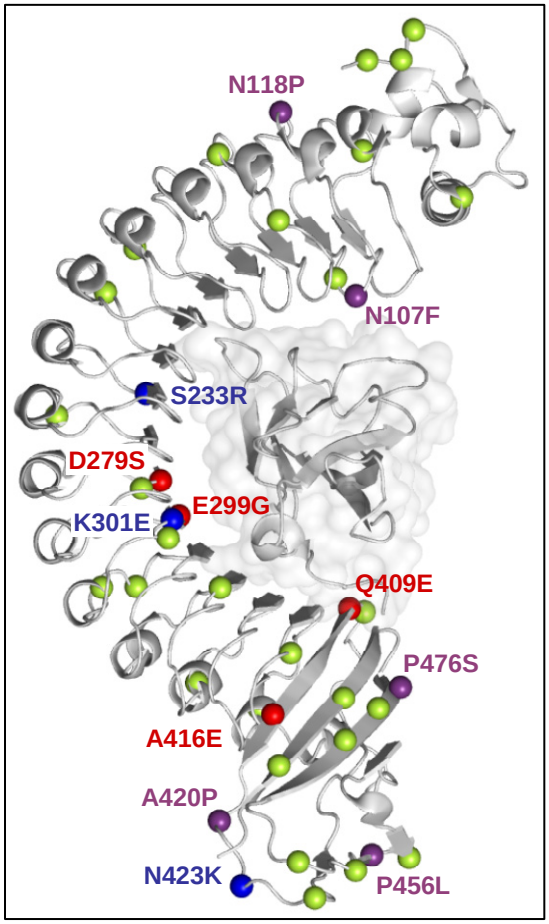

Figure 4.3-1: Mapping conserved and non-conserved amino acid residues of InlA onto the structure of the InlA/hEC1 complex. InlA sequences of 101 listerial isolates were compared (Nightingale *et al.*, 2005a; Tsai *et al.*, 2006). Amino acid residues differing from the consensus sequence in any of the sequences are indicated by spheres (green: conservative exchanges, red/blue: exchanges involving negative/positive charged residues, violet: non-conservative exchanges involving uncharged residues). Only substitutions N107F (3), S233R (1), and K301E (1) could potentially influence recognition of hEC1 (number of exchange carrying isolates).

One scenario why tighter binding could be disadvantageous was proposed to be that release of the bacterium from remnants of the phagomosal membrane could be impaired if the affinity of InlA for E-cadherin is too high (Schubert *et al.*, 2002). This hypothesis was supported by biophysical analyses of the wild-type complex that demonstrated binding affinity to be Ca^{2+}-dependent. As the Ca^{2+}-concentration within cells is 10^7-fold less than that of the extracellular milieu, complex formation was assumed to be favored extracellularly and weakened after uptake (Schubert *et al.*, 2002). Using gentamicin invasion assays, this hypothesis could,

however, not be confirmed. Release of bacteria expressing high affinity InlA-variants appears unaffected. Is weak binding of InlA to hEC1 essential to allow release after uptake? *L. monocytogenes* produces the potent membrane lysing virulence factor LLO that disrupts the phagosomal membrane efficiently (Dramsi and Cossart, 2002). Crosslinking bacterial cell-wall and phagosomal membrane, due to a nanomolar affinity of InlA presumably does not cause phagosomal trapping. Instead the surface of *L. monocytogenes* would be "decorated" with nonfunctional $InlA^m$/E-cadherin complexes potentially interfering with other infection processes. Immune-fluorescence staining of intracellular *L. monocytogenes* demonstrate that InlA continues to be expressed after invasion but co-localization of InlA or $InlA^m$ and E-cadherin 30 min post infection when bacteria start to escape from the phagosome could not be shown (Figure 3.4-8A-B). This indicates that InlA is, presumably, rapidly turned over in common with other cell-wall-anchored proteins (Boneca, 2005). Re-arrangement of the bacterial peptidoglycan can be achieved by cell-wall degrading enzymes and a number of these have been identified (Carroll *et al.*, 2003; Wang and Lin, 2007) and characterized as potential virulence factors (Lenz *et al.*, 2003; Cabanes *et al.*, 2004).

Evolutionary pressures on a versatile bacterium such as *L. monocytogenes*, that colonizes a range of distinct habitats, appear to be divergent at best. Obligate pathogens are more amenable to mutations that enhance their ability to infect their hosts or to be transmitted from one host to another (Brown *et al.*, 2006) because of their dependence on a single ecological niche. The weak selection pressure on *L. monocytogenes*, in contrast, generates a variety of closely related listerial sub-species (or strains) with different pathogenic potential. On the other hand, weak selection pressure in combination with constant exposure to potential hosts suffice to maintain functional virulence factors such as InlA and InlB, but appears to be insufficient to optimize them further.

4.3.3 Insights into the mechanism of InlA mediated uptake

Although the affinity of InlA for E-cadherin has been found to be surprisingly low (Schubert *et al.*, 2002), this affinity clearly suffices to recruit E-cadherin from cell-cell-contacts and induce bacterial uptake. E-cadherin/E-cadherin interactions of neighboring cells similarly rely on low binding affinities (Haussinger *et al.*, 2004). Coupled to high molecule densities, low binding affinity may be crucial to ensure cadherin specificity (Chen *et al.*, 2005) especially for tissue sorting during embryogenesis (McNeill, 2000). At the same time, low affinity for

other E-cadherin molecules and the large number of molecules per cell make E-cadherin a perfect target for bacterial adhesion (Braun and Cossart, 2000). Infection studies using InlA-coated beads, indicate that InlA-mediated entry is associated with receptor clustering within cholesterol-rich membrane domains known as lipid rafts and the recruitment of typical lipid raft markers such as ganglioside GM1 to the site of entry (Seveau *et al.*, 2004). Analyzing both Lmo-EGD and Lmo-InlA^{m} induced invasion by immunofluorescence (Figure 3.4-8) reveals a dramatic redistribution of E-cadherin in infected cells. The typical peripheral fluorescence of E-cadherin and α-catenin in confluent epithelial cells (Figure 3.4-8I-J), hallmark of intact adherens junctions, are absent in infected cells (Figure 3.4-8A-D). The invasion strategy of *L. monocytogenes* thus appears to involve the remodeling of adherence junctions.

Combining our observations with previous findings (Seveau *et al.*, 2004), allows us to propose a molecular model of listerial invasion: The first contact between *L. monocytogenes* and a target cell by necessity involves a limited number of InlA/E-cadherin pairs. The high local density of InlA molecules then, however, leads to an accumulation of additional E-cadherin molecules from adjacent areas creating an initial receptor cluster. As in cell-cell-contact formation (Gumbiner, 2000), this initial contact induces intracellular signaling (Nelson and Nusse, 2004) triggering the fusion of E-cadherin containing vesicles with the plasma membrane, extending the initial contact to create a (pseudo-)adherens junction (Bryant and Stow, 2004). Normally, E-cadherin accumulation is tightly regulated to avoid the loss of existing cell-cell contacts by excessive E-cadherin recruitment. *L. monocytogenes*, however, appears to induce an imbalance, triggering massive E-cadherin recruitment to the site of entry (Seveau *et al.*, 2004), disrupting existing adherence junctions (Figure 3.4-8). This induced imbalance may be caused by the high density of InlA-molecules within a small area. As both Lmo-EGD and Lmo-InlA^{m} induce this imbalance to a similar extent, high affinity of InlA for E-cadherin does not appear to be relevant to this process.

The strategy of deregulating the distribution of E-cadherin could be advantageous in two respects. First, the local accumulation of E-cadherin provides a hot-spot of invasion that is maintained after uptake and supports invasion of further bacteria. This was frequently observed in immunofluorescent stains (Figure 3.4-8C-D), where multiple infected cells are surrounded by non-infected ones – even after short infection periods where no intracellular growth took place. Secondly, sequestering E-cadherin locally disrupts the epithelial barrier

function, exposing basolaterally confined E-cadherin of neighboring cells and facilitating their infection.

4.3.4 Studying extended host specificity *in vitro*

The apparent interaction of the mEC1 domain and InlA^m provided a first indication that the binding specificity of InlA^m had been extended. To test this hypothesis in a more natural setting, Lmo-InlA^m expressing full-length InlA^m instead of the C-terminally truncated version, used in biophysical and structural analysis, were incubated with the murine E-cadherin expressing cell line MCA-3D. A natural epithelial monolayer was simulated *in vitro* by growing cells to confluence such that E-cadherin is essentially buried in adherens junctions and InlA^m would need to recruit E-cadherin from adherens junctions to induce invasion.

Unspecific, invasion protein independent uptake of bacteria was analyzed using the InlAB deletion mutant strain *L. monocytogenes* Δ*inlAB*2 and apathogenic *L. innocua* expressing PrfA and LLO (see 3.5.4 on p. 67). Whereas *L. monocytogenes* Δ*inlAB*2 still induced limited uptake, the transgenic *L. innocua* strain was not detectable intracellularly. The non-invasiveness of *L. innocua* is probably caused by the absence of virulence factors necessary for an intracellular lifestyle of *L. monocytogenes*, rather than any missing invasion proteins. Similarly, the deletion of LLO in *L. monocytogenes* Δ*hly* results in phagosomal trapping reducing the likelihood of bacterial release from the phagosome, rather than abolishing phagolysosomal release entirely.

Invasion studies using murine epithelial MCA-3D cells indicate that the strains Lmo-EGD, Lmo-Δ*inlA*2, Lmo-pPL2-*inlA*^{m} and Lmo-InlA^m all invade with similar efficiency. All strains express functional InlB while InlA is either absent (Lmo-Δ*inlA*2), non-functional (Lmo-EGD), functional but weakly expressed (Lmo-pPL2-*inlA*^{m}) or fully functional (Lmo-InlA^m). Invasion is thus clearly independent of InlA. Comparing the invasion rates of Lmo-EGD and Lmo-pPL2-*inlA*^{m} to the amount of InlB being produced (see 3.4.2 on p.51) indicates that reduced levels of InlB for e.g. in Lmo-pPL2-*inlA*^{m} leads to slightly lower invasion rates. The reason for InlA-dependent invasion being masked by InlB is probably due to the immortalization of MCA-3D cells, as this procedure is known to not only induce the down-regulation of the tumor suppressor gene E-cadherin but also the up-regulation of the proto-oncogene c-Met, the receptor of InlB (Peruzzi and Bottaro, 2006).

4.4 InlA-dependent and -independent routes of listerial infection

In depth analysis of the infection process of Lmo-EGD vs. Lmo-InlA^m in mice provides unique insights into the contribution of functional InlA to listerial distribution *in vivo*. It furthermore illuminates common infection routes of both bacterial strains as well as routes, exclusively to Lmo-InlA^m.

In mice, Lmo-EGD primarily targets the Peyer's patches (Marco *et al.*, 1997). Specialized, epithelial-like M-cells (Clark and Hirst, 2002) covering these centers of mucosal immunity actively transport antigens and viable bacteria from the intestinal lumen to the underlying immune-cells (Kraehenbuhl and Neutra, 2000). This sampling process is assumed to be important in immune-regulation, defense against pathogens, and coexistence with commensal microorganisms. A high concentration of macrophages beneath M-cells and the lymph-node like structure, filled with neutrophils and lymphocytes, that forms part of the Peyer's patch reduce the number of pathogens that are able to invade the host via this potential gateway (Newberry and Lorenz, 2005). Food-borne pathogens such as *Salmonellae* or *Shigellae* exploit the indiscriminate uptake by M-cells to gain access to the basolateral side of the epithelium (Vazquez-Torres and Fang, 2000). Both species use type three secretion systems (see 1.3 on p.14) to manipulate host cell functions inducing uptake into host cells. Initial contact between the needle tip and host cells is mediated by IpaB in *Shigellae* that binds CD44 (Lafont *et al.*, 2002) and SipB in *Salmonellae* that binds an as yet unidentified host receptor. Because these receptors are localized basolaterally, both pathogens first need to overcome the intestinal barrier before being able to infect host cells from the basolateral side and spreading to cells of the adjoining epithelium (Jensen *et al.*, 1998). E-cadherin on the basolateral side of M-cells and enterocytes potentially allow Lmo-EGD to employ a similar strategy in humans. Our analyses, however, indicate that colonization of M-cells and Peyer's patches by Lmo-InlA^m in mice is indistinguishable from that of Lmo-EGD. Re-infection of M-cells is thus not part of the listerial invasion strategy. Following their entry through Peyer's patches both Lmo-EGD and Lmo-InlA^m are presumably phagocytosed by macrophages independent of InlA and InlB that traffic to mesenteric lymph nodes and enter the blood stream as early as 12 hours p.i. rapidly reaching deeper tissues (Figure 3.6-2B-F and Figure 4.4-1). Additionally, listerial dissemination to the spleen presumably involve CD8α^+ dendritic cells, again independent of InlA and InlB (Neuenhahn *et al.*, 2006).

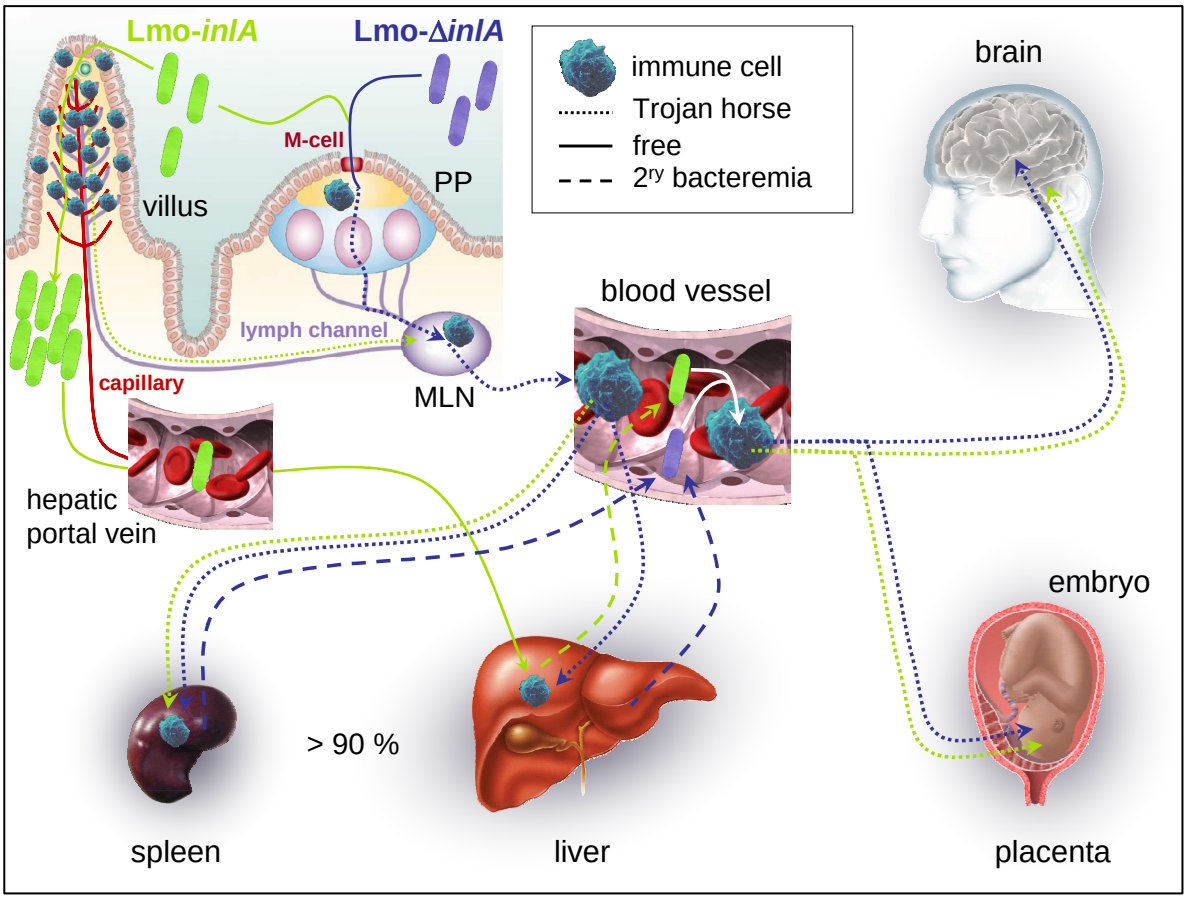

Figure 4.4-1: Schematic representation of listerial infection routes. Lmo-Δ*inlA* (non-functional InlA, blue lines) enters Peyer's patches (PP) through unspecific uptake by M-cells. Within the Peyer's patches they are phagocytosed by immune cells (predominantly macrophages) and transported to mesenteric lymph nodes (MLN), to the blood via the thoracic duct, and are systemically distributed. Liver and spleen initially take up more than 90% of blood-borne bacteria. Bacterial growth in these organs induces a secondary bacteremia resulting in large numbers of bacteria entering the blood stream. Here they are phagocytosed by circulating immune cells and reach the brain or the placenta/embryo. Lmo-*inlA* (functional InlA, green) additionally uses a second route of entry: InlA-mediated uptake into epithelial cells and spreading to sub-epithelial tissue. Via extracellular fluid bacteria reaches MLN and the blood stream. After massive growth in subepithelial tissue, large numbers of bacteria have direct access to the blood stream and are transported to the liver (via the hepatic portal vein), and to other organs. Further distribution also depends on the Trojan horse mechanism. Figure of the intestine adapted from Mowat *et al.*, 2003.

Using the re-engineered strain Lmo-InlA^{m}, we resolve the long-standing debate on which route *L. monocytogenes* uses to enter hosts *in vivo*. Previous studies on orally acquired murine listeriosis ignored or underestimated the fact that murine E-cadherin is not recognized by InlA (Daniels *et al.*, 2000; Czuprynski *et al.*, 2002; Czuprynski *et al.*, 2003; Le Monnier *et al.*, 2006). Infection experiments in guinea pigs, on the other hand failed to discuss that InlB is non-functional in this system (Bakardjiev *et al.*, 2006). This led to conclusions being drawn that potentially do not reflect the true pathophysiology of *L. monocytogenes in vivo*. InlA of Lmo-EGD is functional in humans but non-functional in mice. As infections of Lmo-EGD in

mice do occur notwithstanding, this process must be independent of InlA. During such InlA-independent infections, bacteria do not colonize the intestinal epithelium. Instead they utilize the indiscriminate uptake by M-cells to reach the Peyer's patches, where they induce a localized infection. Mild immune responses observed in intestinal tissue in Lmo-EGD-infected mice after day 3 p.i. (Figure 3.6-4I) are probably caused by immune cells activated in Peyer's patches migrating into the intestinal tissues (Mowat, 2003). Dissemination of bacteria from infected intestinal tissue is thus largely prevented, allowing rapid healing of the localized infection in the intestine and clearance of Lmo-EGD from the liver and spleen after day 3 p.i.

In addition to the Peyer's patches (InlA-independent), Lmo-InlA^m infects the intestinal epithelium (InlA-dependent, Figure 4.4-1) - immunohistochemically observed 24 h p.i. (Figure 3.6-4D). Over the next two days Lmo-InlA^m progressively infects subepithelial connective tissue documented by a steady increase in bacterial numbers in the intestine (Figure 3.6-2B). By day 4 p.i., large numbers of bacteria colonize the intestinal epithelial and subepithelial tissues (Figure 3.6-2B and Figure 3.6-4P) opening a second, dominant route of listerial dissemination. Compared to the InlA-independent route, bacteria now directly access draining lymph nodes and blood as well as the liver via the hepatic portal vein (Figure 4.4-1). This results in a ~10^3-fold increase in bacterial number in the liver of Lmo-InlA^m-infected mice on day 4 p.i. (Figure 3.6-2E). The heavy inflammation of the intestine additionally sequesters immune resources weakening the host.

Bacterial numbers in mesenteric lymph nodes and intestine were also observed to increase until day 3 p.i. using a transgenic mouse model (Lecuit *et al.*, 2001). Overall the efficiency of uptake and hence the number of invading bacteria are much lower, allowing the infection to subside by day 5 p.i.

The course of infection after intravenous inoculation is, surprisingly, indistinguishable for the two listerial strains, implying that InlA may not be essential for the later stages of listerial infections. Instead intracellular trafficking of *L. monocytogenes* could be more important for systemic spreading than previously anticipated. Slightly higher virulence of Lmo-InlA^m may indicate that InlA nevertheless imparts an advantage to the bacterium during this stage of the infection. Overall, InlA is crucial to establish the infection of the intestinal epithelium. InlB and potentially other virulence factors then take over, leading to spread and systemic infection (Hamon *et al.*, 2006).

Taken together, this work establishes the unique mechanism by which *L. monocytogenes* infects its hosts. The food-borne bacterial pathogens *Yersiniae*, *Shigellae*, and *Salmonellae* all rely on indiscriminate uptake by M-cells to overcome the intestinal barrier and furthermore all re-infect M-cells basolaterally as a prelude to spreading to the adjoining epithelium and causing localized inflammation (Cossart and Sansonetti, 2004; Pizarro-Cerda and Cossart, 2006a). *L. monocytogenes*, though similarly transported to the Peyer's patches by M-cells, does not re-infect the latter despite the presence of receptors for both InlA and InlB on M-cells and enterocytes. Dispersal of *L. monocytogenes* as a “Trojan horse” after phagocytosis by macrophages and other immune cells, allows some spreading of the bacterium to deeper tissues, but generally allows the host to clear the infection within a few days. Instead, InlA provides *L. monocytogenes* with a second, dominant route of uptake. Here the bacterium directly invades individual cells of the intestinal epithelium independent of Peyer’s patches, which - though slower than unspecific M-cell mediated uptake - allows sustained infections first of the intestinal epithelium followed by systemic infection.

4.4.1 The role of InlB in systemic listeriosis

The precise role of InlB during infection *in vivo* is currently not known. Cell-culture experiments clearly demonstrate that InlB is responsible for listerial uptake into hepatocytes *in vitro* (Dramsi *et al.*, 1995). Until recently it was, however, not possible to test the contribution of Met to listerial virulence *in vivo*, as Met is essential for embryonic development, making a knock-out lethal (Birchmeier *et al.*, 2003). The recent generation of a healthy conditional *met* knock-out (Borowiak *et al.*, 2004; Huh *et al.*, 2004) could represent the ideal system to distinguish the roles of InlA and InlB, especially in combination with Lmo-InlA^{m}.

Intravenous inoculation of mice with Lmo-EGD or listerial strains deficient in InlA and/or InlB have also been used to analyze the contribution of InlB in systemic listeriosis *in vivo* (Conlan, 1999; Cousens and Wing, 2000). Although artificial, these studies demonstrate the importance of resident hepatic macrophages (Kupffer cells) in early immune defense against *L. monocytogenes*. While they also reveal hepatocytes to be the primary target of *L. monocytogenes* (Gregory *et al.*, 1996a), they fail to establish the precise role of InlB as hepatocytes are also efficiently infected by *L. monocytogenes* lacking both InlA and InlB (Gregory *et al.*, 1996b). This result indicates either that hepatocytes possess phagocytic

activity or that Kupffer cells initially take up *L. monocytogenes* which then spread to adjacent hepatocytes.

Reduced virulence of *L. monocytogenes* deficient for InlB established its critical role during infection (Lingnau *et al.*, 1995). The existence of two different trafficking mechanisms, via the blood or as "Trojan horses", however, makes it difficult to analyze or quantify the contribution of each pathway independent of the other.

Using Lmo-InlA^{m} it should now be possible to analyze the role of InlB in human-like listeriosis more precisely as the physiological route of listerial uptake may now be addressed in mice. By comparing Lmo-InlA^{m} with Lmo-InlA^{m}/ InlB, it should be possible to distinguish between InlA and InlB dependent uptake and dissemination *in vivo*. Additionally, both strains could be instrumental to reveal the precise target of InlB *in vivo* as several potential receptors have been identified but not yet analyzed in a natural system.

4.4.2 *L. monocytogenes* infection in pregnant mice

Pregnancy in humans increases susceptibility towards *L. monocytogenes* (Vazquez-Boland *et al.*, 2001) and InlA appears crucial for listerial crossing of the blood-placental barrier (Lecuit *et al.*, 2004). Both pregnant mice (Le Monnier *et al.*, 2007) and guinea pigs (Bakardjiev *et al.*, 2006) have been used to investigate this link. The usefulness of these models are, however, limited by the respective host specificities of InlA and InlB (see above). Lmo-InlA^{m} overcomes these limitations by providing active InlA and InlB for the murine system. Infecting pregnant mice orally with Lmo-InlA^{m} mimics the human course of infections and vertical transmission.

We, however, do not observe a significant difference between Lmo-EGD and Lmo-InlA^{m} both by intravenous and oral infection of pregnant mice. This would indicate that the natural route of placental infection in mice is not dependent on functional InlA and/or InlB. The uniquely invasive form of trophoblast-cell mediated haemochorial placentation in humans (Moffett and Loke, 2006) may result in a higher susceptibility for listerial infections in humans. Alternatively, vertical transmission could occur as discussed for the blood-brain-barrier, in which the vast majority of *L. monocytogenes* enter the placental barrier using the "Trojan horse" strategy (Figure 4.4-1) via infected monocytes or macrophages (Drevets, 1999). In this case InlA-mediated entry would be subordinate to "Trojan horse" type uptake

and would therefore only be detectable *in vitro* or *ex vivo* where the latter mechanism is absent.

4.4.3 InlA- and InlB-independent transmission to the brain?

Although not directly analyzed, the InlA/InlB-independent infection of the murine placenta may serve to shed some light onto the mechanisms of listerial breaching of the blood-brain barrier. The blood-brain barrier is composed of the capillary endothelium and a thin basement membrane surrounded by synapse-like extensions of astrocytes. Tight junctions between endothelial cells prohibit paracellular transport (Huber *et al.*, 2001) allowing precise control of substances to be transported over this barrier by transcytosis (Tuma and Hubbard, 2003). The mechanism by which *L. monocytogenes* crosses the barrier has been controversially discussed: Enterocytes of brain capillaries or the choroid plexus express both E-cadherin and c-Met, potentially making them susceptible to InlA- and/or InlB-mediated uptake. *In vitro*, InlB enables uptake into microvascular endothelial cells (Greiffenberg *et al.*, 1998) implying direct invasion of endothelial cells by *L. monocytogenes*. Cell-to-cell spread would then allow subsequent bacterial transmission to the CNS. On the other hand, E-cadherin could allow for InlA-dependent entry of *L. monocytogenes* into endothelial cells (Lecuit, 2005). Its contribution has, however, not yet been tested. All of these studies suffer from having been performed *in vitro*. In these transformed cells expressing altered levels of Met and E-cadherin, InlB- and/or InlA-dependent entry may be observed. To what extent this reflects the situation *in vivo*, however, remains to be investigated. Other hypotheses stress the "Trojan horse" mechanisms as responsible for listerial transmission into the brain (Join-Lambert *et al.*, 2005) or a bacteremia induced translocation (Berche, 1995).

To establish the bacterial factors involved in breaching the blood-brain barriers requires an *in vivo* system expressing functional InlA and InlB (Khelef *et al.*, 2006; Ireton, 2007). This prerequisite is met by Lmo-InlA^{m}. Our preliminary analyses, however, do not indicate that InlA is involved in breaching the blood-brain barrier. Taking studies of infected pregnant mice into account, it would appear most probable that the “Trojan horse” mechanism would be responsible for transmission to the CNS. Further studies, possibly utilizing Lmo-InlA^{m}, may potentially help to resolve this question.

5 Outlook

The combination of structural and biophysical analysis of distinct changes within interaction interfaces has improved the knowledge of how protein-protein interactions are enthalpically and entropically stabilized and shed light on synergy effects and particularly on long-range cooperativity.

This study supports the crucial role of water in protein interaction interfaces and quantifies its role in terms of changes in entropy and enthalpy. These data may prove useful in analyzing other protein-protein complexes or in refining sophisticated force fields, used in computational protein design, molecular dynamics simulations (Karplus and McCammon, 2002) or docking studies (Sousa *et al.*, 2006). In particular, an improved understanding of the precise role of water would allow appropriate constraints to be introduced into existing computational protocols that usually operate *in vacuo* to reduce the calculation times (Levy and Onuchic, 2006) to improve the precision and efficiency of such algorithms.

On the other hand, our rational protein interface design approach has allowed the binding specificity of InlA to be extended to include murine E-cadherin, thereby creating a new model for orally acquired listeriosis in mice. The re-engineered listerial strain Lmo-InlA^{m} will have a broad application in immunology, as any mutant mouse strain can directly be used to genetically dissect innate and adaptive host immune response to *L. monocytogenes* by employing the natural route of infection. Experimental listeriosis has in the past been instrumental in establishing major paradigms in contemporary immunology including MHC-restriction (Bouwer *et al.*, 1997), macrophage activation (Goldfine and Wadsworth, 2002) and the role of $CD4^{+}$ / $CD8^{+}$ T cells in host defense (Lara-Tejero and Pamer, 2004). The response of the immune system to intracellular pathogens *in vivo* may be analyzed using the modified listerial strain Lmo-InlA^{m}. Additionally, other yet unidentified or uncharacterized factors, involved in listerial pathogenicity, may be analyzed in an *in vivo* setting. Examples include InlC, InlE, InlG, InlH and InlJ, that have been characterized as potential virulence factor because listerial knock-out strains showed reduced virulence, though their precise role remains unknown (Raffelsbauer *et al.*, 1998; Bergmann *et al.*, 2002; Luo *et al.*, 2004; Sabet *et al.*, 2005).

Furthermore, the methodology may be applicable to other pathogens, that like *L. monocytogenes* are non-pathogenic in animals and hence prevent animal-models being used to investigate the *in vivo* mechanisms of infection in humans. HIV is probably the most prominent example and efforts to adapt it to animal hosts have been described in the recent literature (Potash *et al.*, 2005; Hatziioannou *et al.*, 2006). Another viral pathogen that has recently emerged, SARS, was murinized by serial passage in mice, selecting for viral variants with adapted molecular repertoire (Roberts *et al.*, 2007).

Animal models are pivotal in pre-clinical trials to establish the potential of future drugs. Unavailable animal models appreciably slow down the process of approving new drugs – resulting in significant financial and economical impact. Rational pathogen design may thus prove advantageous in generating new model systems to allow more rapid screening of new forms of anti-infectives.

6 Literature

Alberti-Segui, C., Goeden, K.R., and Higgins, D.E. (2007). Differential function of *Listeria monocytogenes* listeriolysin O and phospholipases C in vacuolar dissolution following cell-to-cell spread. Cell Microbiol. *9*, 179-195.

Alrutz, M.A. and Isberg, R.R. (1998). Involvement of focal adhesion kinase in invasin-mediated uptake. Proc. Natl. Acad. Sci. USA *95*, 13658-13663.

Altekruse, S.F., Cohen, M.L., and Swerdlow, D.L. (1997). Emerging foodborne diseases. Emerg. Infect. Dis. *3*, 285-293.

Aravind, L. and Koonin, E.V. (1999). Gleaning non-trivial structural, functional and evolutionary information about proteins by iterative database searches. J. Mol. Biol. *287*, 1023-1040.

Ausubel, F.M., Brent, R., Kingston, R.E., Moor, D.D., Seidman, J.G., Smith, J.A., and Struhl, K. (2007). Current protocols in molecular biology. (New York: John Wiley & Sons Inc.).

Bakardjiev, A.I., Stacy, B.A., Fisher, S.J., and Portnoy, D.A. (2004). Listeriosis in the pregnant guinea pig: a model of vertical transmission. Infect. Immun. *72*, 489-497.

Bakardjiev, A.I., Theriot, J.A., and Portnoy, D.A. (2006). *Listeria monocytogenes* traffics from maternal organs to the placenta and back. PLoS. Pathog. *2*, e66.

Basar, T., Shen, Y., and Ireton, K. (2005). Redundant roles for Met docking site tyrosines and the Gab1 pleckstrin homology domain in InlB-mediated entry of *Listeria monocytogenes*. Infect. Immun. *73*, 2061-2074.

Bell, J.K., Mullen, G.E., Leifer, C.A., Mazzoni, A., Davies, D.R., and Segal, D.M. (2003). Leucine-rich repeats and pathogen recognition in Toll-like receptors. Trends Immunol. *24*, 528-533.

Berche, P. (1995). Bacteremia is required for invasion of the murine central nervous system by *Listeria monocytogenes*. Microb. Pathog. *18*, 323-336.

Bergmann, B., Raffelsbauer, D., Kuhn, M., Goetz, M., Hom, S., and Goebel, W. (2002). InlA- but not InlB-mediated internalization of *Listeria monocytogenes* by non-phagocytic mammalian cells needs the support of other internalins. Mol. Microbiol. *43*, 557-570.

Bershadsky, A. (2004). Magic touch: how does cell-cell adhesion trigger actin assembly? Trends Cell Biol. *14*, 589-593.

Bierne, H. (2001). A role for cofilin and LIM kinase in Listeria-induced phagocytosis. J. Cell Biol. *155*, 101-112.

Bierne, H., Miki, H., Innocenti, M., Scita, G., Gertler, F.B., Takenawa, T., and Cossart, P. (2005). WASP-related proteins, Abi1 and Ena/VASP are required for Listeria invasion induced by the Met receptor. J. Cell Sci. *118*, 1537-1547.

Birchmeier, C., Birchmeier, W., Gherardi, E., and Vande Woude, G.F. (2003). Met, metastasis, motility and more. Nat. Rev. Mol. Cell Biol. *4*, 915-925.

Blanchoin, L., Amann, K.J., Higgs, H.N., Marchand, J.B., Kaiser, D.A., and Pollard, T.D. (2000). Direct observation of dendritic actin filament networks nucleated by Arp2/3 complex and WASP/Scar proteins. Nature *404*, 1007-1011.

Boggon, T.J., Murray, J., Chappuis-Flament, S., Wong, E., Gumbiner, B.M., and Shapiro, L. (2002). C-cadherin ectodomain structure and implications for cell adhesion mechanisms. Science *296*, 1308-1313.

Boneca, I.G. (2005). The role of peptidoglycan in pathogenesis. Curr. Opin. Microbiol. *8*, 46-53.

Borowiak, M., Garratt, A.N., Wustefeld, T., Strehle, M., Trautwein, C., and Birchmeier, C. (2004). Met provides essential signals for liver regeneration. Proc. Natl Acad. Sci. USA *101*, 10608-10613.

Bottaro, D.P., Rubin, J.S., Faletto, D.L., Chan, A.M., Kmiecik, T.E., Vande Woude, G.F., and Aaronson, S.A. (1991). Identification of the hepatocyte growth factor receptor as the c-met proto-oncogene product. Science *251*, 802-804.

Boujemaa-Paterski, R., Gouin, E., Hansen, G., Samarin, S., Le Clainche, C., Didry, D., Dehoux, P., Cossart, P., Kocks, C., Carlier, M.F., and Pantaloni, D. (2001). Listeria protein ActA mimics WASp family proteins: it activates filament barbed end branching by Arp2/3 complex. Biochemistry *40*, 11390-11404.

Bouwer, H.G., Barry, R.A., and Hinrichs, D.J. (1997). Acquired immunity to an intracellular pathogen: immunologic recognition of L. monocytogenes-infected cells. Immunol. Rev. *158*, 137-146.

Braun, L., Dramsi, S., Dehoux, P., Bierne, H., Lindahl, G., and Cossart, P. (1997). InlB: an invasion protein of *Listeria monocytogenes* with a novel type of surface association. Mol. Microbiol. *25*, 285-294.

Braun, L. and Cossart, P. (2000). Interactions between *Listeria monocytogenes* and host mammalian cells. Microbes. Infect. *2*, 803-811.

Braun, L., Ghebrehiwet, B., and Cossart, P. (2000). gC1q-R/p32, a C1q-binding protein, is a receptor for the InlB invasion protein of *Listeria monocytogenes*. EMBO J. *19*, 1458-1466.

Brown, N.F., Wickham, M.E., Coombes, B.K., and Finlay, B.B. (2006). Crossing the line: selection and evolution of virulence traits. PLoS. Pathog. *2*, e42.

Bryant, D.M. and Stow, J.L. (2004). The ins and outs of E-cadherin trafficking. Trends Cell Biol. *14*, 427-434.

Cabanes, D., Dehoux, P., Dussurget, O., Frangeul, L., and Cossart, P. (2002). Surface proteins and the pathogenic potential of *Listeria monocytogenes*. Trends Microbiol. *10*, 238-245.

Cabanes, D., Dussurget, O., Dehoux, P., and Cossart, P. (2004). Auto, a surface associated autolysin of *Listeria monocytogenes* required for entry into eukaryotic cells and virulence. Mol. Microbiol. *51*, 1601-1614.

Carroll, S.A., Hain, T., Technow, U., Darji, A., Pashalidis, P., Joseph, S.W., and Chakraborty, T. (2003). Identification and characterization of a peptidoglycan hydrolase, MurA, of *Listeria monocytogenes*, a muramidase needed for cell separation. J. Bacteriol. *185*, 6801-6808.

CCP4 (Collaborative Computational Project 4) (1994). The CCP4 suite: programs for protein crystallography. Acta Crystallogr. D *50*, 760-763.

Chakraborty, T., Leimeister-Wächter, M., Domann, E., Hartl, M., Goebel, W., Nichterlein, T., and Notermans, S. (1992). Coordinate regulation of virulence genes in *Listeria monocytogenes* requires the product of the *prfA* gene. J. Bacteriol. *174*, 568-574.

Changeux, J.P. and Edelstein, S.J. (2005). Allosteric mechanisms of signal transduction. Science *308*, 1424-1428.

Charlton, K.M. and Garcia, M.M. (1977). Spontaneous listeric encephalitis and neuritis in sheep. Light microscopic studies. Vet. Pathol. *14*, 297-313.

Cheers, C., Mandel, T.E., and McKenzie, I.F. (1979). Genetics and mechanisms of resistance or susceptibility to murine listeriosis. Adv. Exp. Med. Biol. *114*, 703-707.

Chen, C.P., Posy, S., Ben Shaul, A., Shapiro, L., and Honig, B.H. (2005). Specificity of cell-cell adhesion by classical cadherins: Critical role for low-affinity dimerization through beta-strand swapping. Proc. Natl. Acad. Sci. USA *102*, 8531-8536.

Chico-Calero, I., Suarez, M., Gonzalez-Zorn, B., Scortti, M., Slaghuis, J., Goebel, W., and Vazquez-Boland, J.A. (2002). Hpt, a bacterial homolog of the microsomal glucose- 6-phosphate translocase, mediates rapid intracellular proliferation in Listeria. Proc. Natl. Acad. Sci. USA *99*, 431-436.

Cho, S., Swaminathan, C.P., Yang, J., Kerzic, M.C., Guan, R., Kieke, M.C., Kranz, D.M., Mariuzza, R.A., and Sundberg, E.J. (2005). Structural Basis of Affinity Maturation and Intramolecular Cooperativity in a Protein-Protein Interaction. Structure. (Camb.) *13*, 1775-1787.

Christensen, J.J., Hansen, L.D., and Izatt, R.M. (1976). Handbook of proton ionization heats and related thermodynamic quantities. (New York: John Wiley and Sons).

Clark, M.A. and Hirst, B.H. (2002). Expression of junction-associated proteins differentiates mouse intestinal M cells from enterocytes. Histochem. Cell Biol. *118*, 137-147.

Coligan, J.E., Dunn, B.M., Ploegh, H.L., Speicher, D.W., and Wingfield, P.T. (2002). Current protocols in protein science. (New York: John Wiley & Sons Inc.).

Conlan, J.W. (1999). Early host-pathogen interactions in the liver and spleen during systemic murine listeriosis: an overview. Immunobiology *201*, 178-187.

Cooper, A. (1999). Thermodynamic analysis of biomolecular interactions. Curr. Opin. Chem. Biol. *3*, 557-563.

Cordy, D. and Osebold, J. (1959). The neuropathogenesis of listeria encephalomyelitis in sheep and mice. J. Infect. Dis. *104*, 164-173.

Cossart, P. and Sansonetti, P.J. (2004). Bacterial invasion: the paradigms of enteroinvasive pathogens. Science *304*, 242-248.

Cousens, L.P. and Wing, E.J. (2000). Innate defenses in the liver during Listeria infection. Immunol. Rev. *174*, 150-159.

Czuprynski, C.J., Faith, N.G., and Steinberg, H. (2002). Ability of the *Listeria monocytogenes* strain Scott A to cause systemic infection in mice infected by the intragastric route. Appl. Environ. Microbiol. *68*, 2893-2900.

Czuprynski, C.J., Faith, N.G., and Steinberg, H. (2003). A/J mice are susceptible and C57BL/6 mice are resistant to *Listeria monocytogenes* infection by intragastric inoculation. Infect. Immun. *71*, 682-689.

D'Souza-Schorey, C. (2005). Disassembling adherens junctions: breaking up is hard to do. Trends Cell Biol. *15*, 19-26.

Daniels, J.J., Autenrieth, I.B., and Goebel, W. (2000). Interaction of *Listeria monocytogenes* with the intestinal epithelium. FEMS Microbiol. Lett. *190*, 323-328.

Dietrich, G., Bubert, A., Gentschev, I., Sokolovic, Z., Simm, A., Catic, A., Kaufmann, S.H., Hess, J., Szalay, A.A., and Goebel, W. (1998). Delivery of antigen-encoding plasmid DNA into the cytosol of macrophages by attenuated suicide *Listeria monocytogenes*. Nat. Biotechnol. *16*, 181-185.

Dramsi, S., Biswas, I., Maguin, E., Braun, L., Mastroeni, P., and Cossart, P. (1995). Entry of *Listeria monocytogenes* into hepatocytes requires expression of *inIB*, a surface protein of the internalin multigene family. Mol. Microbiol. *16*, 251-261.

Dramsi, S., Dehoux, P., Lebrun, M., Goossens, P.L., and Cossart, P. (1997). Identification of four new members of the internalin multigene family of *Listeria monocytogenes* EGD. Infect. Immun. *65*, 1615-1625.

Dramsi, S., Levi, S., Triller, A., and Cossart, P. (1998). Entry of *Listeria monocytogenes* into neurons occurs by cell-to-cell spread: an *in vitro* study. Infect. Immun. *66*, 4461-4468.

Dramsi, S. and Cossart, P. (2002). Listeriolysin O: a genuine cytolysin optimized for an intracellular parasite. J. Cell Biol. *156*, 943-946.

Drevets, D.A. (1999). Dissemination of *Listeria monocytogenes* by infected phagocytes. Infect. Immun. *67*, 3512-3517.

Dubail, I., Autret, N., Beretti, J.L., Kayal, S., Berche, P., and Charbit, A. (2001). Functional assembly of two membrane-binding domains in listeriolysin O, the cytolysin of *Listeria monocytogenes*. Microbiology *147*, 2679-2688.

Dunitz, J.D. (1994). The entropic cost of bound water in crystals and biomolecules. Science *264*, 670.

Dunitz, J.D. (1995). Win some, lose some: enthalpy-entropy compensation in weak intermolecular interactions. Chem. Biol. *2*, 709-712.

Dussurget, O., Pizarro-Cerda, J., and Cossart, P. (2004). Molecular determinants of *Listeria monocytogenes* virulence. Annu. Rev. Microbiol. *58*, 587-610.

Elsinghorst, E.A. (1994). Measurement of invasion by gentamicin resistance. Methods Enzymol. *236*, 405-420.

Emsley, P. and Cowtan, K. (2004). Coot: model-building tools for molecular graphics. Acta Crystallogr. D *60*, 2126-2132.

Feng, H.P. (2005). Crossing the species barrier. Nat. Struct. Mol. Biol. *12*, 831.

Gaillard, J.L., Berche, P., Frehel, C., Gouin, E., and Cossart, P. (1991). Entry of *L. monocytogenes* into cells is mediated by internalin, a repeat protein reminiscent of surface antigens from gram-positive cocci. Cell *65*, 1127-1141.

Galan, J.E. (2000). Alternative strategies for becoming an insider: lessons from the bacterial world. Cell *103*, 363-366.

Galan, J.E. and Wolf-Watz, H. (2006). Protein delivery into eukaryotic cells by type III secretion machines. Nature *444*, 567-573.

Gates, J. and Peifer, M. (2005). Can 1000 Reviews Be Wrong? Actin, alpha-Catenin, and Adherens Junctions. Cell *123*, 769-772.

Glaser, P.*et al.* (2001). Comparative genomics of Listeria species. Science *294*, 849-852.

Goldfine, H. and Wadsworth, S.J. (2002). Macrophage intracellular signaling induced by *Listeria monocytogenes*. Microbes. Infect. *4*, 1335-1343.

Gouin, E., Mengaud, J., and Cossart, P. (1994). The virulence gene cluster of *Listeria monocytogenes* is also present in *Listeria ivanovii*, an animal pathogen, and *Listeria seeligeri*, a nonpathogenic species. Infect. Immun. *62*, 3550-3553.

Gregory, S.H., Sagnimeni, A.J., and Wing, E.J. (1996a). Bacteria in the bloodstream are trapped in the liver and killed by immigrating neutrophils. J. Immunol. *157*, 2514-2520.

Gregory, S.H., Sagnimeni, A.J., and Wing, E.J. (1996b). Expression of the *inlAB* operon by *Listeria monocytogenes* is not required for entry into hepatic cells *in vivo*. Infect. Immun. *64*, 3983-3986.

Greiffenberg, L., Goebel, W., Kim, K.S., Weiglein, I., Bubert, A., Engelbrecht, F., Stins, M., and Kuhn, M. (1998). Interaction of *Listeria monocytogenes* with human brain microvascular endothelial cells: InlB-dependent invasion, long-term intracellular growth, and spread from macrophages to endothelial cells. Infect. Immun. *66*, 5260-5267.

Guimaraes, V.D., Gabriel, J.E., Lefevre, F., Cabanes, D., Gruss, A., Cossart, P., Azevedo, V., and Langella, P. (2005). Internalin-expressing *Lactococcus lactis* is able to invade small intestine of guinea pigs and deliver DNA into mammalian epithelial cells. Microbes. Infect. *7*, 836-844.

Gumbiner, B.M. (2000). Regulation of cadherin adhesive activity. J. Cell Biol. *148*, 399-404.

Gumbiner, B.M. (2005). Regulation of cadherin-mediated adhesion in morphogenesis. Nat. Rev. Mol. Cell Biol. *6*, 622-634.

Guruge, J.L., Falk, P.G., Lorenz, R.G., Dans, M., Wirth, H.P., Blaser, M.J., Berg, D.E., and Gordon, J.I. (1998). Epithelial attachment alters the outcome of *Helicobacter pylori* infection. Proc. Natl. Acad. Sci. USA *95*, 3925-3930.

Hamon, M., Bierne, H., and Cossart, P. (2006). *Listeria monocytogenes*: a multifaceted model. Nat Rev Micro *4*, 423-434.

Hatziioannou, T., Princiotta, M., Piatak, M., Jr., Yuan, F., Zhang, F., Lifson, J.D., and Bieniasz, P.D. (2006). Generation of simian-tropic HIV-1 by restriction factor evasion. Science *314*, 95.

Haussinger, D., Ahrens, T., Aberle, T., Engel, J., Stetefeld, J., and Grzesiek, S. (2004). Proteolytic E-cadherin activation followed by solution NMR and X-ray crystallography. EMBO J. *23*, 1699-1708.

Heeney, J.L., Dalgleish, A.G., and Weiss, R.A. (2006). Origins of HIV and the evolution of resistance to AIDS. Science *313*, 462-466.

Helwani, F.M., Kovacs, E.M., Paterson, A.D., Verma, S., Ali, R.G., Fanning, A.S., Weed, S.A., and Yap, A.S. (2004). Cortactin is necessary for E-cadherin-mediated contact formation and actin reorganization. J. Cell Biol. *164*, 899-910.

Hoess, R.H. (2001). Protein design and phage display. Chem. Rev. *101*, 3205-3218.

Hof, H. and Hefner, P. (1988). Pathogenicity of *Listeria monocytogenes* in comparison to other *Listeria* species. Infection *16 Suppl 2*, S141-S144.

Hof, H. (2001). *Listeria monocytogenes*: a causative agent of gastroenteritis? Eur. J. Clin. Microbiol. Infect. Dis. *20*, 369-373.

Hopkins, A.L., Mason, J.S., and Overington, J.P. (2006). Can we rationally design promiscuous drugs? Curr. Opin. Struct. Biol. *16*, 127-136.

Huber, J.D., Egleton, R.D., and Davis, T.P. (2001). Molecular physiology and pathophysiology of tight junctions in the blood-brain barrier. Trends Neurosci. *24*, 719-725.

Huh, C.G., Factor, V.M., Sanchez, A., Uchida, K., Conner, E.A., and Thorgeirsson, S.S. (2004). Hepatocyte growth factor/c-met signaling pathway is required for efficient liver regeneration and repair. Proc. Natl. Acad. Sci. USA *101*, 4477-4482.

Inohara, Chamaillard, McDonald, C., and Nunez, G. (2005). NOD-LRR proteins: role in host-microbial interactions and inflammatory disease. Annu. Rev. Biochem. *74*, 355-383.

Ireton, K. (1996). A role for phosphoinositide 3-kinase in bacterial invasion. Science *274*, 780-782.

Ireton, K., Payrastre, B., and Cossart, P. (1999). The *Listeria monocytogenes* protein InlB is an agonist of mammalian phosphoinositide 3-kinase. J. Biol. Chem. *274*, 17025-17032.

Ireton, K. (2007). Entry of the bacterial pathogen *Listeria monocytogenes* into mammalian cells. Cell Microbiol.

Isberg, R.R. and Leong, J.M. (1990). Multiple beta 1 chain integrins are receptors for invasin, a protein that promotes bacterial penetration into mammalian cells. Cell *60*, 861-871.

Jelesarov, I. and Bosshard, H.R. (1999). Isothermal titration calorimetry and differential scanning calorimetry as complementary tools to investigate the energetics of biomolecular recognition. J. Mol. Recognit. *12*, 3-18.

Jensen, V.B., Harty, J.T., and Jones, B.D. (1998). Interactions of the invasive pathogens *Salmonella typhimurium*, *Listeria monocytogenes*, and *Shigella flexneri* with M cells and murine Peyer's patches. Infect. Immun. *66*, 3758-3766.

Join-Lambert, O.F., Ezine, S., Le Monnier, A., Jaubert, F., Okabe, M., Berche, P., and Kayal, S. (2005). *Listeria monocytogenes*-infected bone marrow myeloid cells promote bacterial invasion of the central nervous system. Cell Microbiol. *7*, 167-180.

Jones, S. and Thornton, J.M. (1996). Principles of protein-protein interactions. Proc. Natl. Acad. Sci. USA *93*, 13-20.

Jonquieres, R., Bierne, H., Fiedler, F., Gounon, P., and Cossart, P. (1999). Interaction between the protein InlB of *Listeria monocytogenes* and lipoteichoic acid: a novel mechanism of protein association at the surface of gram-positive bacteria. Mol. Microbiol. *34*, 902-914.

Jonquieres, R., Pizarro-Cerda, J., and Cossart, P. (2001). Synergy between the N- and C-terminal domains of InlB for efficient invasion of non-phagocytic cells by *Listeria monocytogenes*. Mol. Microbiol. *42*, 955-965.

Kabsch, W. (1988). Evaluation of single-crystal X-ray diffraction data from a position-sensitive detector. Journal of Applied Crystallography *21*, 916-924.

Karplus, M. and McCammon, J.A. (2002). Molecular dynamics simulations of biomolecules. Nat. Struct. Biol. *9*, 646-652.

Kayal, S. and Charbit, A. (2006). Listeriolysin O: a key protein of *Listeria monocytogenes* with multiple functions. FEMS Microbiol. Rev. *30*, 514-529.

Keskin, O., Ma, B., and Nussinov, R. (2005). Hot regions in protein-protein interactions: the organization and contribution of structurally conserved hot spot residues. J. Mol. Biol. *345*, 1281-1294.

Khelef, N., Lecuit, M., Bierne, H., and Cossart, P. (2006). Species specificity of the *Listeria monocytogenes* InlB protein. Cell Microbiol. *8*, 457-470.

Kissinger, C.R., Gehlhaar, D.K., and Fogel, D.B. (1999). Rapid automated molecular replacement by evolutionary search. Acta Crystallogr. D *55*, 484-491.

Kobe, B. and Deisenhofer, J. (1994). The leucine-rich repeat: a versatile binding motif. Trends Biochem. Sci. *19*, 415-421.

Kobe, B. and Kajava, A.V. (2001). The leucine-rich repeat as a protein recognition motif. Curr. Opin. Struct. Biol. *11*, 725-732.

Kobielak, A., Pasolli, H.A., and Fuchs, E. (2004). Mammalian formin-1 participates in adherens junctions and polymerization of linear actin cables. Nat. Cell Biol. *6*, 21-30.

Koch, J. and Stark, K. (2006). Significant increase of listeriosis in Germany - epidemiological patterns 2001-2005. Euro. Surveill *11*, 85-88.

Kocks, C., Gouin, E., Tabouret, M., Berche, P., Ohayon, H., and Cossart, P. (1992). *L. monocytogenes*-induced actin assembly requires the *actA* gene product, a surface protein. Cell *68*, 521-531.

Kortemme, T. and Baker, D. (2004). Computational design of protein-protein interactions. Curr. Opin. Chem. Biol. *8*, 91-97.

Kraehenbuhl, J.P. and Neutra, M.R. (2000). Epithelial M cells: differentiation and function. Annu. Rev. Cell Dev. Biol. *16*, 301-332.

Kussel-Andermann, P., El Amraoui, A., Safieddine, S., Nouaille, S., Perfettini, I., Lecuit, M., Cossart, P., Wolfrum, U., and Petit, C. (2000). Vezatin, a novel transmembrane protein, bridges myosin VIIA to the cadherin-catenins complex. EMBO J. *19*, 6020-6029.

Lafont, F., Tran, V.N., Hanada, K., Sansonetti, P., and van der Goot, F.G. (2002). Initial steps of *Shigella* infection depend on the cholesterol/sphingolipid raft-mediated CD44-IpaB interaction. EMBO J. *21*, 4449-4457.

Lamzin, V.S. and Wilson, K.S. (1993). Automated refinement of protein models. Acta Crystallogr. D *49*, 129-147.

Lara-Tejero, M. and Pamer, E.G. (2004). T cell responses to *Listeria monocytogenes*. Curr. Opin. Microbiol. *7*, 45-50.

Lassnig, C., Sanchez, C.M., Egerbacher, M., Walter, I., Majer, S., Kolbe, T., Pallares, P., Enjuanes, L., and Muller, M. (2005). Development of a transgenic mouse model susceptible to human coronavirus 229E. Proc. Natl. Acad. Sci. USA *102*, 8275-8280.

Lauer, P., Chow, M.Y., Loessner, M.J., Portnoy, D.A., and Calendar, R. (2002). Construction, characterization, and use of two *Listeria monocytogenes* site-specific phage integration vectors. J. Bacteriol. *184*, 4177-4186.

Le Monnier, A., Join-Lambert, O.F., Jaubert, F., Berche, P., and Kayal, S. (2006). Invasion of the placenta during murine listeriosis. Infect. Immun. *74*, 663-672.

Le Monnier, A., Autret, N., Join-Lambert, O.F., Jaubert, F., Charbit, A., Berche, P., and Kayal, S. (2007). ActA is required for crossing of the fetoplacental barrier by *Listeria monocytogenes*. Infect. Immun. *75*, 950-957.

Leavitt, S. and Freire, E. (2001). Direct measurement of protein binding energetics by isothermal titration calorimetry. Curr. Opin. Struct. Biol. *11*, 560-566.

Lecuit, M., Ohayon, H., Braun, L., Mengaud, J., and Cossart, P. (1997). Internalin of *Listeria monocytogenes* with an intact leucine-rich repeat region is sufficient to promote internalization. Infect. Immun. *65*, 5309-5319.

Lecuit, M., Dramsi, S., Gottardi, C., Fedor-Chaiken, M., Gumbiner, B., and Cossart, P. (1999). A single amino acid in E-cadherin responsible for host specificity towards the human pathogen *Listeria monocytogenes*. EMBO J. *18*, 3956-3963.

Lecuit, M., Hurme, R., Pizarro-Cerda, J., Ohayon, H., Geiger, B., and Cossart, P. (2000). A role for alpha-and beta-catenins in bacterial uptake. Proc. Natl. Acad. Sci. USA *97*, 10008-10013.

Lecuit, M., Vandormael-Pournin, S., Lefort, J., Huerre, M., Gounon, P., Dupuy, C., Babinet, C., and Cossart, P. (2001). A transgenic model for listeriosis: role of internalin in crossing the intestinal barrier. Science *292*, 1722-1725.

Lecuit, M. and Cossart, P. (2002). Genetically-modified-animal models for human infections: the Listeria paradigm. Trends Mol. Med. *8*, 537-542.

Lecuit, M., Nelson, D.M., Smith, S.D., Khun, H., Huerre, M., Vacher-Lavenu, M.C., Gordon, J.I., and Cossart, P. (2004). Targeting and crossing of the human maternofetal barrier by *Listeria monocytogenes*: role of internalin interaction with trophoblast E-cadherin. Proc. Natl. Acad. Sci. USA *101*, 6152-6157.

Lecuit, M. (2005). Understanding how *Listeria monocytogenes* targets and crosses host barriers. Clin. Microbiol. Infect. *11*, 430-436.

Lenz, L.L., Mohammadi, S., Geissler, A., and Portnoy, D.A. (2003). SecA2-dependent secretion of autolytic enzymes promotes *Listeria monocytogenes* pathogenesis. Proc. Natl. Acad. Sci. USA *100*, 12432-12437.

Levy, Y. and Onuchic, J.N. (2006). Water mediation in protein folding and molecular recognition. Annu. Rev. Biophys. Biomol. Struct. *35*, 389-415.

Lewis, D.B. (2006). Avian flu to human influenza. Annu. Rev. Med. *57*, 139-154.

Li, F., Li, W., Farzan, M., and Harrison, S.C. (2005). Structure of SARS coronavirus spike receptor-binding domain complexed with receptor. Science *309*, 1864-1868.

Liberles, J.S., Thorolfsson, M., and Martinez, A. (2005). Allosteric mechanisms in ACT domain containing enzymes involved in amino acid metabolism. Amino. Acids *28*, 1-12.

Lingnau, A., Domann, E., Hudel, M., Bock, M., Nichterlein, T., Wehland, J., and Chakraborty, T. (1995). Expression of the *Listeria monocytogenes* EGD *inlA* and *inlB* genes, whose products mediate bacterial entry into tissue culture cell lines, by PrfA-dependent and -independent mechanisms. Infect. Immun. *63*, 3896-3903.

Lorber, B. (1997). Listeriosis. Clin. Infect. Dis. *24*, 1-9.

Luo, Q., Rauch, M., Marr, A.K., Muller-Altrock, S., Luo, Q., and Goebel, W. (2004). *In vitro* transcription of the *Listeria monocytogenes* virulence genes *inl*C and *mpl* reveals overlapping PrfA-dependent and -independent promoters that are differentially activated by GTP. Mol. Microbiol. *52*, 39-52.

Lynch, M., Painter, J., Woodruff, R., and Braden, C. (2006). Surveillance for foodborne-disease outbreaks - United States, 1998-2002. MMWR Surveill Summ. *55*, 1-42.

Marco, A.J., Altimira, J., Prats, N., Lopez, S., Dominguez, L., Domingo, M., and Briones, V. (1997). Penetration of *Listeria monocytogenes* in mice infected by the oral route. Microb. Pathog. *23*, 255-263.

Marino, M., Banerjee, M., Jonquieres, R., Cossart, P., and Ghosh, P. (2002). GW domains of the *Listeria monocytogenes* invasion protein InlB are SH3-like and mediate binding to host ligands. EMBO J. *21*, 5623-5634.

McCammon, J.A. (2005). Target flexibility in molecular recognition. Biochim. Biophys. Acta *1754*, 221-224.

McLauchlin, J., Mitchell, R.T., Smerdon, W.J., and Jewell, K. (2004). *Listeria monocytogenes* and listeriosis: a review of hazard characterisation for use in microbiological risk assessment of foods. Int. J. Food Microbiol. *92*, 15-33.

McNeill, H. (2000). Sticking together and sorting things out: adhesion as a force in development. Nat. Rev. Genet. *1*, 100-108.

Mengaud, J., Ohayon, H., Gounon, P., Mege, R.-M., and Cossart, P. (1996). E-cadherin is the receptor for internalin, a surface protein required for entry of *L. monocytogenes* into epithelial cells. Cell *84*, 923-932.

Meyer, E.A., Castellano, R.K., and Diederich, F. (2003). Interactions with aromatic rings in chemical and biological recognition. Angew. Chem. Int. Ed Engl. *42*, 1210-1250.

Moffett, A. and Loke, C. (2006). Immunology of placentation in eutherian mammals. Nat. Rev. Immunol. *6*, 584-594.

Mowat, A.M. (2003). Anatomical basis of tolerance and immunity to intestinal antigens. Nat. Rev. Immunol. *3*, 331-341.

Moza, B., Buonpane, R.A., Zhu, P., Herfst, C.A., Rahman, A.K., McCormick, J.K., Kranz, D.M., and Sundberg, E.J. (2006). Long-range cooperative binding effects in a T cell receptor variable domain. Proc. Natl. Acad. Sci. USA *103*, 9867-9872.

Munder, A., Zelmer, A., Schmiedl, A., Dittmar, K.E., Rohde, M., Dorsch, M., Otto, K., Hedrich, H.J., Tümmler, B., Weiss, S., and Tschernig, T. (2005). Murine pulmonary infection with *Listeria monocytogenes*: differential susceptibility of BALB/c, C57BL/6 and DBA/2 mice. Microbes. Infect. *7*, 600-611.

Murphy, K.P. (1995). Noncovalent forces important to the conformational stability of protein structures. Methods Mol. Biol. *40*, 1-34.

Murshudov, G.N., Vagin, A.A., and Dodson, E.J. (1997). Refinement of macromolecular structures by the maximum-likelihood method. Acta Crystallogr. D *53*, 240-255.

Navarro, P., Gomez, M., Pizarro, A., Gamallo, C., Quintanilla, M., and Cano, A. (1991). A role for the E-cadherin cell-cell adhesion molecule during tumor progression of mouse epidermal carcinogenesis. J. Cell Biol. *115*, 517-533.

Nelson, W.J. and Nusse, R. (2004). Convergence of Wnt, beta-catenin, and cadherin pathways. Science *303*, 1483-1487.

Neuenhahn, M.*et al.* (2006). CD8α^+ dendritic cells are required for efficient entry of *Listeria monocytogenes* into the spleen. Immunity. *25*, 619-630.

Newberry, R.D. and Lorenz, R.G. (2005). Organizing a mucosal defense. Immunol. Rev. *206*, 6-21.

Niemann, H.H., Jäger, V., Butler, P.J.G., van den Heuvel, J., Schmidt, S., Ferraris, D., Gherardi, E., and Heinz, D.W. (2007). Structure of the human receptor tyrosine kinase Met in complex with the *Listeria monocytogenes* invasion protein InlB. Cell *in press*.

Nightingale, K.K., Windham, K., Martin, K.E., Yeung, M., and Wiedmann, M. (2005a). Select *Listeria monocytogenes* subtypes commonly found in foods carry distinct nonsense mutations in *inlA*, leading to expression of truncated and secreted internalin A, and are associated with a reduced invasion phenotype for human intestinal epithelial cells. Appl. Environ. Microbiol. *71*, 8764-8772.

Nightingale, K.K., Windham, K., and Wiedmann, M. (2005b). Evolution and molecular phylogeny of *Listeria monocytogenes* isolated from human and animal listeriosis cases and foods. J. Bacteriol. *187*, 5537-5551.

Olier, M., Pierre, F., Rousseaux, S., Lemaitre, J.P., Rousset, A., Piveteau, P., and Guzzo, J. (2003). Expression of truncated Internalin A is involved in impaired internalization of some *Listeria monocytogenes* isolates carried asymptomatically by humans. Infect. Immun. *71*, 1217-1224.

Orndorff, P.E., Hamrick, T.S., Smoak, I.W., and Havell, E.A. (2006). Host and bacterial factors in listeriosis pathogenesis. Vet. Microbiol. *114*, 1-15.

Ottemann, K.M., Xiao, W., Shin, Y.K., and Koshland, D.E., Jr. (1999). A piston model for transmembrane signaling of the aspartate receptor. Science *285*, 1751-1754.

Otwinowski, Z. and Minor, W. (1997). Processing of x-ray diffraction data collected in oscillation mode. Methods in Enzymology *276*, 307-321.

Ozawa, M., Baribault, H., and Kemler, R. (1989). The cytoplasmic domain of the cell adhesion molecule uvomorulin associates with three independent proteins structurally related in different species. EMBO J. *8*, 1711-1717.

Pamer, E.G. (2004). Immune responses to *Listeria monocytogenes*. Nat. Rev. Immunol. *4*, 812-823.

Park, S.F. and Stewart, G.S. (1990). High-efficiency transformation of *Listeria monocytogenes* by electroporation of penicillin-treated cells. Gene *94*, 129-132.

Pasche, B., Kalaydjiev, S., Franz, T.J., Kremmer, E., Gailus-Durner, V., Fuchs, H., Hrabé de Angelis, M., Lengeling, A., and Busch, D.H. (2005). Sex-dependent susceptibility to *Listeria monocytogenes* infection is mediated by differential interleukin-10 production. Infect. Immun. *73*, 5952-5960.

Patterson, J.B., Manchester, M., and Oldstone, M.B. (2001). Disease model: dissecting the pathogenesis of the measles virus. Trends Mol. Med. *7*, 85-88.

Pentecost, M., Otto, G., Theriot, J.A., and Amieva, M.R. (2006). *Listeria monocytogenes* invades the epithelial junctions at sites of cell extrusion. PLoS. Pathog. *2*, e3.

Perozzo, R., Folkers, G., and Scapozza, L. (2004). Thermodynamics of protein-ligand interactions: history, presence, and future aspects. J. Recept. Signal. Transduct. Res. *24*, 1-52.

Perrella, M. (1999). Understanding mechanisms in a cooperative protein: the CO ligation intermediates of hemoglobin. Biophys. Chem. *81*, 157-178.

Peruzzi, B. and Bottaro, D.P. (2006). Targeting the c-Met signaling pathway in cancer. Clin. Cancer Res. *12*, 3657-3660.

Pizarro-Cerda, J. and Cossart, P. (2006a). Bacterial adhesion and entry into host cells. Cell *124*, 715-727.

Pizarro-Cerda, J. and Cossart, P. (2006b). Subversion of cellular functions by *Listeria monocytogenes*. J. Pathol. *208*, 215-223.

Pohl, M.A., Wiedmann, M., and Nightingale, K.K. (2006). Associations among *Listeria monocytogenes* genotypes and distinct clinical manifestations of listeriosis in cattle. Am. J. Vet. Res. *67*, 616-626.

Poltorak, A., He, X., Smirnova, I., Liu, M.Y., Van Huffel, C., Du, X., Birdwell, D., Alejos, E., Silva, M., Galanos, C., Freudenberg, M., Ricciardi-Castagnoli, P., Layton, B., and Beutler, B. (1998). Defective LPS signaling in C3H/HeJ and C57BL/10ScCr mice: mutations in *Tlr4* gene. Science *282*, 2085-2088.

Potash, M.J., Chao, W., Bentsman, G., Paris, N., Saini, M., Nitkiewicz, J., Belem, P., Sharer, L., Brooks, A.I., and Volsky, D.J. (2005). A mouse model for study of systemic HIV-1 infection, antiviral immune responses, and neuroinvasiveness. Proc. Natl. Acad. Sci. USA *102*, 3760-3765.

Pust, S., Morrison, H., Wehland, J., Sechi, A.S., and Herrlich, P. (2005). *Listeria monocytogenes* exploits ERM protein functions to efficiently spread from cell to cell. EMBO J. *24*, 1287-1300.

Raffelsbauer, D., Bubert, A., Engelbrecht, F., Scheinpflug, J., Simm, A., Hess, J., Kaufmann, S.H., and Goebel, W. (1998). The gene cluster *inl*C2DE of *Listeria monocytogenes* contains additional new *internalin* genes and is important for virulence in mice. Mol. Gen. Genet. *260*, 144-158.

Reichmann, D., Rahat, O., Cohen, M., Neuvirth, H., and Schreiber, G. (2007). The molecular architecture of protein-protein binding sites. Curr. Opin. Struct. Biol. *17*, 67-76.

Roberts, A., Deming, D., Paddock, C.D., Cheng, A., Yount, B., Vogel, L., Herman, B.D., Sheahan, T., Heise, M., Genrich, G.L., Zaki, S.R., Baric, R., and Subbarao, K. (2007). A Mouse-Adapted SARS-Coronavirus Causes Disease and Mortality in BALB/c Mice. PLoS. Pathog. *3*, e5.

Rosenberg, M. and Goldblum, A. (2006). Computational protein design: a novel path to future protein drugs. Curr. Pharm. Des *12*, 3973-3997.

Sabet, C., Lecuit, M., Cabanes, D., Cossart, P., and Bierne, H. (2005). LPXTG protein InlJ, a newly identified internalin involved in *Listeria monocytogenes* virulence. Infect. Immun. *73*, 6912-6922.

Sambrook, J. and Russell, D.W. (2000). Molecular Cloning - a laboratory manual. (Cold Spring Harbor: Cold Spring Harbor Laboratory Press).

Schimmele, B. and Plückthun, A. (2005). Identification of a functional epitope of the Nogo receptor by a combinatorial approach using ribosome display. J. Mol. Biol. *352*, 229-241.

Schubert, W.D., Goebel, G., Diepholz, M., Darji, A., Kloer, D., Hain, T., Chakraborty, T., Wehland, J., Domann, E., and Heinz, D.W. (2001). Internalins from the human pathogen *Listeria monocytogenes* combine three distinct folds into a contiguous internalin domain. J. Mol. Biol. *312*, 783-794.

Schubert, W.D., Urbanke, C., Ziehm, T., Beier, V., Machner, M.P., Domann, E., Wehland, J., Chakraborty, T., and Heinz, D.W. (2002). Structure of internalin, a major invasion protein of *Listeria monocytogenes*, in complex with its human receptor E-cadherin. Cell *111*, 825-836.

Schubert, W.D. and Heinz, D.W. (2003). Structural aspects of adhesion to and invasion of host cells by the human pathogen *Listeria monocytogenes*. Chembiochem. *4*, 1285-1291.

Seveau, S., Bierne, H., Giroux, S., Prevost, M.C., and Cossart, P. (2004). Role of lipid rafts in E-cadherin- and HGF-R/Met-mediated entry of *Listeria monocytogenes* into host cells. J. Cell Biol. *166*, 743-753.

Seveau, S., Tham, T.N., Payrastre, B., Hoppe, A.D., Swanson, J.A., and Cossart, P. (2007). A FRET analysis to unravel the role of cholesterol in Rac1 and PI 3-kinase activation in the InlB/Met signalling pathway. Cell Microbiol. *9*, 790-803.

Sharma, S.K., Ramsey, T.M., and Bair, K.W. (2002). Protein-protein interactions: lessons learned. Curr. Med. Chem. Anticancer Agents *2*, 311-330.

Shen, Y., Naujokas, M., Park, M., and Ireton, K. (2000). InIB-dependent internalization of Listeria is mediated by the Met receptor tyrosine kinase. Cell *103*, 501-510.

Sleator, R.D. and Hill, C. (2006). Patho-biotechnology: using bad bugs to do good things. Curr. Opin. Biotechnol. *17*, 211-216.

Sousa, S., Cabanes, D., Archambaud, C., Colland, F., Lemichez, E., Popoff, M., Boisson-Dupuis, S., Gouin, E., Lecuit, M., Legrain, P., and Cossart, P. (2005). ARHGAP10 is necessary for alpha-catenin recruitment at adherens junctions and for Listeria invasion. Nat. Cell Biol. *7*, 954-960.

Sousa, S.F., Fernandes, P.A., and Ramos, M.J. (2006). Protein-ligand docking: current status and future challenges. Proteins *65*, 15-26.

Stevens, J., Blixt, O., Tumpey, T.M., Taubenberger, J.K., Paulson, J.C., and Wilson, I.A. (2006). Structure and receptor specificity of the hemagglutinin from an H5N1 influenza virus. Science *312*, 404-410.

Stites, W.E. (1997). Protein-protein interactions: interface structure, binding thermodynamics, and mutational analysis. Chem. Rev. *97*, 1233-1250.

Storoni, L.C., McCoy, A.J., and Read, R.J. (2004). Likelihood-enhanced fast rotation functions. Acta Crystallogr. D *60*, 432-438.

Sun, H., Ringdahl, U., Homeister, J.W., Fay, W.P., Engleberg, N.C., Yang, A.Y., Rozek, L.S., Wang, X., Sjobring, U., and Ginsburg, D. (2004). Plasminogen is a critical host pathogenicity factor for group A streptococcal infection. Science *305*, 1283-1286.

Takahashi, N., Takahashi, Y., and Putnam, F.W. (1985). Periodicity of leucine and tandem repetition of a 24-amino acid segment in the primary structure of leucine-rich alpha 2-glycoprotein of human serum. Proc. Natl. Acad. Sci. USA *82*, 1906-1910.

Tilney, L.G. and Portnoy, D.A. (1989). Actin filaments and the growth, movement, and spread of the intracellular bacterial parasite, *Listeria monocytogenes*. J. Cell Biol. *109*, 1597-1608.

Ton-That, H., Liu, G., Mazmanian, S.K., Faull, K.F., and Schneewind, O. (1999). Purification and characterization of sortase, the transpeptidase that cleaves surface proteins of *Staphylococcus aureus* at the LPXTG motif. Proc. Natl. Acad. Sci. USA *96*, 12424-12429.

Tsai, Y.H., Orsi, R.H., Nightingale, K.K., and Wiedmann, M. (2006). *Listeria monocytogenes* internalins are highly diverse and evolved by recombination and positive selection. Infect. Genet. Evol. *6*, 378-389.

Tuma, P.L. and Hubbard, A.L. (2003). Transcytosis: crossing cellular barriers. Physiol Rev. *83*, 871-932.

Vazquez-Boland, J.A., Kuhn, M., Berche, P., Chakraborty, T., Dominguez-Bernal, G., Goebel, W., Gonzalez-Zorn, B., Wehland, J., and Kreft, J. (2001). Listeria pathogenesis and molecular virulence determinants. Clin. Microbiol. Rev. *14*, 584-640.

Vazquez-Torres, A. and Fang, F.C. (2000). Cellular routes of invasion by enteropathogens. Curr. Opin. Microbiol. *3*, 54-59.

Vriend, G. (1990). WHAT IF: a molecular modeling and drug design program. J. Mol. Graph. *8*, 52-6, 29.

Wang, L. and Lin, M. (2007). Identification of IspC, an 86-kilodalton protein target of humoral immune response to infection with *Listeria monocytogenes* serotype 4b, as a novel surface autolysin. J. Bacteriol. *189*, 2046-2054.

Wang, T.W., Zhu, H., Ma, X.Y., Zhang, T., Ma, Y.S., and Wei, D.Z. (2006). Mutant library construction in directed molecular evolution: casting a wider net. Mol. Biotechnol. *34*, 55-68.

Weaver, A.M., Young, M.E., Lee, W.L., and Cooper, J.A. (2003). Integration of signals to the Arp2/3 complex. Curr. Opin. Cell Biol. *15*, 23-30.

Weis, J. and Seeliger, H.P. (1975). Incidence of *Listeria monocytogenes* in nature. Appl. Microbiol. *30*, 29-32.

Wheelock, M.J. and Johnson, K.R. (2003). Cadherin-mediated cellular signaling. Curr. Opin. Cell Biol. *15*, 509-514.

Wodak, S.J. and Janin, J. (2002). Structural basis of macromolecular recognition. Adv. Protein Chem. *61*, 9-73.

Yamada, S.*et al.* (2006). Haemagglutinin mutations responsible for the binding of H5N1 influenza A viruses to human-type receptors. Nature *444*, 378-382.

Yu, E.W. and Koshland, D.E., Jr. (2001). Propagating conformational changes over long (and short) distances in proteins. Proc. Natl. Acad. Sci. USA *98*, 9517-9520.

Danksagung

Mein besonderer Dank gilt Dr. Wolf-Dieter Schubert für die Aufnahme in seine Arbeitsgruppe, die Bereitstellung des interessanten Projektes und seine ständige Unterstützung. Neben dem überaus großen Interesse an meiner Arbeit, hat sein Engagement und seine Diskussionsbereitschaft entscheidend zum Gelingen dieser Arbeit beigetragen. Vielen Dank für die Überarbeitungen der Veröffentlichungen und dieser Dissertation. Große Herausforderungen, bedingt nicht nur durch die Methodenvielfalt in dieser Arbeit, konnten nicht zuletzt durch seine Unterstützung bewältigt werden.

Prof. Dr. Dirk Heinz danke ich für die Möglichkeit meine Doktorarbeit im Bereich Strukturbiologie anfertigen zu können und für die ausgezeichneten Arbeitsbedingungen, die nicht nur im neuen Gründerzentrum sondern auch in unserem alten C-Gebäude oft keine Wünsche offen gelassen haben. Für sein großes Interesse an meiner Arbeit, seine ständige Unterstützung, die vielen Diskussionsanstöße die entscheidend zum Fortschritt der Arbeit beigetragen haben und seiner Hilfe bei der weiteren Planung meiner wissenschaftlichen Laufbahn bin ich ihm sehr dankbar.

Für die Übernahme des Zweitgutachtens bedanke ich mich herzlich bei Prof. Dr. Petra Dersch.

Ebenso möchte ich mich für die Übernahme des Prüfungsvorsitzes bei Prof. Dr. Ralf Mendel bedanken.

Ich danke Dr. Bastian Pasche und Dr. Andreas Lengeling für die ausgezeichnete Kooperation, ohne die die Etablierung des neuen Listerien-Stammes nicht möglich gewesen wäre. Die gute Zusammenarbeit hat einen wichtigen Beitrag zum Gelingen der Arbeit geleistet.

In diesem Zusammenhang soll die sehr gute Kooperation mit Dr. Stefanie Deppenmeier und Prof. Dr. Achim Gruber nicht unerwähnt bleiben. Die schnelle histologische Begutachtung

der Proben ebenso wie die konstruktive Mitarbeit insbesondere von Prof. Dr. Achim Gruber waren eine große Hilfe.

Dr. Joop van den Heuvel danke ich für die Planung bei schwierigen Klonierungsprojekten, insbesondere bei der Herstellung des transgenen Listerien-Stammes, sowie der Hilfe bei der Beantragung der S2-Arbeiten und für das Korrekturlesen der Veröffentlichungen.
Daniela Gebauer danke ich für die Unterstützung bei der Klonierung des pAUL-A Konstruktes.

Dr. Theresia Stradal möchte ich herzlich für die Einführung in die experimentelle Zell- und Infektionsbiologie sowie die Fluoreszenzmikroskopie danken. Die vielen Anregungen für weitere Experimente haben dazu beigetragen, den Listerien-Stamm umfassend zu charakterisieren.

Dr. Uwe Kärst danke ich für die technische Unterstützung bezüglich des Isothermen Titrations-Kalorimeters, insbesondere dessen Reparatur ohne die abschließende Messungen äußerst schwierig geworden wären.

Ute Widow und Sabine Schmidt danke ich nicht nur für die kontinuierliche Unterstützung im Labor, sondern auch für die unglaubliche Arbeitsatmosphäre und die lustigen Kaffeerunden. Angefangen vom Anfeuerungsteam beim Behördenmarathon bis hin zu den Geburtstags-veranstaltungen haben wir eine ganze Menge Spaß gehabt.

Zu dem besonders guten Arbeitsklima hat natürlich auch das „Kompetenz-Zentrum für Strukturbiologische Vernetzung“ mit dem „Sekret-Ariat“ Maike Rochon sowie dem „inneren Führungskreis“ Gregor Hagelüken beigetragen. Nicht nur die überaus humorvollen Rezitationen oder die vielleicht nicht immer der Jahreszeit angepassten Dekoration des Büros haben zu einem unschlagbarem „Humorfaktor“ beigetragen.

Dem gesamten Team des Bereiches Strukturbiologie danke ich für das gute Arbeitsklima. Besonderer Dank gilt dabei Dr. Hartmut Niemann für seine ständige Hilfsbereitschaft und dass er als „assoziiertes Mitglied des Kompetenzzentrums“ immer für einen Scherz zu haben war. Dr. Joachim Reichelt danke ich für seine Hilfe rund um Computer und Röntgengerät.

Meiner Familie danke ich für die große Unterstützung während meiner gesamten akademischen Ausbildung. Ohne Euch wäre es nicht möglich gewesen Studium und Doktorarbeit so „reibungslos“ hinter sich zu bringen.

Lebenslauf

Persönliche Daten

Thomas Wollert

geb. 31.05.1979 in Magdeburg

ledig

deutsch

Schulische Ausbildung

1985-1989	Grundschule in Wefensleben
1989-1991	Realschule in Wefensleben
1991-1997	Allertal Gymnasium Eilsleben
	Abschluss: Abitur

Wehrdienst

1997-1998	General-Feldmarschall-Rommel Kaserne, Augustdorf

Akademisch Ausbildung

10/1998-10/2000	Grundstudium Biochemie an der Universität Potsdam
10/2000-02/2004	Hauptstudium Biochemie an der Universität Hannover Abschluss: Diplom (mit Auszeichnung)
07/2003-01/2004	Diplomarbeit an der Gesellschaft für Biotechnologische Forschung (seit 2006: Helmholtz-Zentrum für Infektionsforschung) Braunschweig: Optimierung des Komplexes zwischen Internalin aus *Listeria monocytogenes* und humanem E-Cadherin durch Mutagenese
03/2004-07/2007	Promotion am Helmholtz-Zentrum für Infektionsforschung, AG Molekulare Wirt-Pathogen Interaktionen im Bereich Strukturbiologie, Braunschweig